Implementation and Testing of Elemental Flooding and Drying in the ADCIRC Hydrodynamic Model

Richard A. Luettich, Jr.
University of North Carolina at Chapel Hill
Institute of Marine Sciences
3431 Arendell St.
Morehead City, NC 28557

Joannes J. Westerink
Dept. of Civil Engineering and Geological Sciences
University of Notre Dame
Notre Dame, IN 46556

July 14, 1995

Final Contractors Report

Prepared for the DEPARTMENT OF THE ARMY
Coastal Engineering Research Center
Waterways Experiment Station
US Army Corps of Engineers
Vicksburg, MS 39180

Under Contract No. DACW39-94-M-5869

TABLE OF CONTENTS

INTRODUCTION

Previous implementations (version 26.XX and lower) of the 2D/3D hydrodynamic model ADCIRC (Luettich et al, 1992, Westerink et al, 1994) made no allowance for the flooding or drying of tidal flats during the course of a tidal cycle or for the inundation and recession of water from low lying coastal lands in response to coastal storms. Rather, ADCIRC assumed the land-water boundary was fixed regardless of the water surface elevation. To accommodate this assumption, (i) bathymetric water depths had to be artificially deepened near shore so that nodes never became dry during falling water levels and (ii) coastlines were assumed to represent infinitely high vertical walls which water piled up against during rising water levels. While these assumptions are reasonable for modeling large scale coastal flows, they improperly represent frictional dissipation and finite amplitude nonlinearities in near shore regions and they also prohibit the over land propagation of flood waters associated with storm surge. As a result, coastal storm surge elevations are often over-estimated and the extent of inundation, a critical parameter in the use of hydrodynamic models for coastal planning, can not accurately be assessed.

Prior to implementing any flooding and drying capability into ADCIRC, a review was completed of flooding and drying algorithms and performance as reported in the published literature. A summary of this review is presented below. An initial assessment of several flooding and drying algorithms was conducted using a one-dimensional (vertically and laterally integrated, constant width) analogue of ADCIRC and is described in Luettich and Westerink (1995). Results from this 1D study suggested element based wetting and drying was generally superior to drag coefficient and nodal based wetting and drying. However, drag coefficient and nodal based solutions were reasonably realistic and their algorithms were much simpler than the element based approach. Therefore these methods were recommended for initial implementation in the full ADCIRC model. Unfortunately, the performances of the drag coefficient and nodal approaches were found to be unsatisfactory in 2D test cases as both methods resulted in the spurious addition of unacceptable amounts of mass to the system. Therefore, an element based scheme has been implemented in ADCIRC and results from this approach are presented in this report. Only flooding and drying due to subcritical flow over sloping inclines has been considered.

LITERATURE SURVEY

The inclusion of flooding and drying capabilities in a hydrodynamic model is a difficult problem. Past attempts to deal with these processes can be broadly lumped into two categories, spatially deforming computational grid schemes and spatially fixed computational grid schemes.

The use of spatially deforming grids requires the transformation of the governing equations into a horizontal coordinate system that is advected with the mean flow. At every time step the water level, the horizontal velocity and the position of the grid is recomputed. Although this approach is conceptually attractive, in practice it can lead to highly deformed grids and is typified by high computational costs. Consequently, it has primarily been restricted to applications involving idealized test problems, (Sielecki and Wurtele, 1970; Lynch and Gray,

1980; Johns 1982; Akanbi and Katopodes, 1988; Siden and Lynch, 1988; Austria and Aldama, 1990).

The most common approach to flooding and drying in operational hydrodynamic models assumes the computational grid is fixed in space. The majority of these schemes designate cells (finite difference models) or elements (finite element models) as being either "wet" or "dry". Wet areas participate in the hydrodynamic calculations while dry areas do not. At selected time intervals (which may or may not be every model time step) an assessment is made of whether additional areas in the grid have become wet or dry. In its simplest form, areas are restricted to wetting or drying in whole grid increments (e.g., Reid and Bodine, 1968; Flather and Heaps, 1975; Yeh and Chou, 1979; Leendertse, 1987; Thomas et al., 1990; Yu et al., 1990; Cialone, 1991; Jelesnianski et al., 1992; Hervouet and Janin, 1994), although efforts have also been made to wet and dry more gradually. The latter is generally accomplished by modifying the governing equations to include some type of element or cell "size factor" that varies from 0 to 1 as a function of water depth. Examples of this include the "marsh porosity method" in RMA-2V (version 4.2), (Thomas et al., 1990) and similar techniques by Flather and Hubbert (1990) and Defina et al. (1994). In addition to flooding and drying in whole or fractional grid increments, algorithms for computational grids that are fixed in space differ in the basic governing equations used to represent the flooding and drying process. For example WIFM assumes cells wet and dry according to a broad crested weir formula, (Cialone, 1991). Other models use the long wave equations, but often without the advective terms included, (Reid and Bodine, 1968; Leendertse, 1987; Thomas et al., 1990; Jelesnianski et al., 1992). Finally, several operational models allow for the possibility of sub grid scale barriers by using weir formulae in place of, or in combination with, the long wave equations when these features are encountered (Leendertse, 1987; Jelesnianski et al., 1992).

Our general assessment of the literature is that while flooding and drying algorithms utilizing deforming grids appear to offer solutions that closely adhere to the long wave equations, their significant computational expense makes them impractical for use in operational models. Schemes utilizing computational grids that are fixed in space, despite their often ad hoc nature, have been implemented in operational models and appear to give realistic flooding and drying estimates. A frequently mentioned problem with these algorithms is numerical noise generated when grid cells are turned on and off. This problem along with the potential to account for sub-grid scale bathymetric variability are the primary motivating factors for the gradual flooding and drying strategies mentioned above. However, we have found that bottom friction is fairly effective at damping this noise in shallow water. Also, the robustness of the wave equation based finite element approach (as utilized in ADCIRC) ensures that minor noise sources do not excite spurious numerical oscillations as might occur in a primitive equation based finite element model. Finally, the difficulty of defining a "size factor" that accurately captures the relationship between water depth and water surface area throughout a model domain makes the use of a gradual wetting and drying approach problematic. Therefore, we have chosen to initially implement a fixed grid flooding and drying strategy in ADCIRC in which whole elements are turned on and off. If important bathymetric features exist at scales below the finite element grid size, we recommend utilizing the power of the finite element method and refining the grid locally to explicitly include these features.

MODIFICATIONS MADE TO ADCIRC TO FACILITATE FLOODING AND DRYING

Several modifications have been made to the base ADCIRC formulation (e.g., as described in Luettich et al., 1992, Westerink et al, 1994) to facilitate implementation of a flooding and drying scheme and to enhance overall model performance. Results from test problems and field applications showed that these changes had minimal effect on the model solutions, except as noted below.

First, ADCIRC was modified to allow the option of using either a fully consistent or a lumped formulation of the linear time derivative terms in the GWCE. (The desired formulation is selected during the model setup.) Mathematically, this means that the Galerkin weighted residual statement for the GWCE was changed from

$$\left\langle \frac{\partial^2 \zeta}{\partial t^2}, \phi_i \right\rangle_\Omega + \left\langle \tau_o \frac{\partial \zeta}{\partial t}, \phi_i \right\rangle_\Omega + \left\langle gh \frac{\partial \zeta}{\partial x}, \frac{\partial \phi_i}{\partial x} \right\rangle_\Omega + \left\langle gh \frac{\partial \zeta}{\partial y}, \frac{\partial \phi_i}{\partial y} \right\rangle_\Omega$$

$$= -E_{h2} \left\langle \frac{\partial^2 \zeta}{\partial x \partial t}, \frac{\partial \phi_i}{\partial x} \right\rangle_\Omega - E_{h2} \left\langle \frac{\partial^2 \zeta}{\partial y \partial t}, \frac{\partial \phi_i}{\partial y} \right\rangle_\Omega + \left\langle U \frac{\partial \zeta}{\partial t}, \frac{\partial \phi_i}{\partial x} \right\rangle_\Omega + \left\langle V \frac{\partial \zeta}{\partial t}, \frac{\partial \phi_i}{\partial y} \right\rangle_\Omega \qquad (1)$$

$$+ \left\langle W_x, \frac{\partial \phi_i}{\partial x} \right\rangle_\Omega + \left\langle W_y, \frac{\partial \phi_i}{\partial y} \right\rangle_\Omega - \int_{\Gamma_Q} \left(\frac{\partial Q_{n^*}}{\partial t} + \tau_o Q_{n^*} \right) \phi_i \, d\Gamma \qquad i = 1, \ldots\ldots N$$

to

$$\left(\frac{\partial^2 \zeta}{\partial t^2} + \tau_o \frac{\partial \zeta}{\partial t} \right) \phi_i + \left\langle gh \frac{\partial \zeta}{\partial x}, \frac{\partial \phi_i}{\partial x} \right\rangle_\Omega + \left\langle gh \frac{\partial \zeta}{\partial y}, \frac{\partial \phi_i}{\partial y} \right\rangle_\Omega$$

$$= -E_{h2} \left\langle \frac{\partial^2 \zeta}{\partial x \partial t}, \frac{\partial \phi_i}{\partial x} \right\rangle_\Omega - E_{h2} \left\langle \frac{\partial^2 \zeta}{\partial y \partial t}, \frac{\partial \phi_i}{\partial y} \right\rangle_\Omega + \left\langle U \frac{\partial \zeta}{\partial t}, \frac{\partial \phi_i}{\partial x} \right\rangle_\Omega + \left\langle V \frac{\partial \zeta}{\partial t}, \frac{\partial \phi_i}{\partial y} \right\rangle_\Omega \qquad (2)$$

$$+ \left\langle W_x, \frac{\partial \phi_i}{\partial x} \right\rangle_\Omega + \left\langle W_y, \frac{\partial \phi_i}{\partial y} \right\rangle_\Omega - \int_{\Gamma_Q} \left(\frac{\partial Q_{n^*}}{\partial t} + \tau_o Q_{n^*} \right) \phi_i \, d\Gamma \qquad i = 1, \ldots\ldots N$$

where all variables are as defined in Luettich et al., (1992).

For any node j, the consistent formulation distributes the contribution of the first two terms in Equation (1) between node j and all of its immediately adjacent nodes. The lumped formulation concentrates the contribution of these terms at node j and therefore on the diagonal of the GWCE system matrix. Our experience utilizing the lumped GWCE formulation on test problems indicates that it is more stable but slightly less accurate (primarily in phase propagation) than the consistent formulation at low grid size to wave length ratios.

Second, ADCIRC was modified so that the dependent variable computed in the solution of the GWCE is the change in water level from the previous time step $\Delta\zeta^{k+1}$ rather than the water level itself ζ^{k+1}. Thus the time discretized, weak weighted residual form of the GWCE was changed from

$$\left\langle \frac{\zeta^{k+1}-2\zeta^{k}+\zeta^{k-1}}{\Delta t^2},\phi_i\right\rangle_\Omega+\tau_o\left\langle \frac{\zeta^{k+1}-\zeta^{k-1}}{2\Delta t},\phi_i\right\rangle_\Omega+\alpha_1\left[\left\langle gh\frac{\partial\zeta^{k+1}}{\partial x},\frac{\partial\phi_i}{\partial x}\right\rangle_\Omega+\left\langle gh\frac{\partial\zeta^{k+1}}{\partial y},\frac{\partial\phi_i}{\partial y}\right\rangle_\Omega\right]$$
$$+\alpha_2\left[\left\langle gh\frac{\partial\zeta^{k}}{\partial x},\frac{\partial\phi_i}{\partial x}\right\rangle_\Omega+\left\langle gh\frac{\partial\zeta^{k}}{\partial y},\frac{\partial\phi_i}{\partial y}\right\rangle_\Omega\right]+\alpha_3\left[\left\langle gh\frac{\partial\zeta^{k-1}}{\partial x},\frac{\partial\phi_i}{\partial x}\right\rangle_\Omega+\left\langle gh\frac{\partial\zeta^{k-1}}{\partial y},\frac{\partial\phi_i}{\partial y}\right\rangle_\Omega\right]$$
$$=\left\langle U^k\left(\frac{\zeta^{k}-\zeta^{k-1}}{\Delta t}\right),\frac{\partial\phi_i}{\partial x}\right\rangle_\Omega+\left\langle V^k\left(\frac{\zeta^{k}-\zeta^{k-1}}{\Delta t}\right),\frac{\partial\phi_i}{\partial y}\right\rangle_\Omega \qquad (3)$$
$$-\left\langle\frac{E_{h2}}{\Delta t}\left(\frac{\partial\zeta^{k}}{\partial x}-\frac{\partial\zeta^{k-1}}{\partial x}\right),\frac{\partial\phi_i}{\partial x}\right\rangle_\Omega-\left\langle\frac{E_{h2}}{\Delta t}\left(\frac{\partial\zeta^{k}}{\partial y}-\frac{\partial\zeta^{k-1}}{\partial y}\right),\frac{\partial\phi_i}{\partial y}\right\rangle_\Omega+\left\langle W_x^k,\frac{\partial\phi_i}{\partial x}\right\rangle_\Omega+\left\langle W_y^k,\frac{\partial\phi_i}{\partial y}\right\rangle_\Omega$$
$$-\int_{\Gamma_Q}\left(\frac{Q_{n^*}^{k+1}-Q_{n^*}^{k-1}}{2\Delta t}+\tau_o\alpha_1Q_{n^*}^{k+1}+\tau_o\alpha_2Q_{n^*}^{k}+\tau_o\alpha_3Q_{n^*}^{k-1}\right)\phi_i\,d\Gamma \qquad i=1,\ldots\ldots N$$

to

$$\left\langle \frac{\Delta\zeta^{k+1}-\Delta\zeta^{k}}{\Delta t^2},\phi_i\right\rangle_\Omega+\tau_o\left\langle \frac{\Delta\zeta^{k+1}+\Delta\zeta^{k}}{2\Delta t},\phi_i\right\rangle_\Omega+\alpha_1\left[\left\langle gh\frac{\partial\Delta\zeta^{k+1}}{\partial x},\frac{\partial\phi_i}{\partial x}\right\rangle_\Omega+\left\langle gh\frac{\partial\Delta\zeta^{k+1}}{\partial y},\frac{\partial\phi_i}{\partial y}\right\rangle_\Omega\right]$$
$$+(\alpha_1+\alpha_2)\left[\left\langle gh\frac{\partial\zeta^{k}}{\partial x},\frac{\partial\phi_i}{\partial x}\right\rangle_\Omega+\left\langle gh\frac{\partial\zeta^{k}}{\partial y},\frac{\partial\phi_i}{\partial y}\right\rangle_\Omega\right]+\alpha_3\left[\left\langle gh\frac{\partial\zeta^{k-1}}{\partial x},\frac{\partial\phi_i}{\partial x}\right\rangle_\Omega+\left\langle gh\frac{\partial\zeta^{k-1}}{\partial y},\frac{\partial\phi_i}{\partial y}\right\rangle_\Omega\right]$$
$$=\left\langle U^k\frac{\Delta\zeta^{k}}{\Delta t},\frac{\partial\phi_i}{\partial x}\right\rangle_\Omega+\left\langle V^k\frac{\Delta\zeta^{k}}{\Delta t},\frac{\partial\phi_i}{\partial y}\right\rangle_\Omega \qquad (4)$$
$$-\left\langle\frac{E_{h2}}{\Delta t}\frac{\partial\Delta\zeta^{k}}{\partial x},\frac{\partial\phi_i}{\partial x}\right\rangle_\Omega-\left\langle\frac{E_{h2}}{\Delta t}\frac{\partial\Delta\zeta^{k}}{\partial y},\frac{\partial\phi_i}{\partial y}\right\rangle_\Omega+\left\langle W_x^k,\frac{\partial\phi_i}{\partial x}\right\rangle_\Omega+\left\langle W_y^k,\frac{\partial\phi_i}{\partial y}\right\rangle_\Omega$$
$$-\int_{\Gamma_Q}\left(\frac{Q_{n^*}^{k+1}-Q_{n^*}^{k-1}}{2\Delta t}+\tau_o\alpha_1Q_{n^*}^{k+1}+\tau_o\alpha_2Q_{n^*}^{k}+\tau_o\alpha_3Q_{n^*}^{k-1}\right)\phi_i\,d\Gamma \qquad i=1,\ldots\ldots N$$

for the consistent formulation or

$$\left(\frac{\Delta\zeta^{k+1}-\Delta\zeta^{k}}{\Delta t^2}+\tau_o\frac{\Delta\zeta^{k+1}+\Delta\zeta^{k}}{2\Delta t}\right)\phi_i+\alpha_1\left[\left\langle gh\frac{\partial\Delta\zeta^{k+1}}{\partial x},\frac{\partial\phi_i}{\partial x}\right\rangle_\Omega+\left\langle gh\frac{\partial\Delta\zeta^{k+1}}{\partial y},\frac{\partial\phi_i}{\partial y}\right\rangle_\Omega\right]$$

$$+(\alpha_1+\alpha_2)\left[\left\langle gh\frac{\partial\zeta^{k}}{\partial x},\frac{\partial\phi_i}{\partial x}\right\rangle_\Omega+\left\langle gh\frac{\partial\zeta^{k}}{\partial y},\frac{\partial\phi_i}{\partial y}\right\rangle_\Omega\right]+\alpha_3\left[\left\langle gh\frac{\partial\zeta^{k-1}}{\partial x},\frac{\partial\phi_i}{\partial x}\right\rangle_\Omega+\left\langle gh\frac{\partial\zeta^{k-1}}{\partial y},\frac{\partial\phi_i}{\partial y}\right\rangle_\Omega\right]$$

$$=\left\langle U^k\frac{\Delta\zeta^{k}}{\Delta t},\frac{\partial\phi_i}{\partial x}\right\rangle_\Omega+\left\langle V^k\frac{\Delta\zeta^{k}}{\Delta t},\frac{\partial\phi_i}{\partial y}\right\rangle_\Omega \tag{5}$$

$$-\left\langle\frac{E_{h2}}{\Delta t}\frac{\partial\Delta\zeta^{k}}{\partial x},\frac{\partial\phi_i}{\partial x}\right\rangle_\Omega-\left\langle\frac{E_{h2}}{\Delta t}\frac{\partial\Delta\zeta^{k}}{\partial y},\frac{\partial\phi_i}{\partial y}\right\rangle_\Omega+\left\langle W_x^k,\frac{\partial\phi_i}{\partial x}\right\rangle_\Omega+\left\langle W_y^k,\frac{\partial\phi_i}{\partial y}\right\rangle_\Omega$$

$$-\int_{\Gamma_Q}\left(\frac{Q_{n^*}^{k+1}-Q_{n^*}^{k-1}}{2\Delta t}+\tau_o\alpha_1Q_{n^*}^{k+1}+\tau_o\alpha_2Q_{n^*}^{k}+\tau_o\alpha_3Q_{n^*}^{k-1}\right)\phi_i\,d\Gamma \qquad i=1,\ldots\ldots N$$

for the lumped formulation.

In Equations (4) and (5), $\Delta\zeta^{k+1}\equiv\zeta^{k+1}-\zeta^{k}$, $\Delta\zeta^{k}\equiv\zeta^{k}-\zeta^{k-1}$, the superscripts k+1, k and k-1 denote variables evaluated at future, present and past time levels, and all other variables are as defined in Luettich et al. (1992). Once $\Delta\zeta^{k+1}$ is determined, the water level at the new time step is computed from $\zeta^{k+1}=\Delta\zeta^{k+1}+\zeta^{k}$. The change from a matrix solution for ζ^{k+1} to one for $\Delta\zeta^{k+1}$ helps decrease numerical roundoff error and simplifies the model implementation in dry areas.

For later convenience, Equations (4) and (5) are written as:

$$\left[\frac{1}{\Delta t^2}\left(1+\frac{\tau_o\Delta t}{2}\right)\right]\left\langle\Delta\zeta^{k+1},\phi_i\right\rangle_\Omega+\alpha_1\left[\left\langle gh\frac{\partial\Delta\zeta^{k+1}}{\partial x},\frac{\partial\phi_i}{\partial x}\right\rangle_\Omega+\left\langle gh\frac{\partial\Delta\zeta^{k+1}}{\partial y},\frac{\partial\phi_i}{\partial y}\right\rangle_\Omega\right]$$

$$=\left[\frac{1}{\Delta t^2}\left(1-\frac{\tau_o\Delta t}{2}\right)\right]\left\langle\Delta\zeta^{k},\phi_i\right\rangle_\Omega$$

$$-(\alpha_1+\alpha_2)\left[\left\langle gh\frac{\partial\zeta^{k}}{\partial x},\frac{\partial\phi_i}{\partial x}\right\rangle_\Omega+\left\langle gh\frac{\partial\zeta^{k}}{\partial y},\frac{\partial\phi_i}{\partial y}\right\rangle_\Omega\right]-\alpha_3\left[\left\langle gh\frac{\partial\zeta^{k-1}}{\partial x},\frac{\partial\phi_i}{\partial x}\right\rangle_\Omega+\left\langle gh\frac{\partial\zeta^{k-1}}{\partial y},\frac{\partial\phi_i}{\partial y}\right\rangle_\Omega\right] \tag{6}$$

$$+\left\langle U^k\frac{\Delta\zeta^{k}}{\Delta t},\frac{\partial\phi_i}{\partial x}\right\rangle_\Omega+\left\langle V^k\frac{\Delta\zeta^{k}}{\Delta t},\frac{\partial\phi_i}{\partial y}\right\rangle_\Omega$$

$$-\left\langle\frac{E_{h2}}{\Delta t}\frac{\partial\Delta\zeta^{k}}{\partial x},\frac{\partial\phi_i}{\partial x}\right\rangle_\Omega-\left\langle\frac{E_{h2}}{\Delta t}\frac{\partial\Delta\zeta^{k}}{\partial y},\frac{\partial\phi_i}{\partial y}\right\rangle_\Omega+\left\langle W_x^k,\frac{\partial\phi_i}{\partial x}\right\rangle_\Omega+\left\langle W_y^k,\frac{\partial\phi_i}{\partial y}\right\rangle_\Omega$$

$$-\int_{\Gamma_Q}\left(\frac{Q_{n^*}^{k+1}-Q_{n^*}^{k-1}}{2\Delta t}+\tau_o\alpha_1Q_{n^*}^{k+1}+\tau_o\alpha_2Q_{n^*}^{k}+\tau_o\alpha_3Q_{n^*}^{k-1}\right)\phi_i\,d\Gamma \qquad i=1,\ldots\ldots N$$

for the consistent formulation or

$$\left[\frac{\phi_i}{\Delta t^2}\left(1+\frac{\tau_o \Delta t}{2}\right)\right]\Delta\zeta^{k+1}+\alpha_1\left[\left\langle gh\frac{\partial \Delta\zeta^{k+1}}{\partial x},\frac{\partial\phi_i}{\partial x}\right\rangle_\Omega+\left\langle gh\frac{\partial \Delta\zeta^{k+1}}{\partial y},\frac{\partial\phi_i}{\partial y}\right\rangle_\Omega\right]$$
$$=\left[\frac{\phi_i}{\Delta t^2}\left(1-\frac{\tau_o \Delta t}{2}\right)\right]\Delta\zeta^{k}$$
$$-(\alpha_1+\alpha_2)\left[\left\langle gh\frac{\partial \zeta^{k}}{\partial x},\frac{\partial\phi_i}{\partial x}\right\rangle_\Omega+\left\langle gh\frac{\partial \zeta^{k}}{\partial y},\frac{\partial\phi_i}{\partial y}\right\rangle_\Omega\right]-\alpha_3\left[\left\langle gh\frac{\partial \zeta^{k-1}}{\partial x},\frac{\partial\phi_i}{\partial x}\right\rangle_\Omega+\left\langle gh\frac{\partial \zeta^{k-1}}{\partial y},\frac{\partial\phi_i}{\partial y}\right\rangle_\Omega\right] \quad (7)$$
$$+\left\langle U^k\frac{\Delta\zeta^{k}}{\Delta t},\frac{\partial\phi_i}{\partial x}\right\rangle_\Omega+\left\langle V^k\frac{\Delta\zeta^{k}}{\Delta t},\frac{\partial\phi_i}{\partial y}\right\rangle_\Omega$$
$$-\left\langle\frac{E_{h2}}{\Delta t}\frac{\partial\Delta\zeta^{k}}{\partial x},\frac{\partial\phi_i}{\partial x}\right\rangle_\Omega-\left\langle\frac{E_{h2}}{\Delta t}\frac{\partial\Delta\zeta^{k}}{\partial y},\frac{\partial\phi_i}{\partial y}\right\rangle_\Omega+\left\langle W_x^k,\frac{\partial\phi_i}{\partial x}\right\rangle_\Omega+\left\langle W_y^k,\frac{\partial\phi_i}{\partial y}\right\rangle_\Omega$$

$$-\int_{\Gamma_Q}\left(\frac{Q_{n^*}^{k+1}-Q_{n^*}^{k-1}}{2\Delta t}+\tau_o\alpha_1 Q_{n^*}^{k+1}+\tau_o\alpha_2 Q_{n^*}^{k}+\tau_o\alpha_3 Q_{n^*}^{k-1}\right)\phi_i d\Gamma \qquad i=1,\ldots\ldots N$$

for the lumped formulation.

Third, ADCIRC was modified to include a simple solver for the GWCE for the case of a diagonal system matrix. This occurs if the code is set up to be fully explicit ($\alpha_1=\alpha_3=0$ and $\alpha_2=1$) and have a lumped formulation. Due to the diagonal GWCE matrix, ADCIRC runs faster and requires less memory in this explicit, lumped mode than in the consistent and/or implicit modes. Results from Test Case 1 reported below indicate that the maximum stable time step using the explicit, lumped mode is only about 60 per cent of the allowable time step in the implicit, consistent mode and 40 per cent of the allowable time step in the implicit, lumped mode.

Forth, ADCIRC was modified to include the option of using a depth dependent drag coefficient:

$$C_f = C_{f\min}\left[1+\left(\frac{H_o}{H}\right)^{\theta}\right]^{\gamma/\theta} \quad (8)$$

where C_f is the standard 2D drag coefficient used in ADCIRC (applied using either a linear or quadratic friction relationship) and H is the total water depth. This relation has the behavior that C_f approaches $C_{f\min}$ in deep water , ($H > H_o$), and approaches $C_{f\min}(H_o/H)^{\gamma}$ in shallow water, ($H < H_o$), Figure 1. The exponent θ determines how rapidly C_f approaches each asymptotic limit and γ determines how rapidly the friction coefficient increases as the water depth decreases. If $C_{f\min} \equiv g n^2/H_o^{\gamma}$ and $\gamma = 1/3$, where g is the gravitational constant and n is

the Manning coefficient, Eq. (1) will provide a Manning equation frictional behavior for $H < H_o$, Figure 1. Examples of the relationship between $C_{f\,\min}$ and n for $\gamma = 1/3$ are given in Table 1.

Table 1. Comparison between $C_{f\,\min}$ and n if $C_{f\,\min} = g n^2 / H_o^{1/3}$

$C_{f\,\min}$	n	n	n	n
	H_o=5m	H_o=10m	H_o=20m	H_o=40m
0.0015	0.016	0.018	0.020	0.023
0.0020	0.019	0.021	0.024	0.026
0.0025	0.021	0.023	0.026	0.030
0.0030	0.023	0.025	0.029	0.032
0.0040	0.026	0.030	0.033	0.037
0.0050	0.030	0.033	0.037	0.042
0.0100	0.042	0.047	0.053	0.059

SUMMARY OF ELEMENT BASED FLOODING AND DRYING IMPLEMENTED IN ADCIRC

The element based approach assumes that flooding and drying can be represented by turning areas of the grid on and off element by element. This approach is similar to most of the fixed grid flooding and drying schemes that have been implemented in finite difference codes. Conceptually, our algorithm assumes the existence of removable barriers along the sides of all elements in the grid and the existence of three different types of nodes, "dry" nodes, "interface" nodes and "wet" nodes. All elements connected to a dry node are assumed to have their barriers in place, thereby preventing any flow through these elements. The water level is maintained at a constant value at these nodes and velocity is set to zero. Interface nodes are connected to both wet elements and dry elements. These are treated as standard land boundary nodes at which the water level rises and falls against the element barriers. Either a no normal flux or a no slip condition can be imposed at the interface nodes, however, the use of a no slip condition considerably simplifies the implementation of the element based approach and cuts the associated CPU time. Since water depths are expected to be relatively shallow at these nodes, the resulting volumetric transport due to tangential slip would be quite small and should not significantly effect the solution. Therefore we have chosen to implement a no slip condition in ADCIRC at all interface nodes. Finally, wet nodes are connected only to wet elements and are handled as in previous versions of ADCIRC.

Nodes can dry under two conditions. First, when receding water levels cause the depth at any node in the grid to fall below a minimum depth, $H_{\min}$, the node is considered to have "dried". $H_{\min}$ is specified in the unit 15 input file. The only exception to this rule occurs immediately after a node "wets" since local water level oscillations can occur when a node changes state. Therefore, after a node wets, the value of $H_{\min}$ is ramped up from zero to the value specified in the input file over a specified number of time steps (typically on the order of 10 to 20). This

permits the node to dry immediately following wetting if the conditions are sufficiently severe (and therefore keeps the solution from blowing up), however, it also allows bottom friction time to damp out small oscillations without reinforcement from additional spurious wetting and drying. A second condition was added to dry "landlocked" interface nodes. Occasionally, it is possible for all elements surrounding an interface node to be turned off without the water level at that node falling below H_{min}. If this happens the interface node is dried.

The condition for a node to wet is more subtle than the condition to dry. Ideally, a node should wet if the water level will rise at that node during subsequent time steps. The only certain way to assess if this will happen is to wet the node, compute the solution for some number of time steps and then examine the water level behavior. If the water level rose at the node, the decision was correct. However, if the water level fell at the node, the node should not have wetted and the model time steps should be repeated without wetting the node. Unfortunately, this approach is computationally impractical, particularly since multiple nodes may be wetting at the same time. Thus a criteria must be used to predict ahead of time if a node should wet.

After trying a variety of alternatives, the following wetting procedure was adopted. An interface node is assumed to change to a fully wet node if (i) the water level gradient and (ii) the vector sum of the water level gradient and the wind stress both favor water motion toward all dry nodes that are connected to the interface node. If this condition is met, the interface node becomes a wet node and the neighboring dry nodes become interface nodes. For the case of tidal forcing only, (i) and (ii) collapse to the commonly used wetting condition of a favorable water level gradient. For the case of wind driven forcing, the use of a water level gradient condition alone proved unsatisfactory since this gradient could be adverse to the wind stress and insufficient to cause flooding. In this case, the force balance in (ii) should be appropriate to determine if flooding will occur. However, in practice (ii) coupled with the numerical dispersion inherent in the finite element method using linear basis functions causes wetting to occur much too quickly for an on shore directed wind stress. Therefore, in addition to the favorable force balance, we somewhat arbitrarily require that enough water accumulates in the wet elements along the flood/dry interface that a favorable water level gradient also exists before flooding can occur. As noted in the results from Test Case 3, this criteria probably still allows flooding to occur too rapidly for an on shore wind.

The only exception to this wetting criteria occurs immediately after a node dries. As discussed above, a change in nodal state can cause local oscillations in the numerical solution which might lead to wetting favorable conditions shortly after a node dries. To minimize this possibility, nodes are not allowed to wet for a specified number of time steps (typically 10 - 20) after they have dried.

Because flow is not permitted across element barriers, this scheme should be nearly mass conserving. Some mass error can be expected because the water level may not be exactly the same when a node dries and when it wets. However, provided element sizes are not excessively large, the resulting error should be small.

Implementation of the flooding and drying scheme in ADCIRC occurs as follows. From a cold start, ADCIRC begins by defining the water surface elevation, ζ, as zero for all "wet" nodes and as $|h| + H_{min}$ for all "dry" nodes, where h is the bathymetric depth. (From a hot start water surface elevations are all read in from the hot start file.) At subsequent time steps, the computation of the water level change (using the GWCE) proceeds as it is presently implemented in ADCIRC for all nodes, except that the contribution of any element to the system matrix and to the forcing at each node is zeroed out if the element has its barriers in place. As a result, the system matrix is no longer stationary in time but rather it must be reconstructed each time a node wets or dries. This is most time consuming when the direct banded matrix solver is used (since the matrix must be re-decomposed each time it changes), and least time consuming when the matrix is diagonal (i.e., using the lumped, explicit formulation). After the water level is computed, the depth at each node is checked to determine whether any flooding or drying has occurred. Velocity is computed from the momentum equations as it is presently implemented in ADCIRC for all nodes, except that the contribution of any element is zeroed out if that element has its barriers in place. No forcing occurs at dry nodes and there is no resulting flow there. At interface nodes the momentum equations can be rotated into a coordinate system that is locally normal and tangential to the interface and the desired velocity component(s) can then be zeroed out. As noted above we have implemented a no slip condition at interface nodes for the present time.

TEST PROBLEMS

The flooding and drying scheme outlined above was tested in four example problems. In all cases the model was run until a dynamic equilibrium was reached in which solutions were stable from one forcing cycle to the next. The Coriolis force and lateral viscous terms were not included in the governing equations, however, all other terms were maintained.

Test Case 1: Tidally Driven Flooding and Drying in a Channel with Uniformly Sloping Bathymetry

This problem is about the simplest possible test case for a flooding and drying routine. It consists of a simulated tidal flow in a straight channel with a linearly sloping bottom, Figure 2. The problem is identical to the Flooding and Drying of a Frictional Incline, Case #1 solved using the 1D ADCIRC analogue (Luettich and Westerink, 1995) except that a smaller minimum depth was used. The specific problem parameters are:

channel length, 24km
bathymetric depth at open end, 5m below still water level
bathymetric depth at closed end, 1m above still water level
linear sloping bathymetry between open and closed end
numerical grid spacing, $\Delta x = 250m$
open end forcing 0.25m amplitude, 6h period.
H_{min} = 0.1 cm

$C_{f\min} = 0.0025, H_o = 1m, \theta = 10, \gamma = 1/3$

maximum time steps:

lumped implicit GWCE, $\Delta t = 60s$, $\left(\Delta t\sqrt{gh}/\Delta x\right)_{\max} = 1.7$

consistent implicit GWCE, $\Delta t = 40s$, $\left(\Delta t\sqrt{gh}/\Delta x\right)_{\max} = 1.1$

lumped explicit GWCE, $\Delta t = 24s$, $\left(\Delta t\sqrt{gh}/\Delta x\right)_{\max} = 0.68$

Water levels and depth-averaged velocities every tenth of a tidal cycle along a transect down the center of the downstream half of the domain are presented in Figures 3a-j. All times are referenced to high tide at the open end of the channel. Results were virtually identical across the channel and for each of the three GWCE formulations (provided the different stability constraints were obeyed). Therefore, only one transect line and one GWCE formulation (lumped implicit) is presented. The wet/dry interface migrates over a lateral distance of approximately 2 km (8 elements) throughout the tidal cycle and at all times the solutions are quite smooth with no signs of significant spatial oscillations. The ADCIRC solution compares closely with the 1D elemental solution in Luettich and Westerink (1995) with slight differences due to the different values of $H_{\min}$ and the different methods used to control noise generated during wetting. (The 1D model used a simple waiting period after both wetting and drying before a node could change state again.)

Time series of water surface elevation and depth-averaged velocity are shown at every time step for four distances along the channel centerline in Figures 4a-d. Well outside of the flood/dry zone the model results are smooth in time and show a small amplification of the input tidal forcing modified by nonlinear effects (primarily finite amplitude) in the channel, Figure 4a. A short distance downstream of the flood/dry zone the model response is strongly influenced by the finite amplitude nonlinearity as evidenced by the shortened flood and prolonged ebb phases of the tide, Figure 4b. A slight oscillation is visible in the elevation and velocity fields during the early part of the flood tide. Inside the flood/dry zone the model results remain reasonably smooth, Figures 4c,d. Elevation shows a slight ripple when the nodal velocity turns on and off (i.e., when the barriers are removed and replaced on the element lying upstream of the node where results have been plotted). Velocity shows a more noticeable oscillation (amplitude of 1-2 cm/s) again primarily during the flood stage of the tide.

Test Case 2: Tidally Driven Flooding and Drying in a Channel with V-Shaped Bathymetry

As a more rigorous test of the flooding and drying algorithm in two dimensions, a second test case was run for the channel shown in Figure 5. The specific problem parameters are:

channel length, 12km
bathymetric depth at open end in channel center, 5m below still water level
bathymetric depth at open end along channel sides, 2 m below still water level
bathymetric depth at closed end in channel center, at still water level
bathymetric depth at closed end along channel sides, 2 m above still water level
linear bathymetric slope in the along channel direction
numerical grid spacing, $\Delta x = 250m$

open end forcing 0.5m amplitude, 6h period.
$H_{\min}$ = 0.1 cm
$C_{f\min} = 0.0025, H_o = 1m, \theta = 10, \gamma = 1/3$
time step, (lumped implicit GWCE), $\Delta t = 30s$, $\left(\Delta t\sqrt{gh}/\Delta x\right)_{\max} = 0.86$

Results are initially presented as contour plots of surface elevation and vector diagrams of depth averaged velocity every 30 minutes (12 intervals) throughout the tidal cycle, Figures 6a-l. All times are referenced to high tide at the open end of the channel. The along channel movement of the wet/dry interface is constrained by the end wall during the flood stage but retreats 2 km along the center axis of the channel during the ebb stage. The lateral range of the wet/dry interface is approximately 1 km on either side of the channel center line. The shape of the interface is rather irregular due to the fact that no attempt was made to place nodes along bathymetric contours, as would typically be done in a field application. The basic model behavior seems realistic as the velocity is closely aligned with the channel axis over most of the channel and turns toward shore near the wet/dry interface. There is a slight indication of noise in the near shore velocity vectors during the onset of the flood stage (e.g., Figure 6h), although this does not appear to propagate to other parts of the domain.

Time series of water surface elevation and depth-averaged velocity are shown at every time step for six locations in the channel in Figures 7a-f. (Channel locations are shown in Figure 8.) The first two locations are on the channel center line and remain wet throughout the tidal cycle, although nodes some distance on either side dry near low tide. The solutions are smooth with the exception of slight ripples in the velocity during flood tide, Figures 7a,b. The third location is also on the channel center line but closer to the closed end. This node dries for a small part of the ebb stage, Figure 7c. Oscillations in the elevation solution are small but visible and are quite evident in the velocity solution (up to approximately 2 cm/s amplitude). Again these are strongest during flooding, although they also appear as adjacent elements dry during ebb tide. The remaining three locations are at the same position along the channel axis as the previous one but are displaced increasing distances away from the channel center line. Consequently they are dry for successively longer portions of the tidal cycle, Figures 7d-f. In each case the elevation shows only slight ripples while the velocities show oscillations of 2 cm/s amplitude or less, primarily during flooding.

Test Case 3: Wind Driven Flooding and Drying in a Channel with Uniformly Sloping Bathymetry

This test uses the same channel as Test Case 1, (Figure 2). Flooding and drying occurs due to the presence of a uniform in space but sinusoidally varying in time wind stress aligned with the axis of the channel. The maximum wind stress corresponds to the open water stress generated by approximately a 50 mile per hour wind. The water level at the open end of the channel is held constant at the still water level. The specific problem parameters are:

channel length, 24km
bathymetric depth at open end, 5m below still water level
bathymetric depth at closed end, 1m above still water level
linear sloping bathymetry between open and closed end

numerical grid spacing, $\Delta x = 250m$
wind stress forcing amplitude = 0.001452 $(m/s)^2$, period = 6 hrs.
$H_{\min} = 0.1$ cm
$C_{f\min} = 0.0025, H_o = 1m, \theta = 10, \gamma = 1/3$
time step, (lumped implicit GWCE), $\Delta t = 30s$, $\left(\Delta t\sqrt{gh}/\Delta x\right)_{\max} = 0.86$

Water levels and depth-averaged velocities every tenth of a tidal cycle on a transect along the center of the downstream half of the channel are presented in Figures 9a-j. Times are referenced to the time of strongest wind directed toward the closed end of the channel. The maximum extent of inundation is limited by the closed end of the channel (Figure 9b) and recedes more than 6 km following the wind reversal (Figures 9g,h). The drying process appears to behave reasonably (Figures 9b-g). However, the flooding process has a somewhat anomalous behavior since a thin (approximately 10 cm) layer of water driven by the wind stress propagates ahead of the main flood wave which is driven by gravity and wind stress (Figures 9i,j,a).

Time series of water surface elevation and depth-averaged velocity are shown at every time step for four distances along the channel centerline in Figures 10a-d. The solutions are generally smooth and comparable to those of the tidal test case.

Test Case 4: Wind Driven Flooding and Drying in a Channel with V-Shaped Bathymetry

As a more rigorous test of the flooding and drying algorithm in two dimensions, a second wind driven test case was run for the same channel used in Test Case 2, (Figure 5). Flooding and drying occurs due to the presence of a uniform in space but sinusoidally varying in time wind stress aligned with the axis of the channel. The maximum wind stress corresponds to the open water stress generated by approximately a 50 mile per hour wind. The water level at the open end of the channel is held constant at the still water level. The specific problem parameters are:

channel length, 12km
bathymetric depth at open end in channel center, 5m below still water level
bathymetric depth at open end along channel sides, 2 m below still water level
bathymetric depth at closed end in channel center, at still water level
bathymetric depth at closed end along channel sides, 2 m above still water level
linear bathymetric slope in the along channel direction
numerical grid spacing, $\Delta x = 250m$
wind stress forcing amplitude = 0.001452 $(m/s)^2$, period = 6 hrs.
$H_{\min} = 0.1$ cm
$C_{f\min} = 0.0025, H_o = 1m, \theta = 10, \gamma = 1/3$
time step, (lumped implicit GWCE), $\Delta t = 30s$, $\left(\Delta t\sqrt{gh}/\Delta x\right)_{\max} = 0.86$

Results are initially presented as contour plots of surface elevation and vector diagrams of depth averaged velocity every 30 minutes (12 intervals) throughout the wind cycle, Figures 11a-l. Times are referenced to the time of strongest wind directed toward the closed end of the channel. The along channel movement of the wet/dry interface is constrained by the end wall during the

flood stage but retreats approximately 3 km along the center axis of the channel during the ebb stage. The lateral range of the wet/dry interface is approximately 1 km on either side of the channel center line. The shape of the interface is rather irregular due to the fact that no attempt was made to place nodes along bathymetric contours, as would typically be done in a field application. The basic model behavior seems quite realistic as the velocity is generally unidirectional and aligned with the water level gradient during periods of weak wind stress (Figures 11 d,e,j,k). During periods of stronger wind stress, velocity is aligned with the wind in shallow water but is in the opposite direction in deep water due to the water level gradient (Figures 11 a,b,c,f,g,h,i).

Time series of water surface elevation and depth-averaged velocity are shown at every time step for six locations in the channel in Figures 12a-f. (Channel locations are shown in Figure 8.) The first two locations are on the channel center line and remain wet throughout the model run. The solutions are smooth except for approximately the first half of flood cycle (e.g., Fig 12b). The remaining locations dry for part of the cycle and exhibit varying amounts of noise upon flooding. These results are consistent with the general observation that elements tended to turn on and off repeatedly during approximately the first half of the flooding cycle in this test case. During this part of the flooding cycle the elevation gradient and the surface stress are opposing each other. In general when an element wets, water sloshes into the element and then back out causing a depression in the water level at the interface nodes. In the present test case, the adverse wind stress enhances the sloshing of water out of the element and therefore causes a further depression in the water level over what occurs in a tide only case.

SUMMARY AND CONCLUSIONS

Based on information available in the literature, we believe a fixed computational grid flooding and drying scheme would be most practical for short term implementation in the operational hydrodynamic model ADCIRC. Of the three fixed grid schemes tested in a 1D analogue of ADCIRC by Luettich and Westerink (1995), preliminary tests in 2D suggested that the element based approach could be implemented most satisfactorily in ADCIRC.

Our element based approach assumes the existence of removable barriers along the sides of all elements in the grid. When barriers are in place along each side of an element, it removes this element from the flow computation. When barriers are in place along only some of the sides of an element, the barriers act as traditional land boundaries, except that a no slip condition is enforced along these barriers.

To facilitate the implementation of the flooding and drying scheme, several changes were made to the basic ADCIRC formulation, (e.g., as described in Luettich et al., 1992, Westerink et al, 1994). Options were added to lump the time derivative terms in the GWCE, to solve the system as a diagonal matrix if the GWCE is lumped and explicit and to allow the drag coefficient to vary as a function of depth (e.g., similar to a Manning equation) in shallow water. In addition

the GWCE was reformed so that the dependent variable is the change in water level each time step rather than actual water level each time step.

Model tests in two tidal channels indicated that the flooding/drying algorithm was reasonably well behaved and gave realistic results. Oscillations, were generated when elements turned on (during flooding) and to a lesser extent when they turned off. However, these oscillations seemed to be effectively dissipated by bottom friction since they did not propagate far from their source, they did not cause elements to repeatedly switch on and off and they did not cause the code to become unstable. We note that initial runs using the flooding and drying scheme on a field problem with tidal forcing show occasional incidences of elements repeatedly turning on and off. However, this has not caused any wide spread corruption of the model run.

Model tests in two wind driven channels were also promising although slightly more problematic than the tidally driven tests. In the test of flooding on a plane sloping beach, a thin layer of water driven by the wind stress inundated the beach in advance of the main flood wave which was driven by gravity and wind stress. In the V-shaped bathymetry test, oscillations generated when elements wetted during the beginning of the flooding cycle were large enough to cause a few elements to repeatedly turn on and off. This only occurred when the water level gradient and the wind stress were opposing each other, in which case the wind stress acted to enhance the initial oscillation. The behavior ceased about mid way through the flood cycle as the wind stress decreased. Again bottom friction seemed to be fairly effective at dissipating these oscillations.

It is our opinion that the element based flood/drying scheme that has been described above brings ADCIRC up to the presently accepted state of the art in flooding and drying capabilities. Never the less, there appears to be a need for considerable additional research on this topic before a fully satisfactory solution is obtained.

REFERENCES

Akanbi A.A., and N.D. Katopodes, 1988, "Model for Flood Propagation on Initially Dry Land", Journal of Hydraulic Engineering, **114**(7): 689-706.

Austria P.M. and A.A. Aldama, 1990, "Adaptive Mesh Scheme for Free Surface Flows with Moving Boundaries", In: Computational Methods in Surface Hydrology, G. Gambolati, A. Rinaldo, C. A. Brebbia, W. G. Gray and G. F. Pinder, eds., Springer-Verlag, pp 456-460.

Cialone, J., 1991, "Coastal Modeling System (CMS) User's Manual", Instruction Report CERC-91-1, Coastal Engineering Research Center, U.S. Army Engineer Waterways Experiment Station, Vicksburg, MS.

Defina, A., L. D'Alpaos and B. Matticchio, 1994, "A New Set of Equations for Very Shallow Water and Partially Dry Areas Suitable to 2D Numerical Models", in Modelling of Flood Propagation Over Initially Dry Areas, P. Molinaro and L. Natale, [eds.], ASCE, New York, NY, pp 72-81.

Flather R.A. and N.S. Heaps, 1975, "Tidal Computations for Morecambe Bay", Geophysical Journal of Royal Astronomical Society, **42:**489-517.

Flather, R.A. and K.P. Hubbert, 1990, "Tide and Surge Models for Shallow Water - Morcambe Bay Revisited", In Modeling Marine Systems, A.M. Davies, [ed.], CRC Press, Inc., Boca Raton, Fl., pp 135-166.

Hervouet, J.-M., J.-M. Janin, 1994, "Finite Element Algorithms for Modelling Flood Propagation" in Modelling of Flood Propagation Over Initially Dry Areas, P. Molinaro and L. Natale, [eds.], ASCE, New York, NY, pp 102-113.

Jelesnianski C.P., J. Chen and W.A. Shaffer, 1992, "SLOSH: Sea, Lake, and Overland Surges from Hurricanes", NOAA Technical Report NWS 48, 71p.

Johns B., 1982, "Numerical Integration of the Shallow Water Equations over a Sloping Shelf", International Journal for Numerical Methods in Fluids, **2:**253-261.

Leendertse J.J., 1987, "Aspects of SIMSYS2D, A System for Two-Dimensional Flow Computation", Rand Corportation report R-3572-USGS, p.

Luettich, R.A., Jr., J.J. Westerink and N.W. Scheffner, 1992, "ADCIRC: An Advanced Three-Dimensional Circulation Model for Shelves, Coasts and Estuaries; Report 1: Theory and Methodology of ADCIRC-2DDI and ADCIRC-3DL", Technical Report DRP-92-6, Coastal Engineering Research Center, U.S. Army Engineer Waterways Experiment Station, Vicksburg, MS.

Luettich, R.A., Jr., and J.J. Westerink, 1995, "An Assessment of Flooding and Drying Techniques for Use in the ADCIRC Hydrodynamic Model", Contractors Report, Contract No. DACW39-94-M-5869, Coastal Engineering Research Center, U.S. Army Engineer Waterways Experiment Station, Vicksburg, MS, 53p.

Lynch D.R. and W.G. Gray, 1980, "Finite Element Simulation of Flow in Deforming Regions", Journal of Computational Physics, **36:**135-153.

Reid R.O. and B.R. Bodine, 1968, "Numerical Model for Storm Surges in Galveston Bay", Journal of the Waterways and Harbors Division, **94**(WW1):33-57.

Siden, G.L.D. and D.R. Lynch, 1988, "Wave Equation Hydrodynamics on Deforming Elements", International Journal for Numerical Methods in Fluids, **8:**1071-1093.

Sielecki A. and M.G. Wurtele, 1970, "The Numerical Integration of the Nonlinear Shallow-Water Equations with Sloping Boundaries", Journal of Computational Physics, **6:**219-236.

Thomas, W.A., W.H. McAnally, Jr., J.V. Letter, Jr., 1990, "Appendix F: User Instructions for RMA-2V, A Two-Dimensional Model for Free Surface Flows", Draft copy, 54 pp.

Westerink, J.J., Blain, C.A., R.A. Luettich, Jr., and N.W. Scheffner, 1994, "ADCIRC: An Advanced Three-Dimensional Circulation Model for Shelves, Coasts and Estuaries; Report 2: User's Manual for ADCIRC-2DDI", Technical Report DRP-92-6, Coastal Engineering Research Center, U.S. Army Engineer Waterways Experiment Station, Vicksburg, MS.

Yeh G. T. and F.K. Chou, 1979, "Moving Boundary Numerical Surge Model", Journal of the Waterway, Port, Coastal and Ocean Division, **105**(WW3):247-263.

Yu C.S., M. Fettweis, F. Rosswo and J. Berlamont, 1990, "A 2D Model with Changing Land-Water Boundaries", In: Computational Methods in Surface Hydrology, G. Gambolati, A. Rinaldo, C. A. Brebbia, W. G. Gray and G. F. Pinder, eds., Springer-Verlag, pp 101-106.

Figure 1. Depth Dependent Drag Coefficient

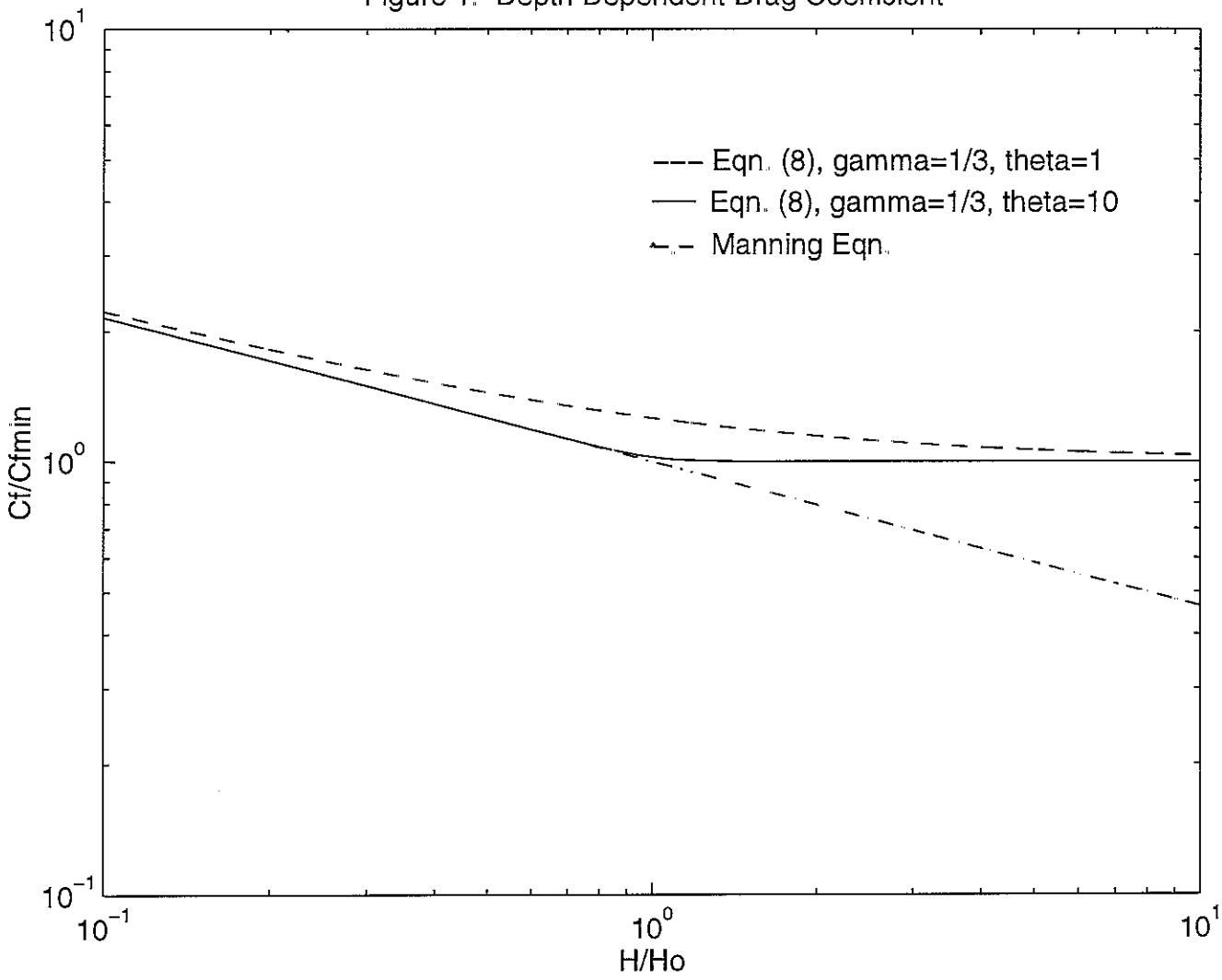

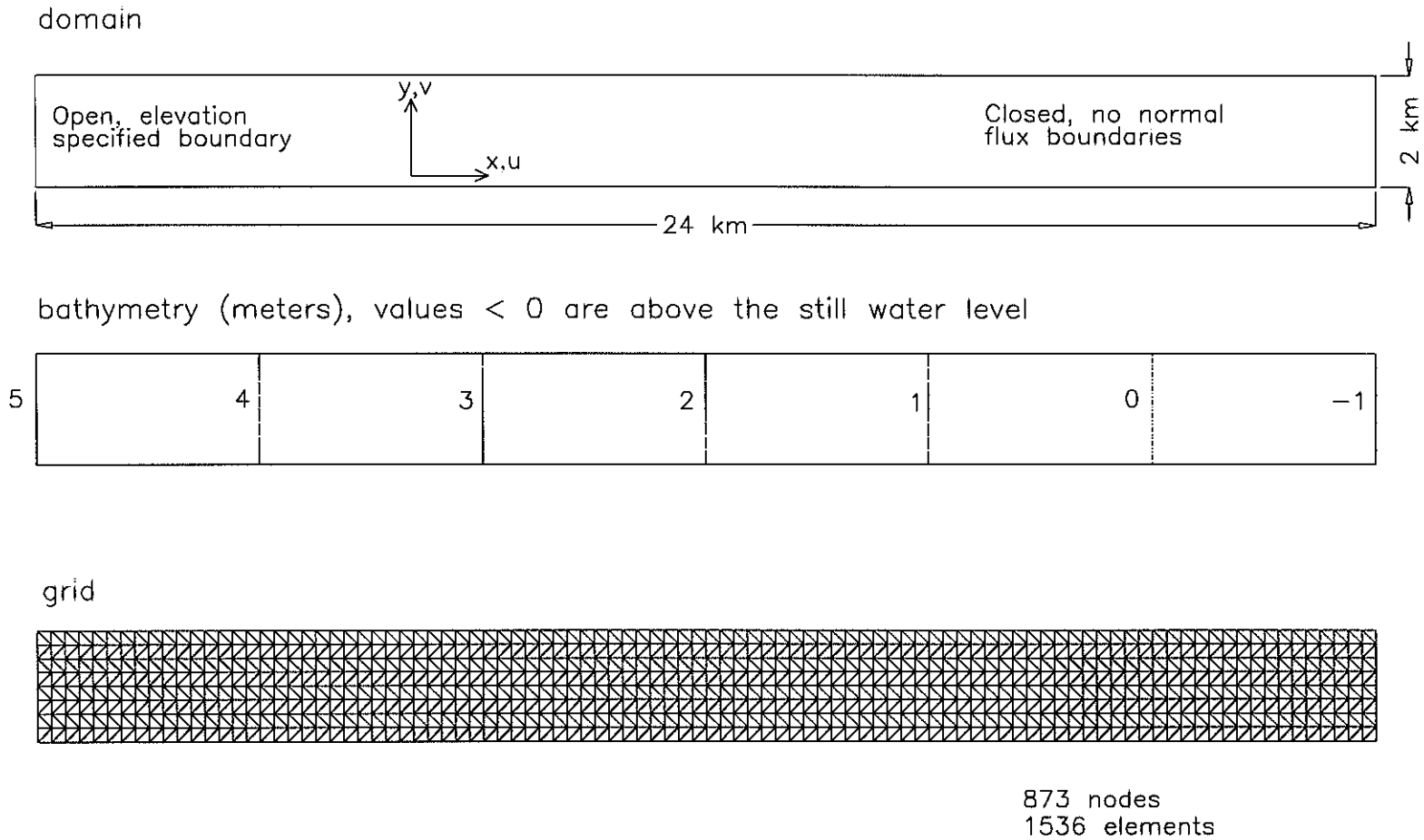

Figure 2. ADCIRC Flooding/Drying Test Cases #1 & #3

Figure 3a. Test Case #1, Time = 0*T/10

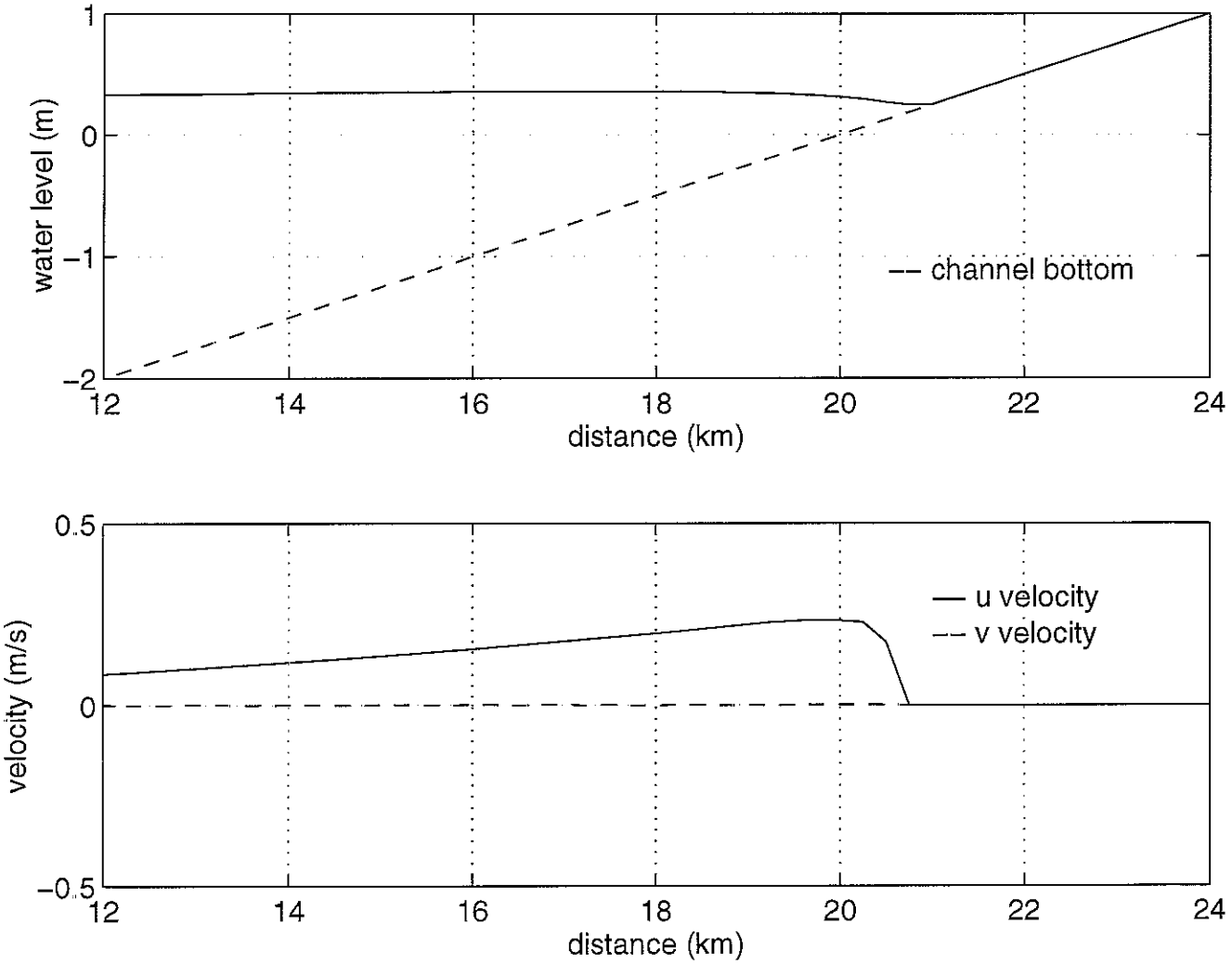

Figure 3b. Test Case #1, Time = 1*T/10

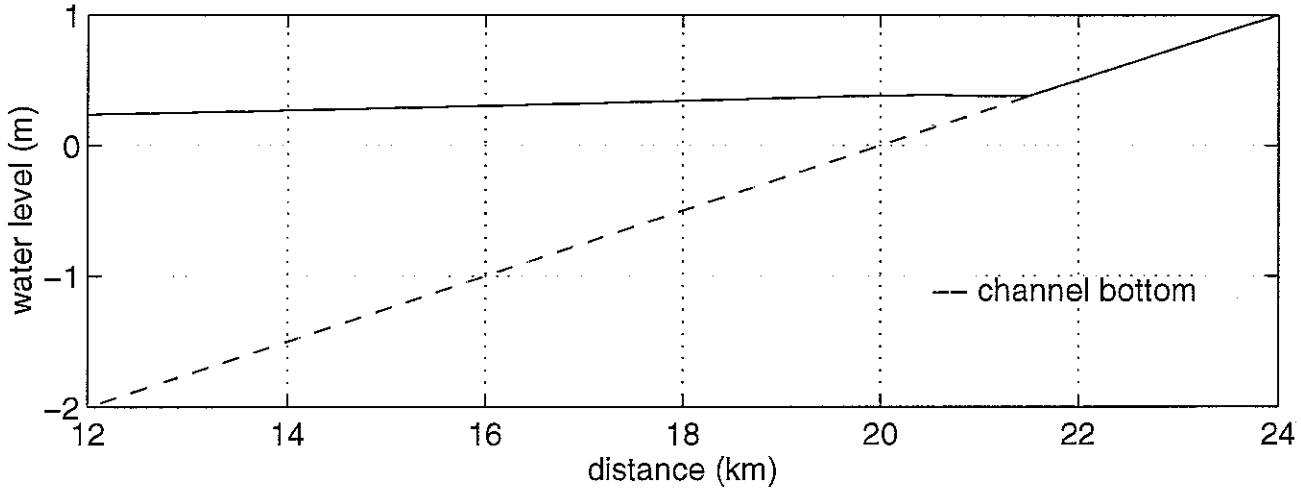

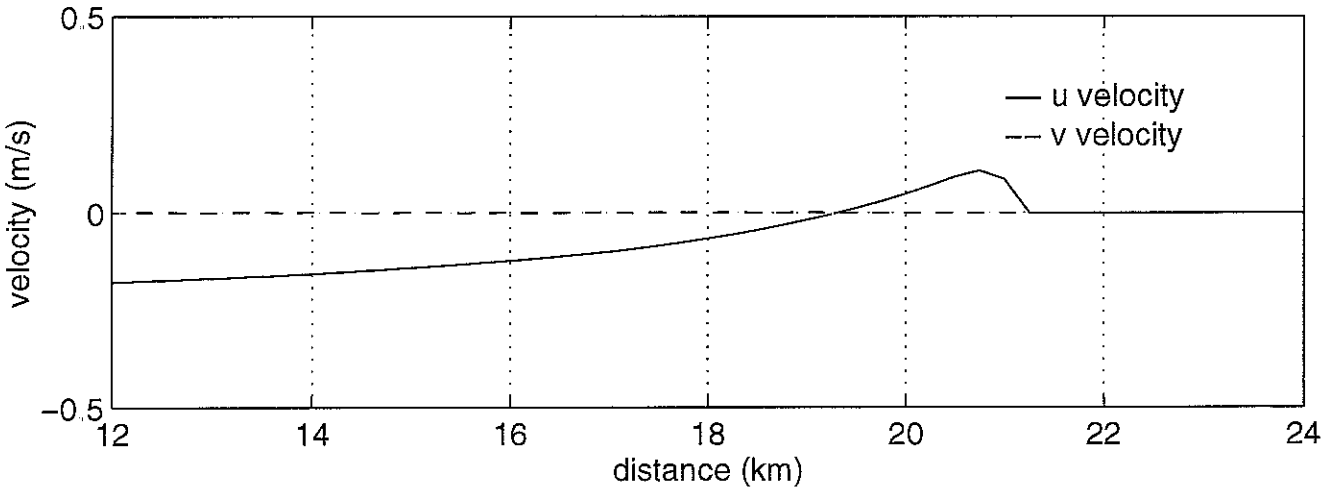

Figure 3c. Test Case #1, Time = 2*T/10

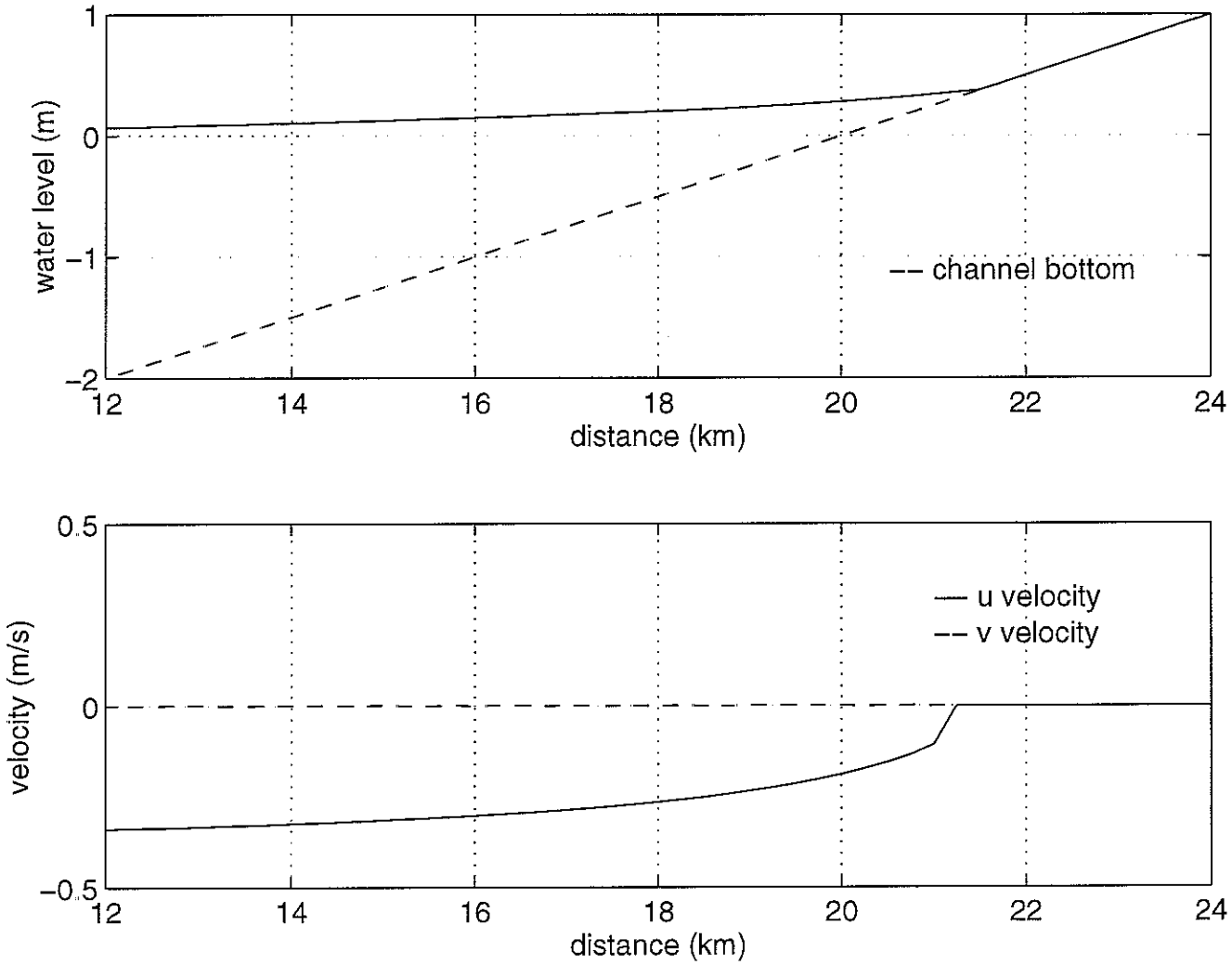

Figure 3d. Test Case #1, Time = 3*T/10

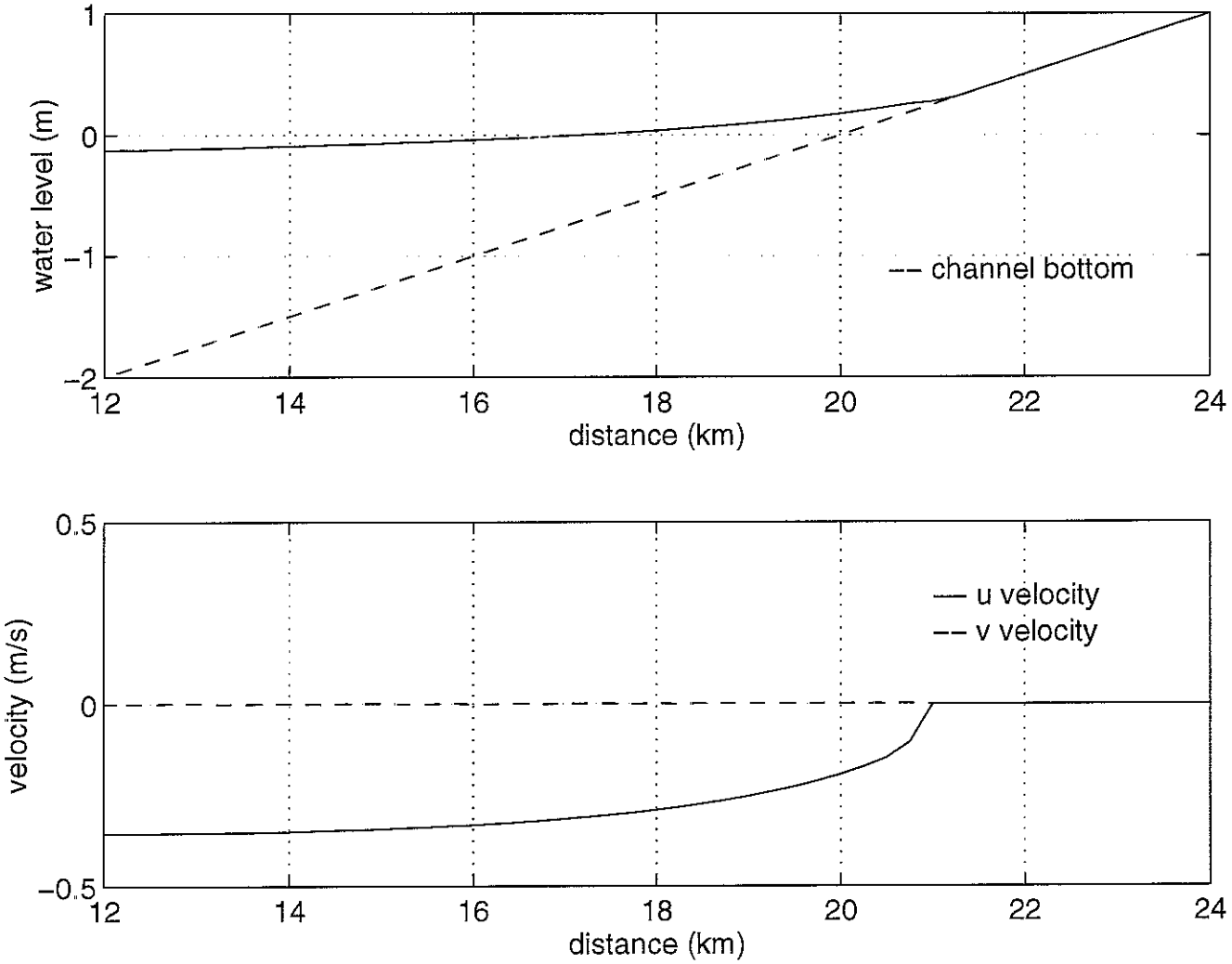

Figure 3e. Test Case #1, Time = 4*T/10

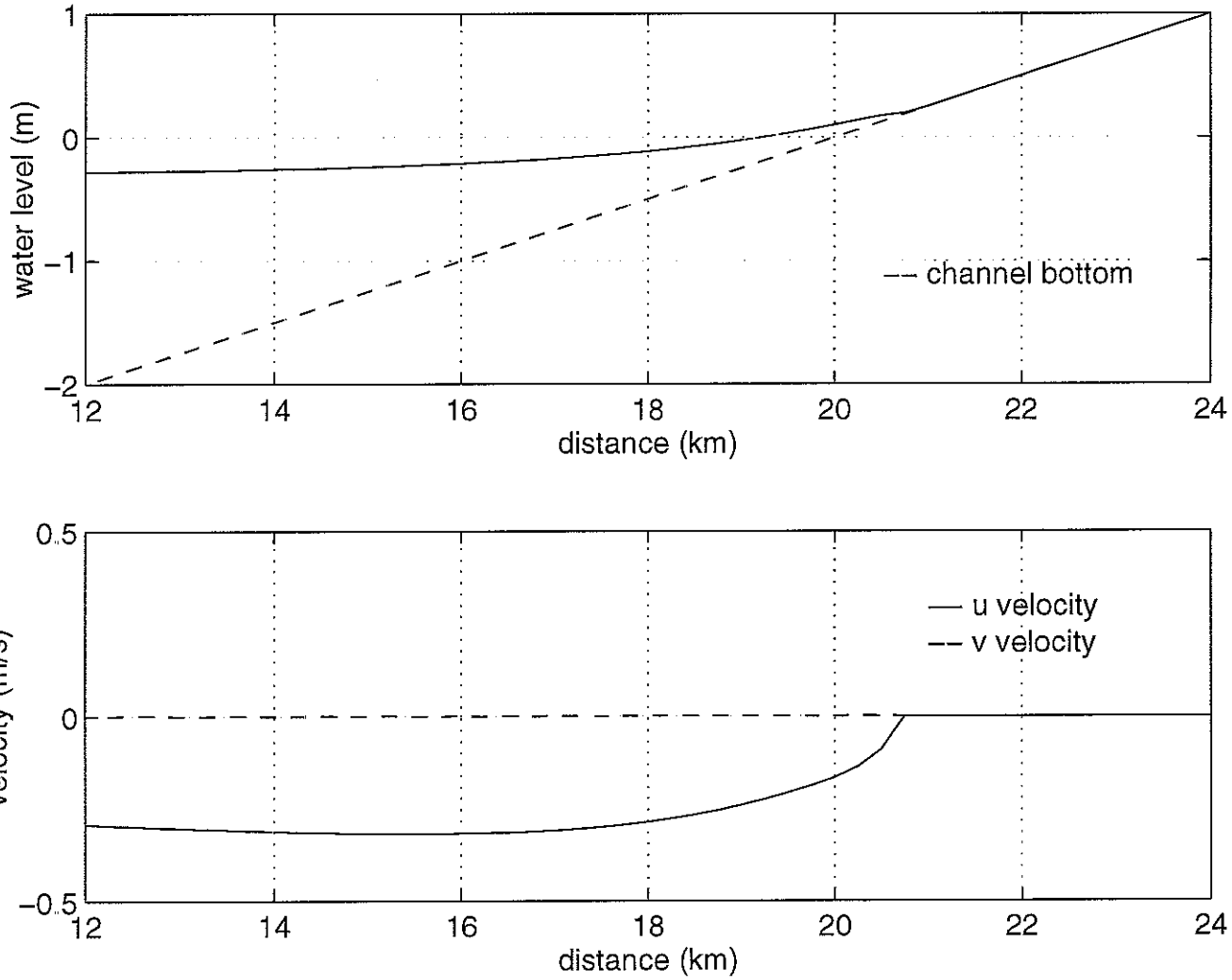

Figure 3f. Test Case #1, Time = 5*T/10

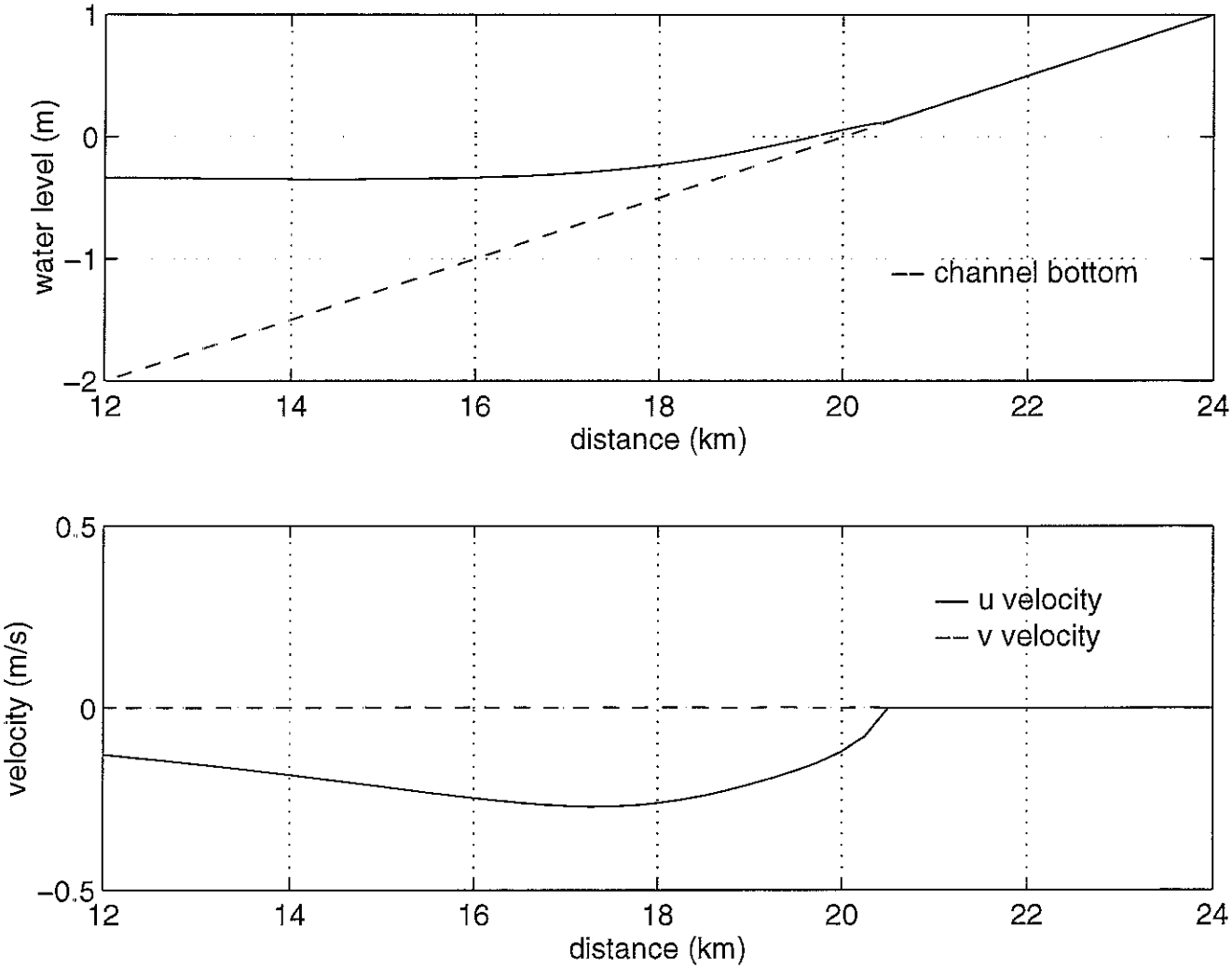

Figure 3g. Test Case #1, Time = 6*T/10

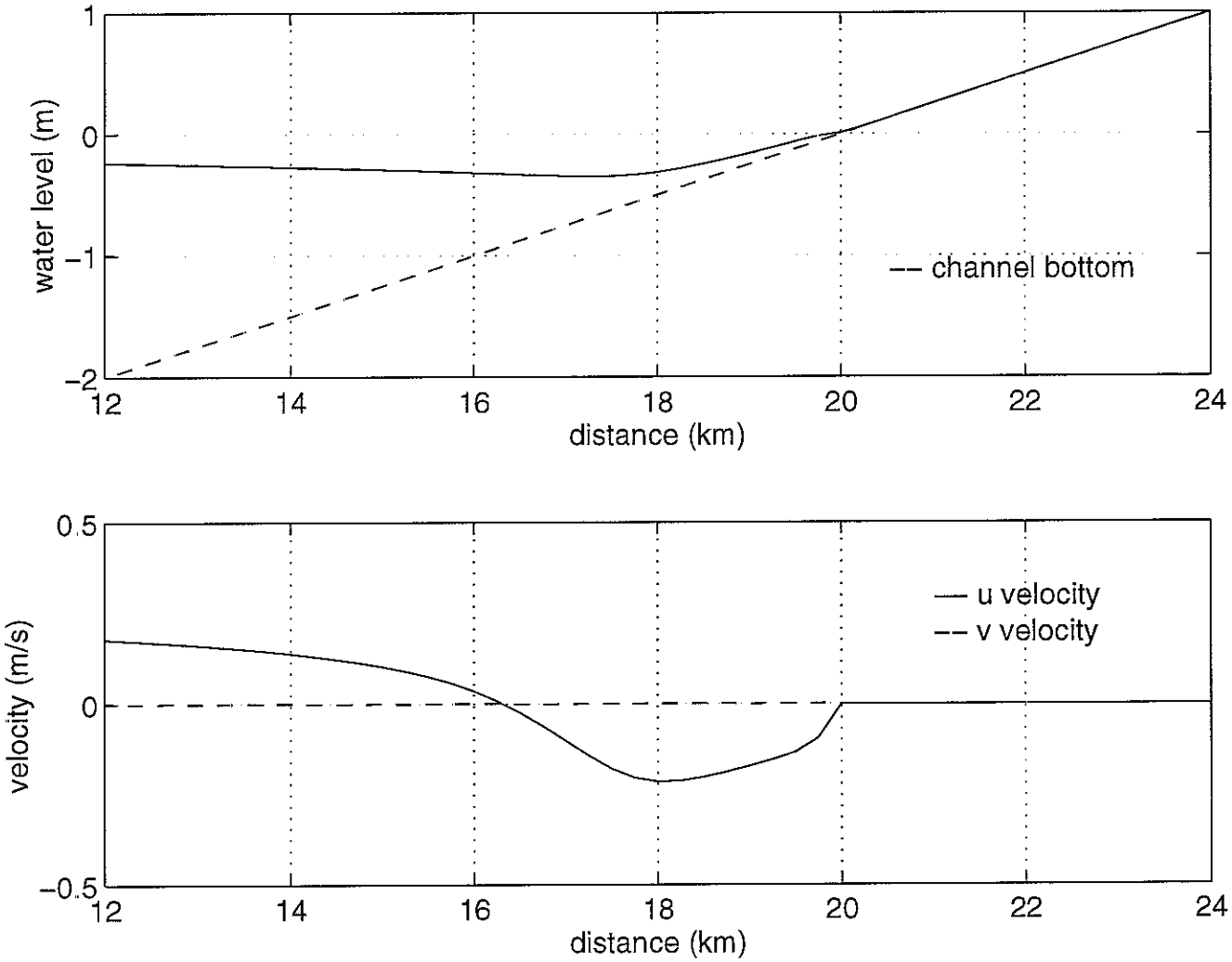

Figure 3h. Test Case #1, Time = 7*T/10

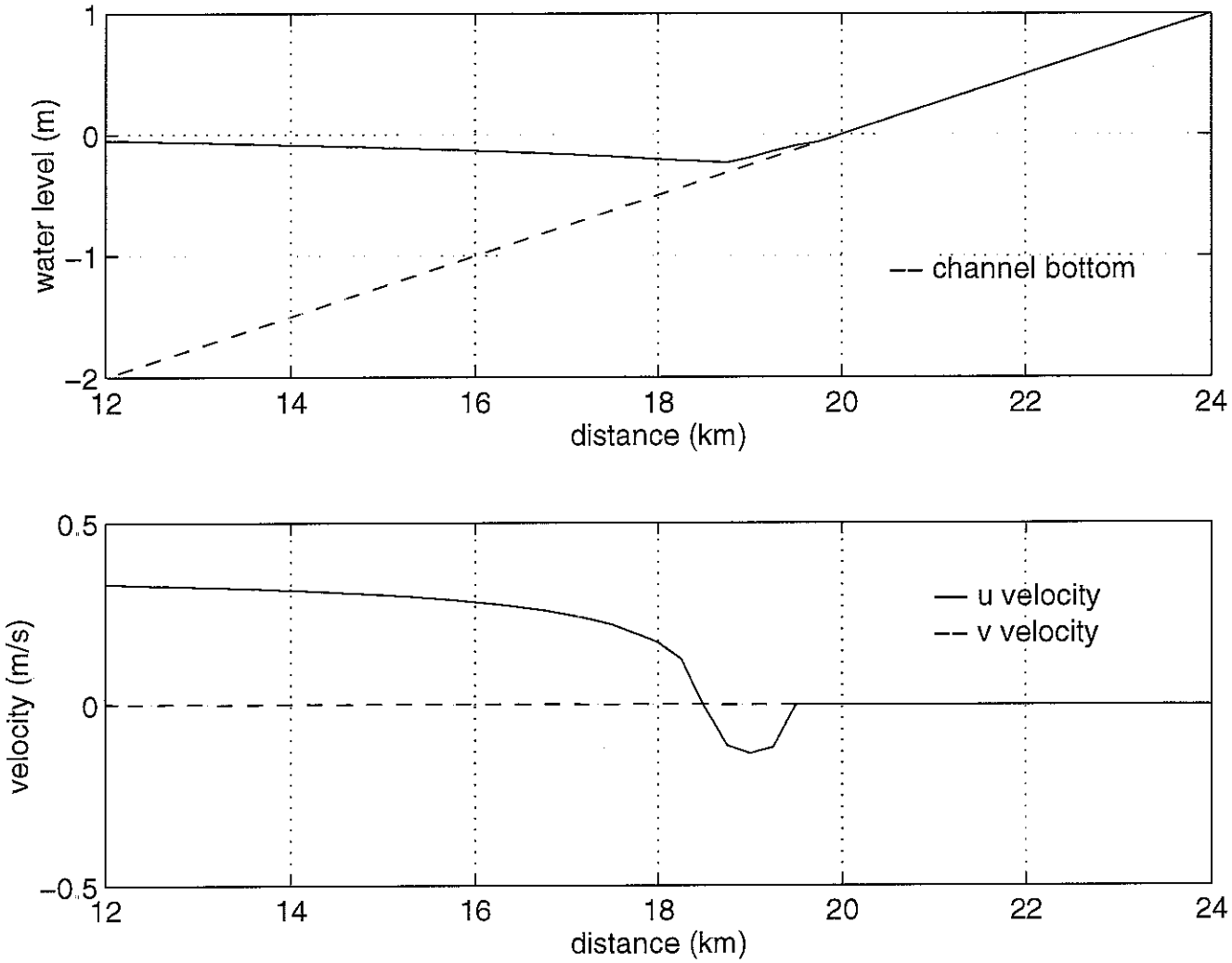

Figure 3i. Test Case #1, Time = 8*T/10

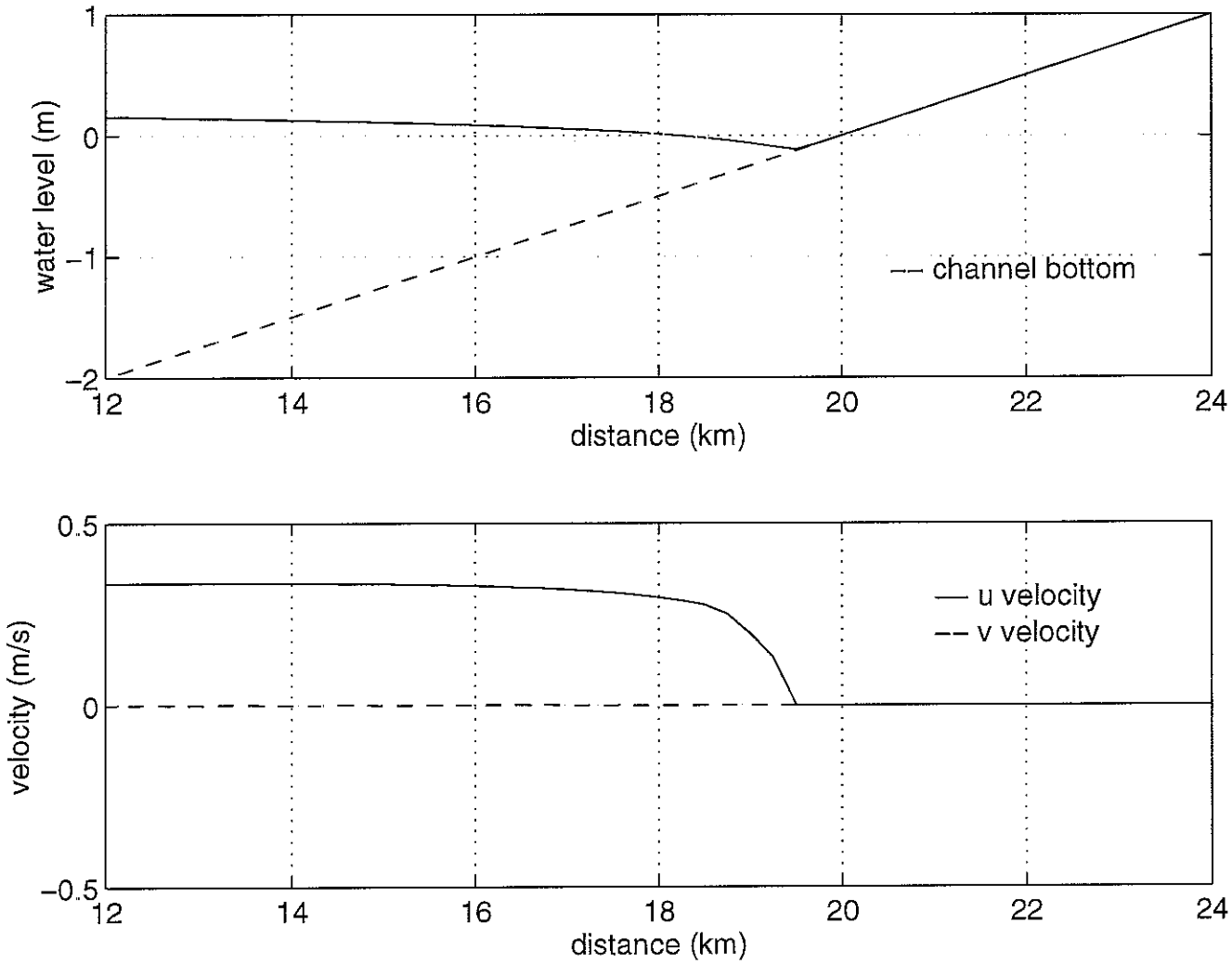

Figure 3j. Test Case #1, Time = 9*T/10

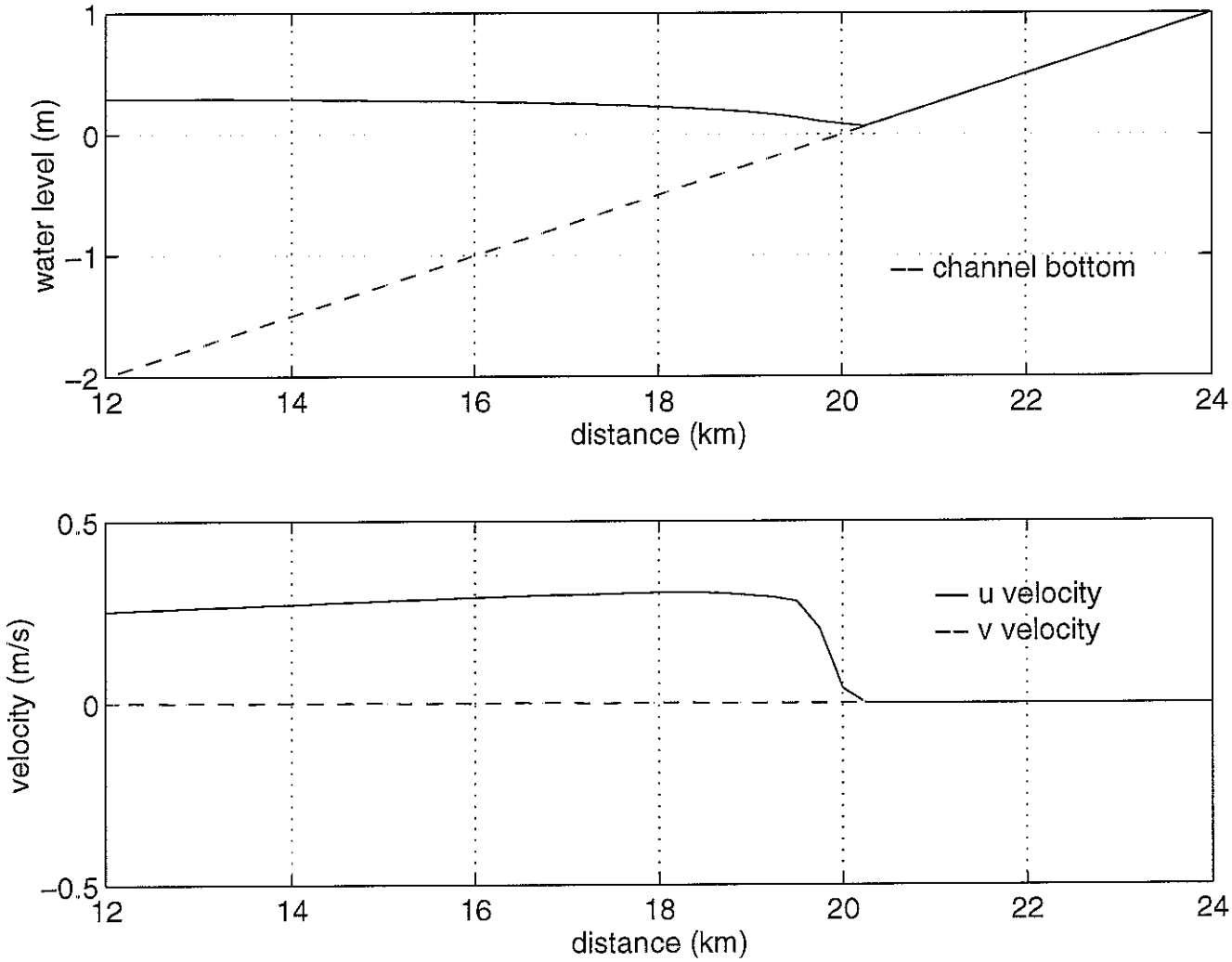

Figure 4a. Test Case #1, Distance = 12.75 km

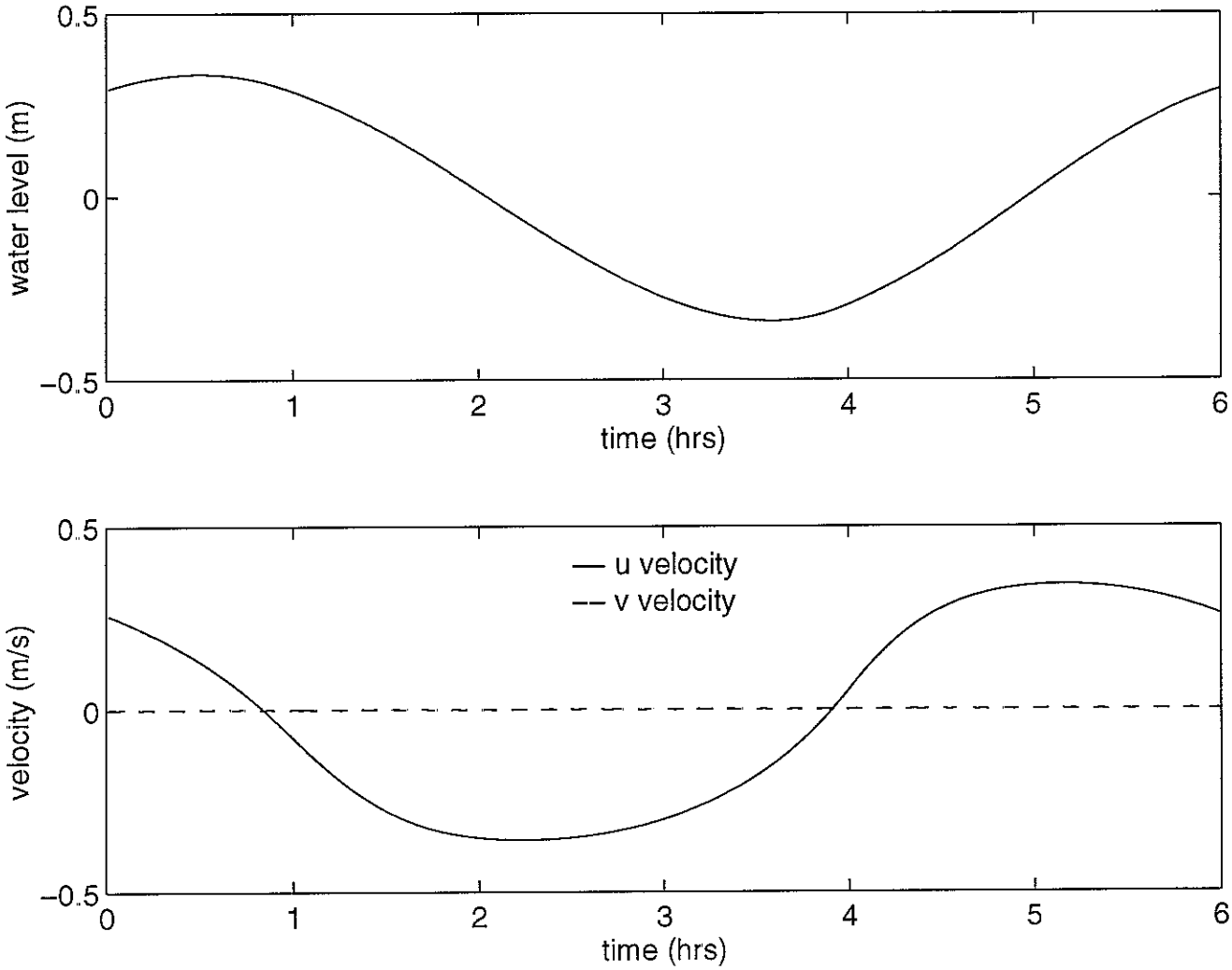

Figure 4b. Test Case #1, Distance = 18.25 km

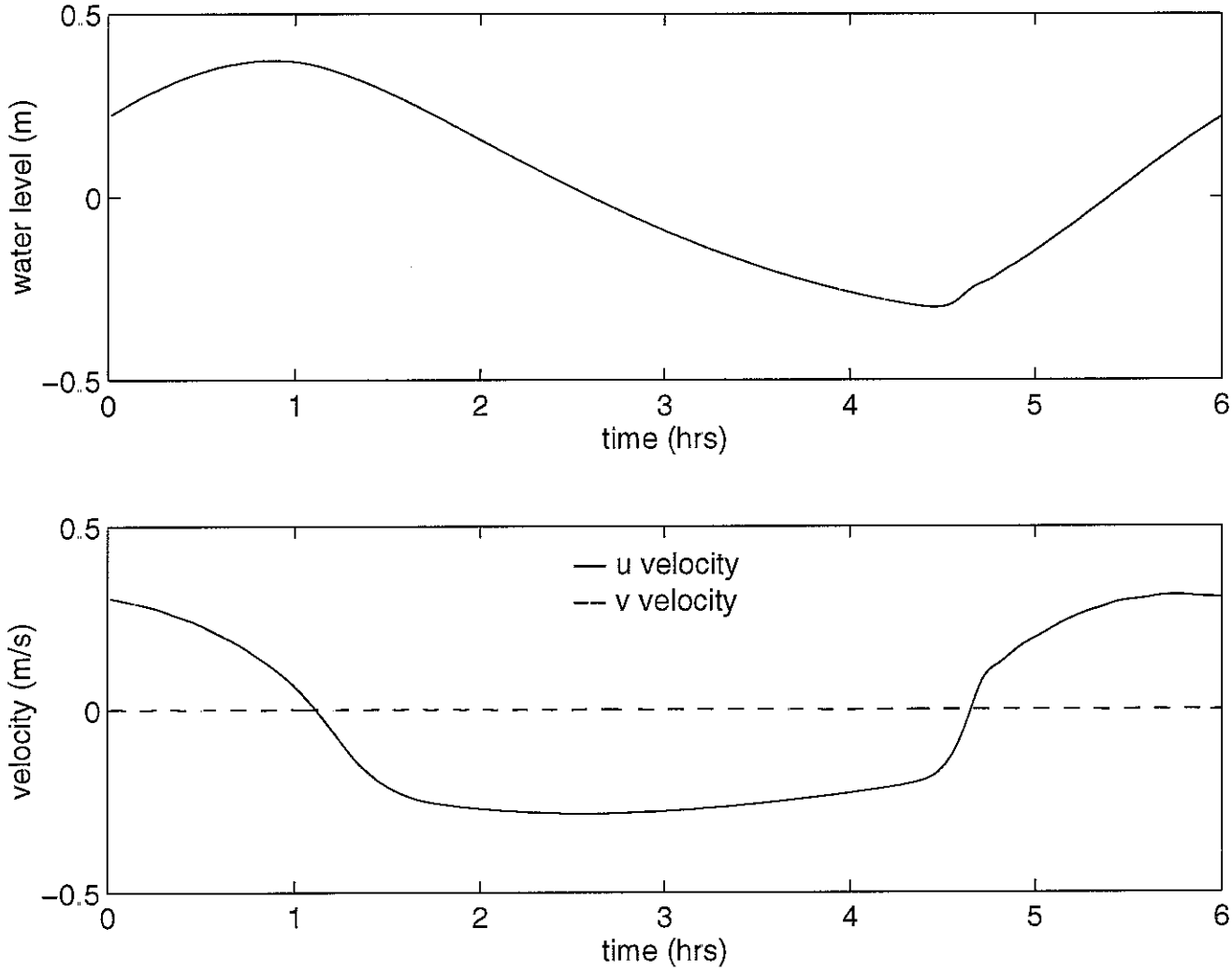

Figure 4c. Test Case #1, Distance = 19.75 km

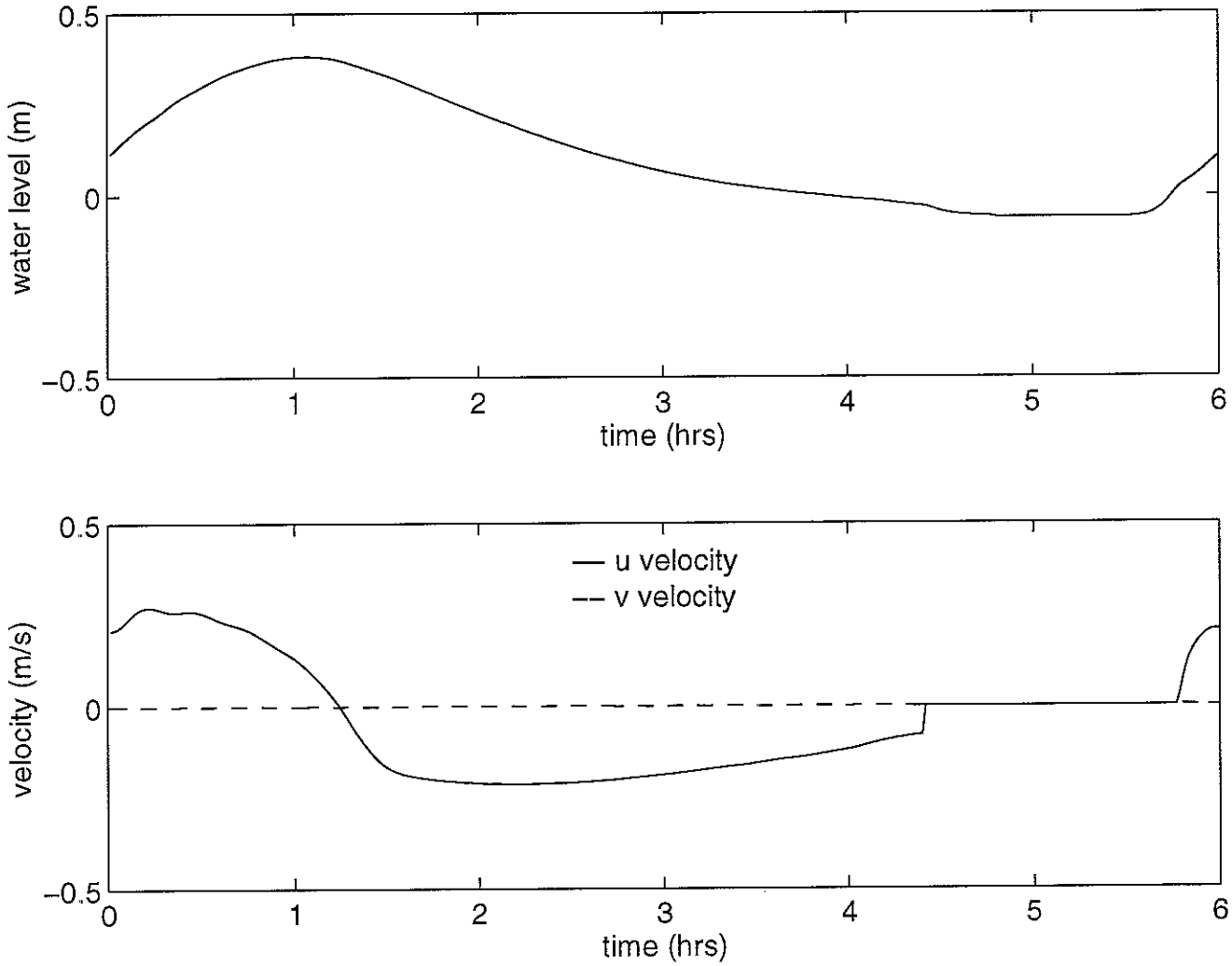

Figure 4d. Test Case #1, Distance = 20.5 km

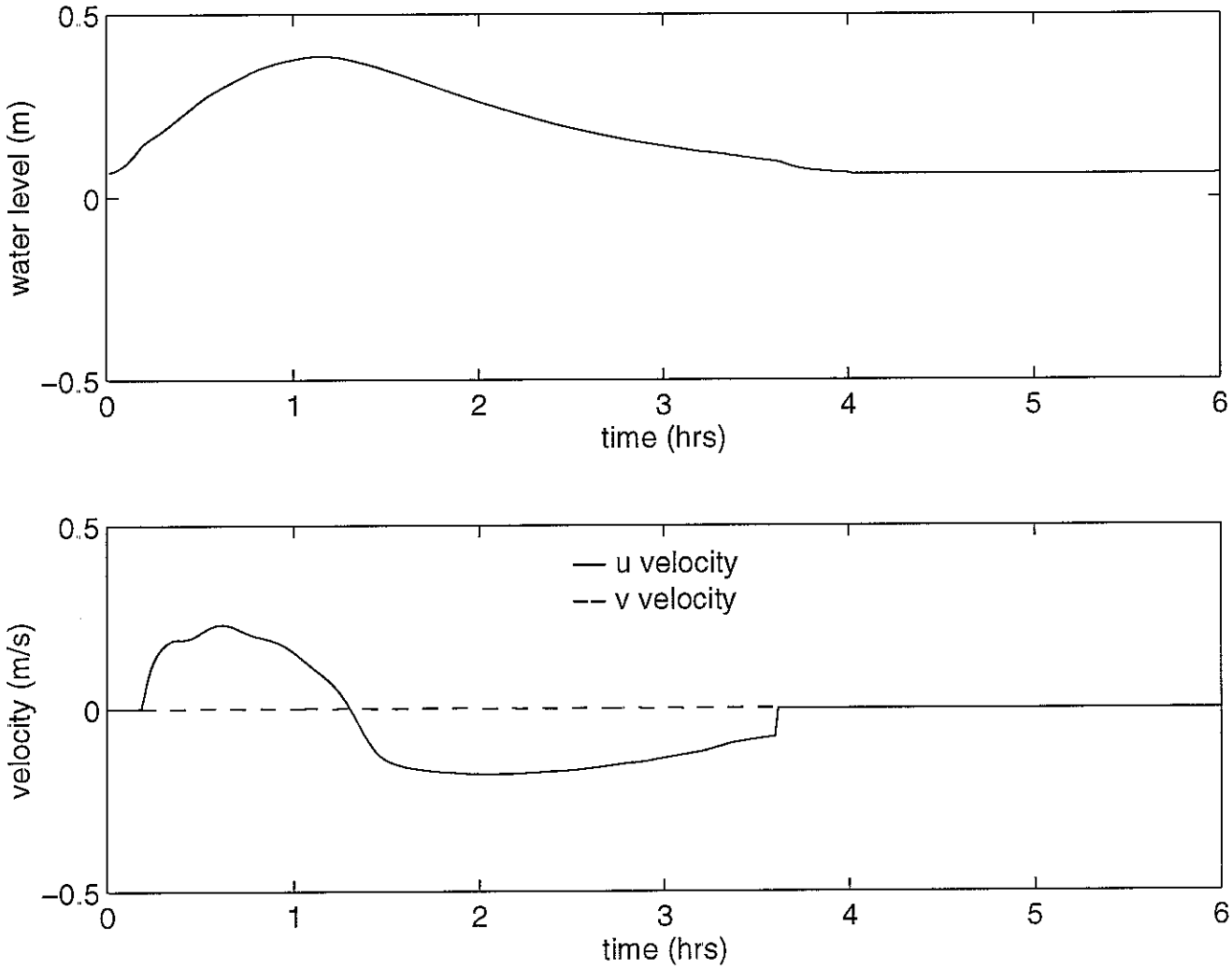

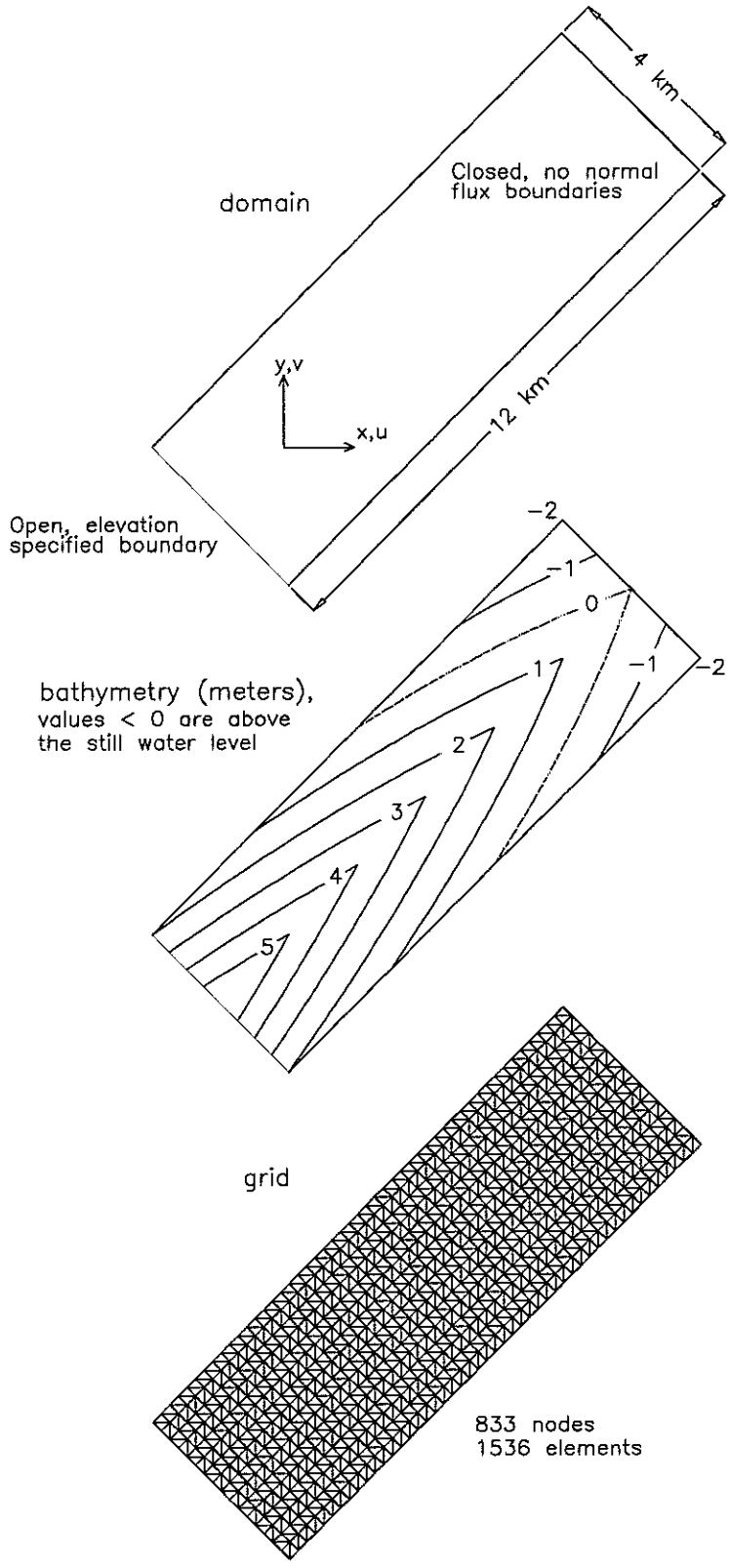

Figure 5. ADCIRC Flooding/Drying Test Cases #2 & #4

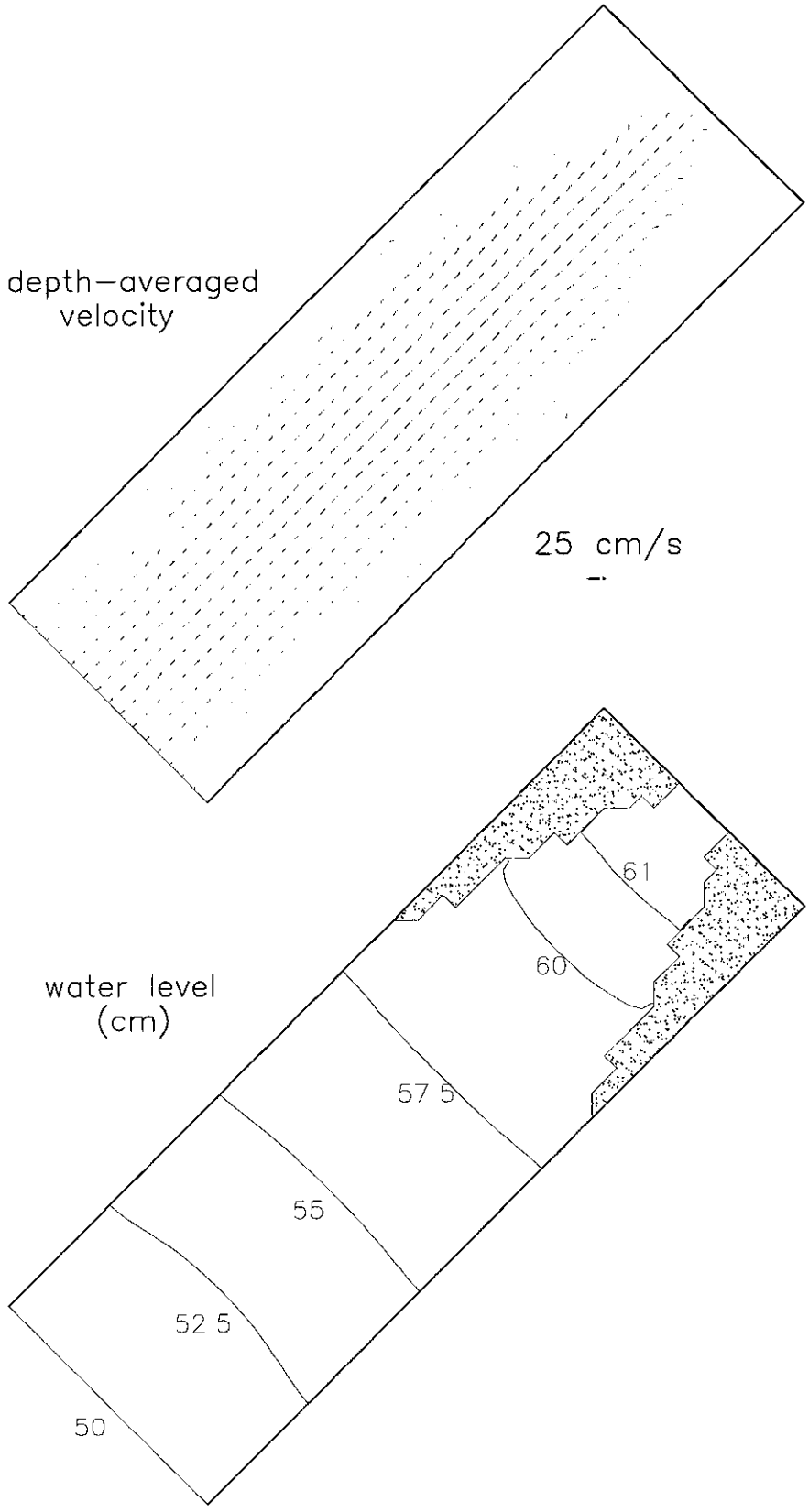

Figure 6a. Test Case #2, time=0.0 hrs

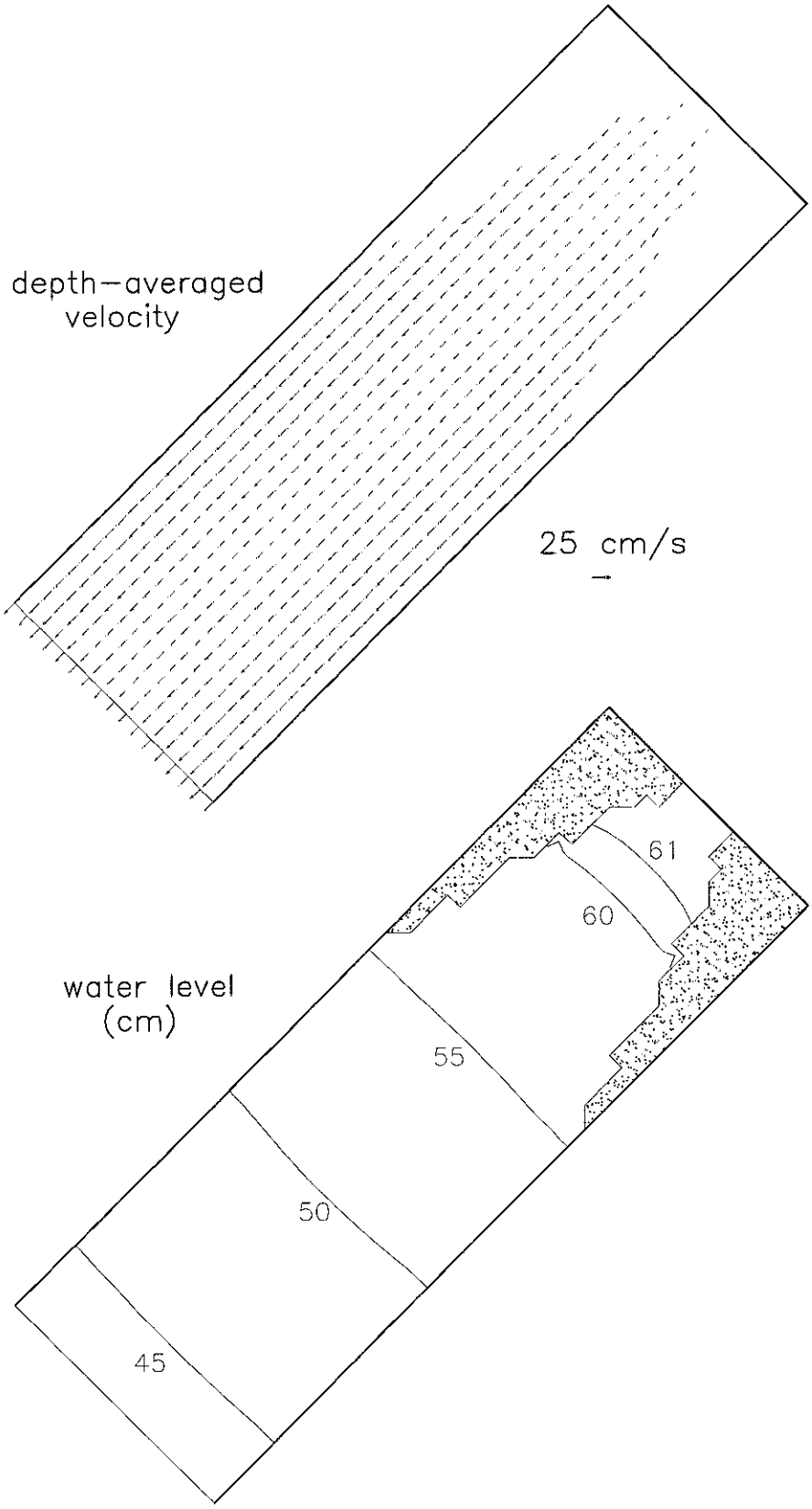

Figure 6b. Test Case #2, time=0.5 hrs

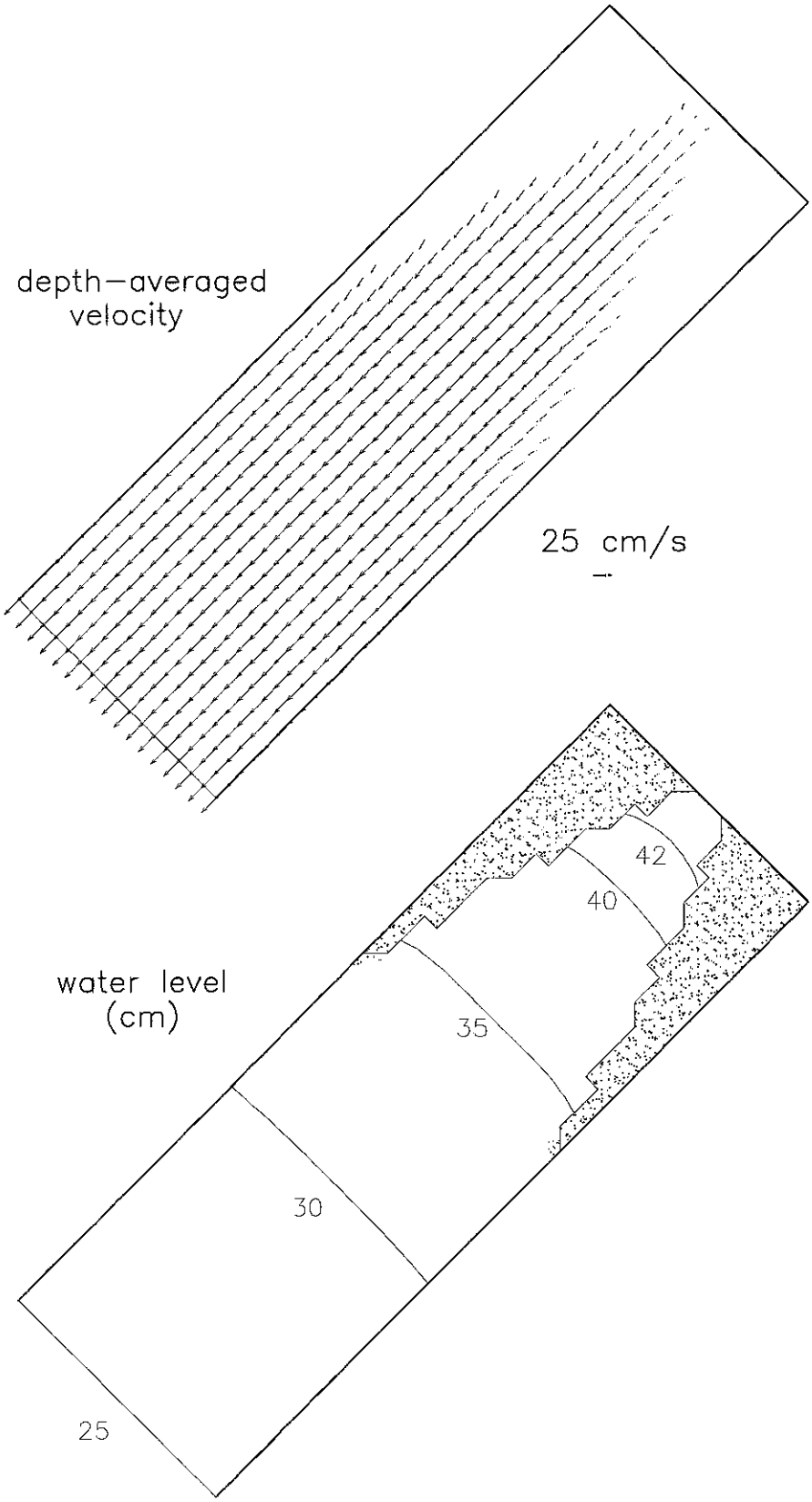

Figure 6c. Test Case #2, time=1.0 hrs

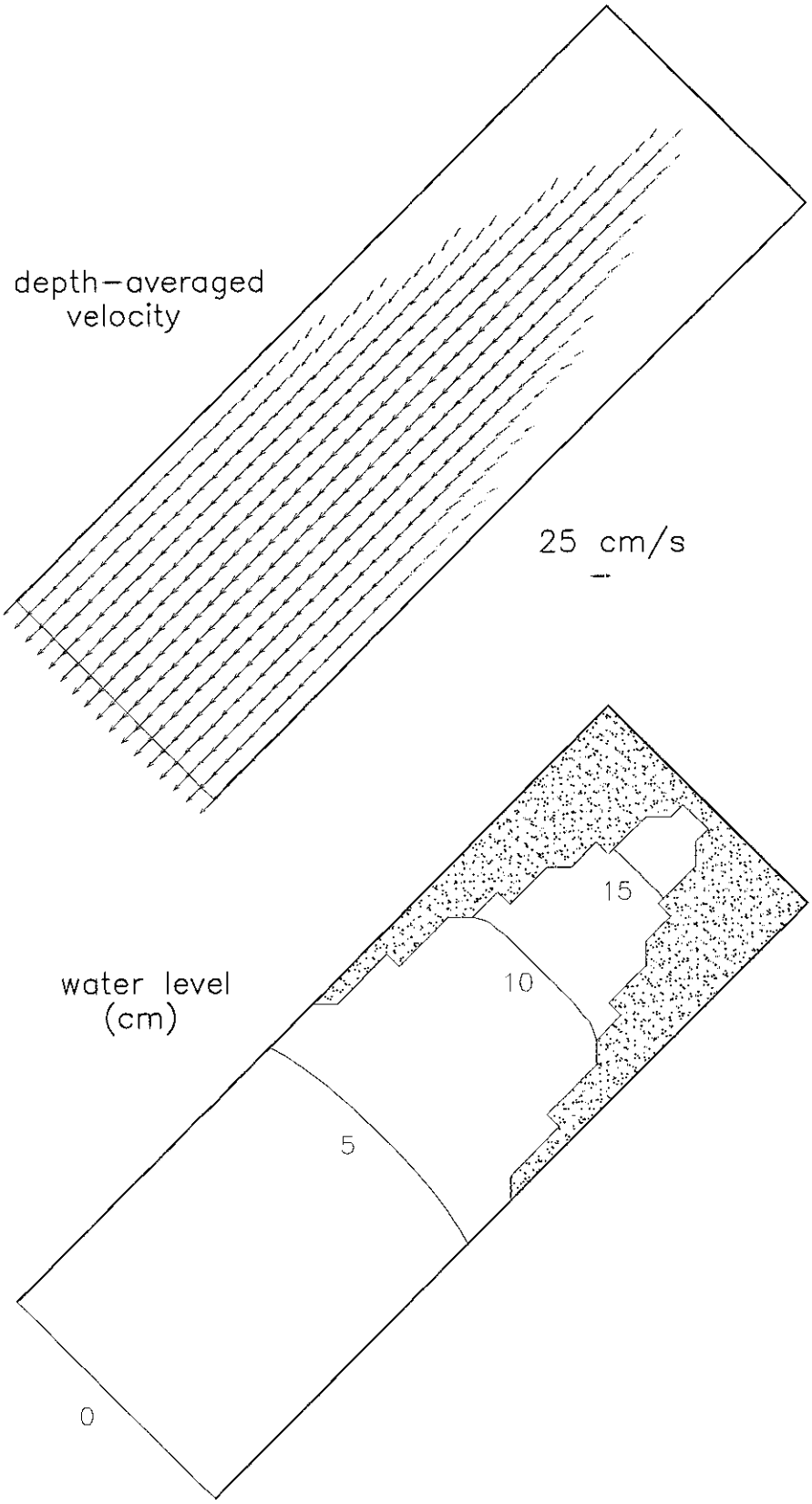

Figure 6d. Test Case #2, time=1.5 hrs

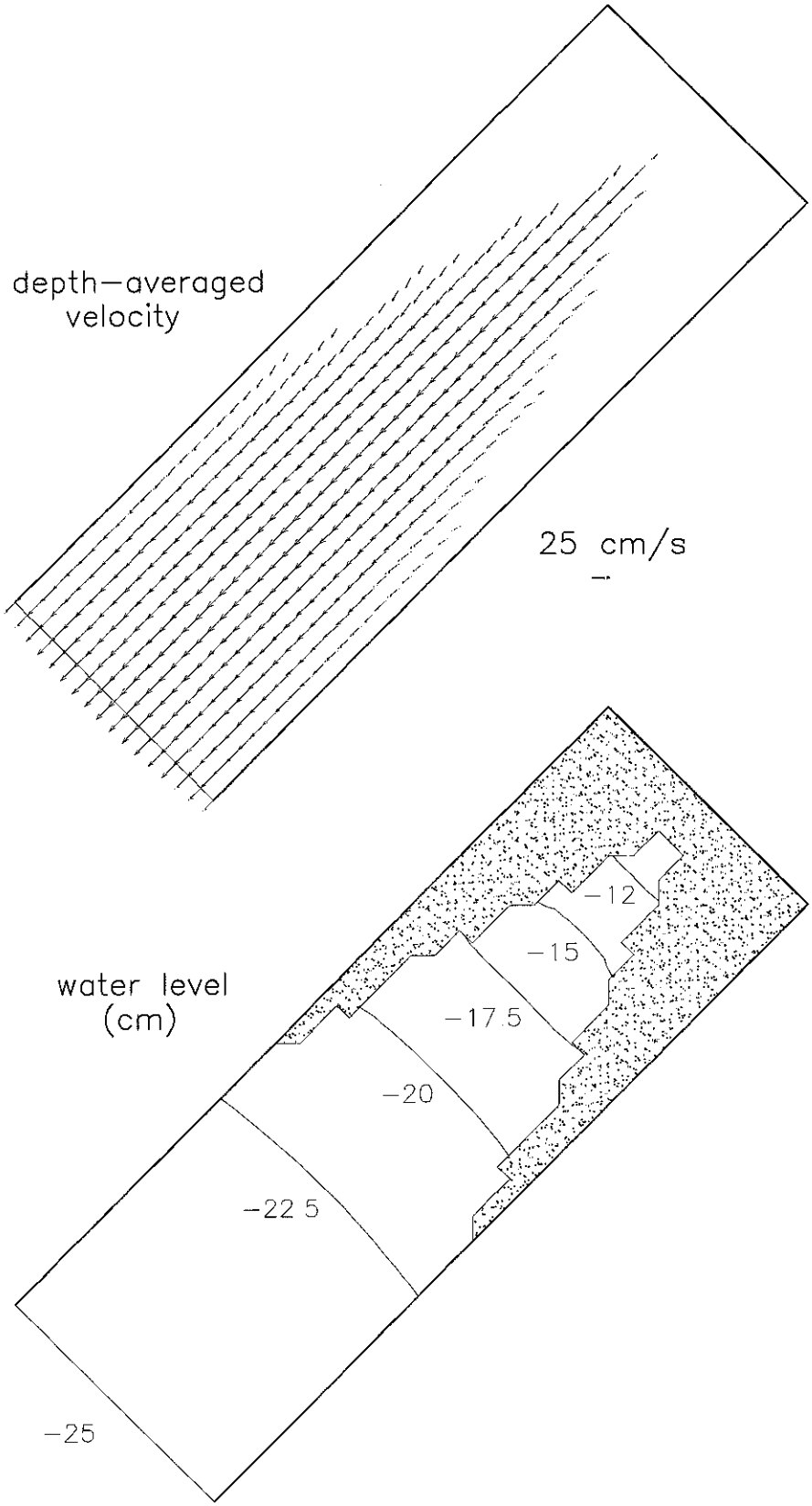

Figure 6e. Test Case #2, time=2.0 hrs

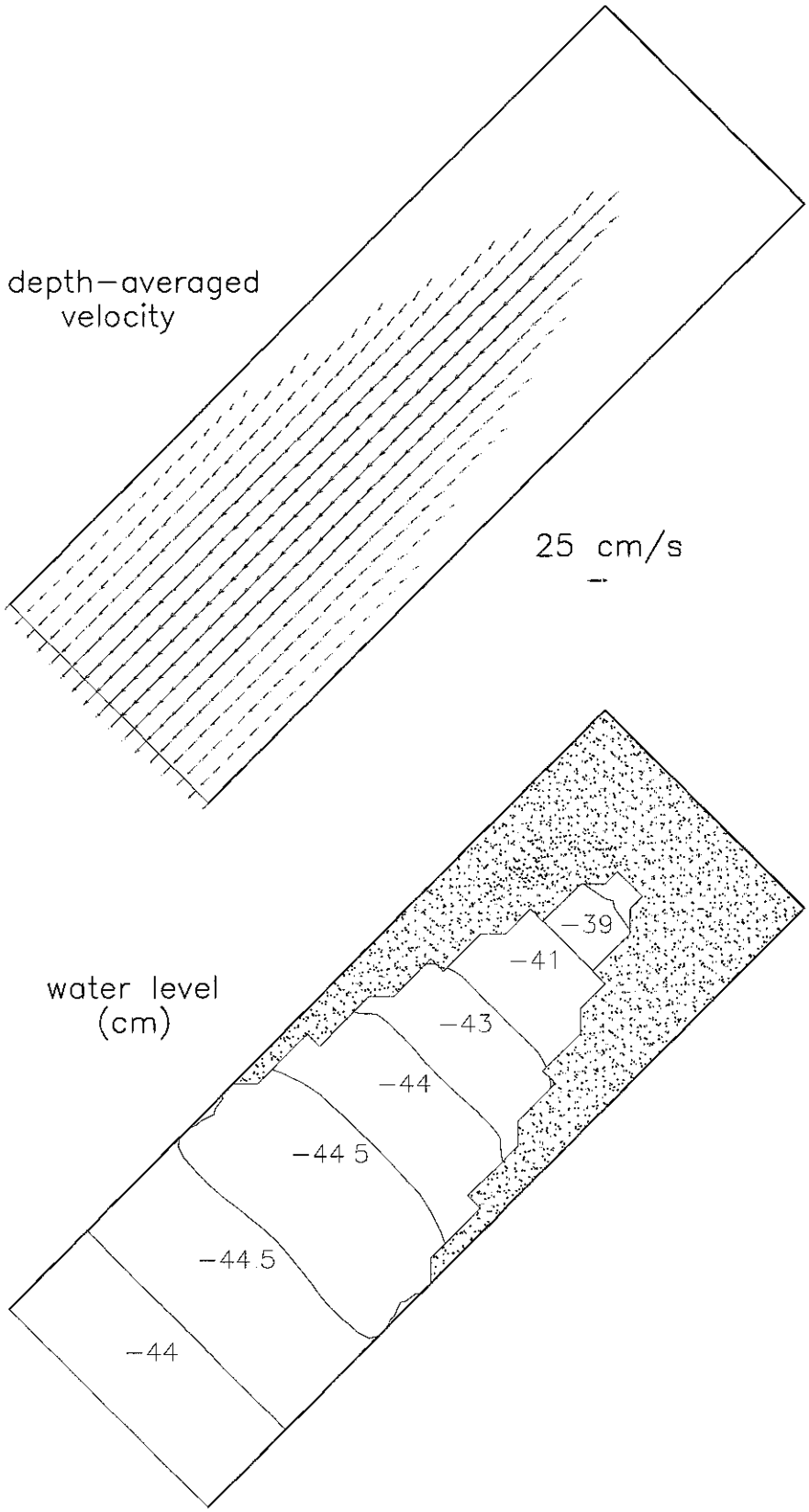

Figure 6f. Test Case #2, time=2.5 hrs

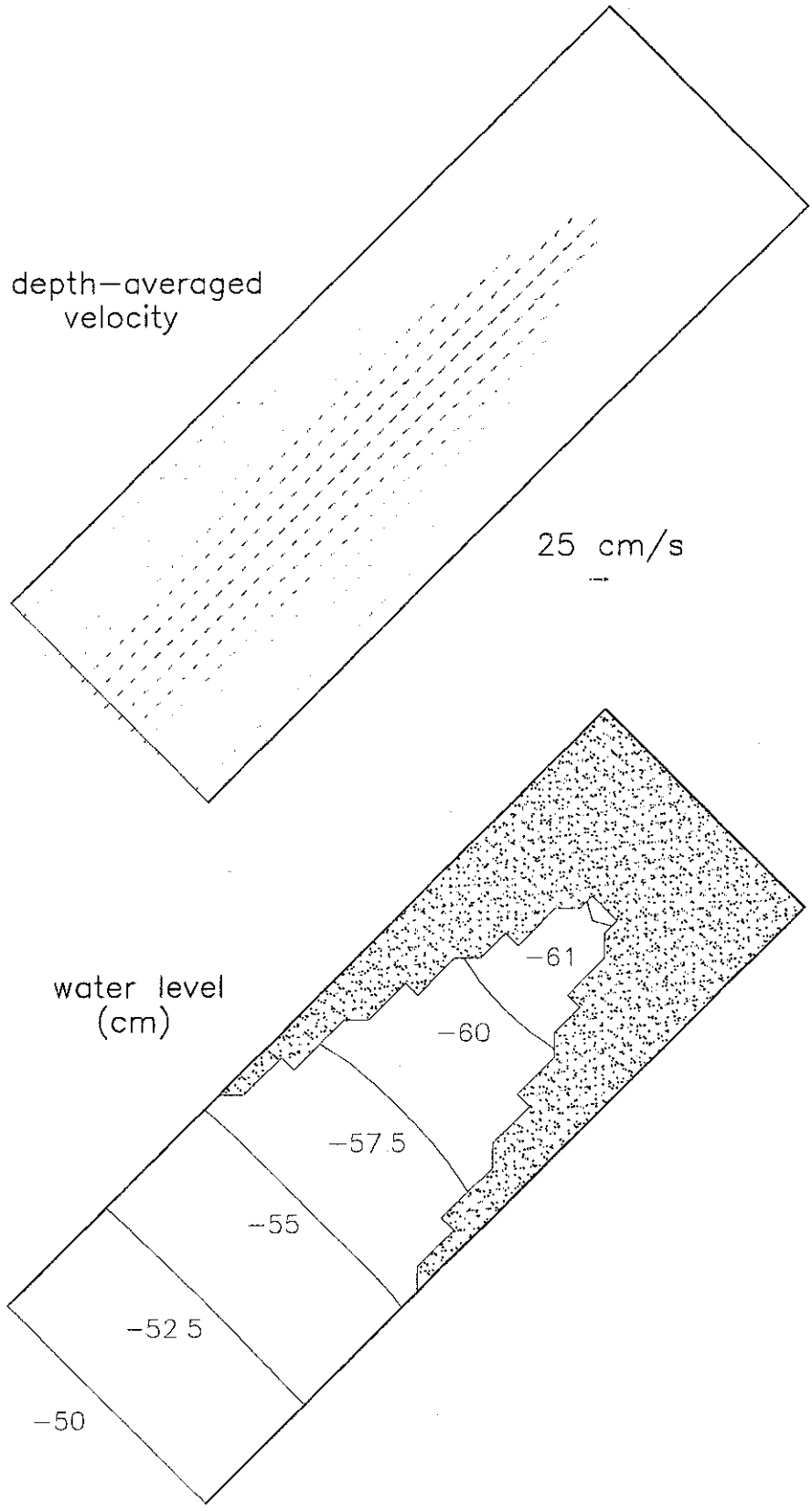

Figure 6g. Test Case #2, time=3.0 hrs

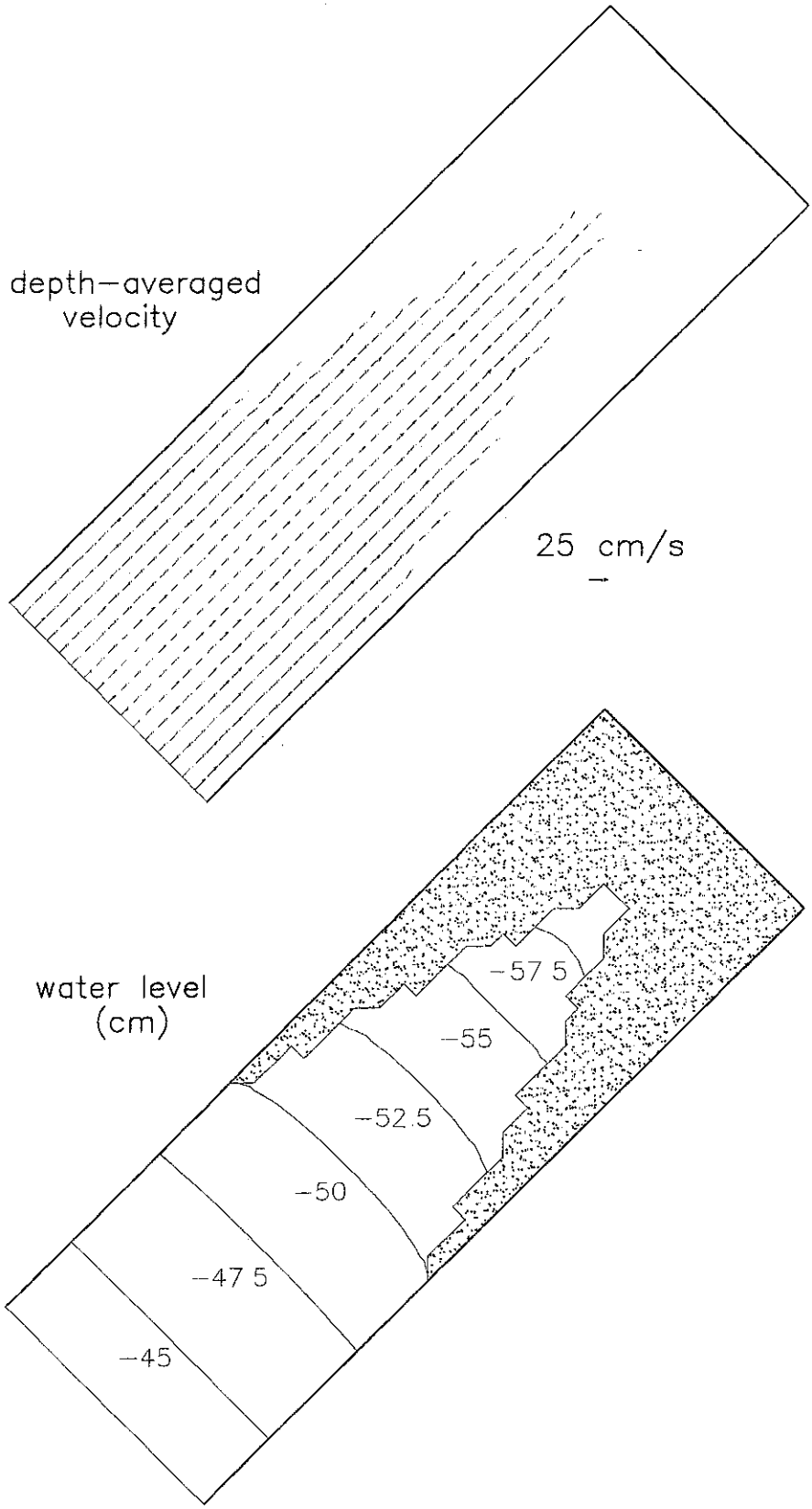

Figure 6h. Test Case #2, time=3.5 hrs

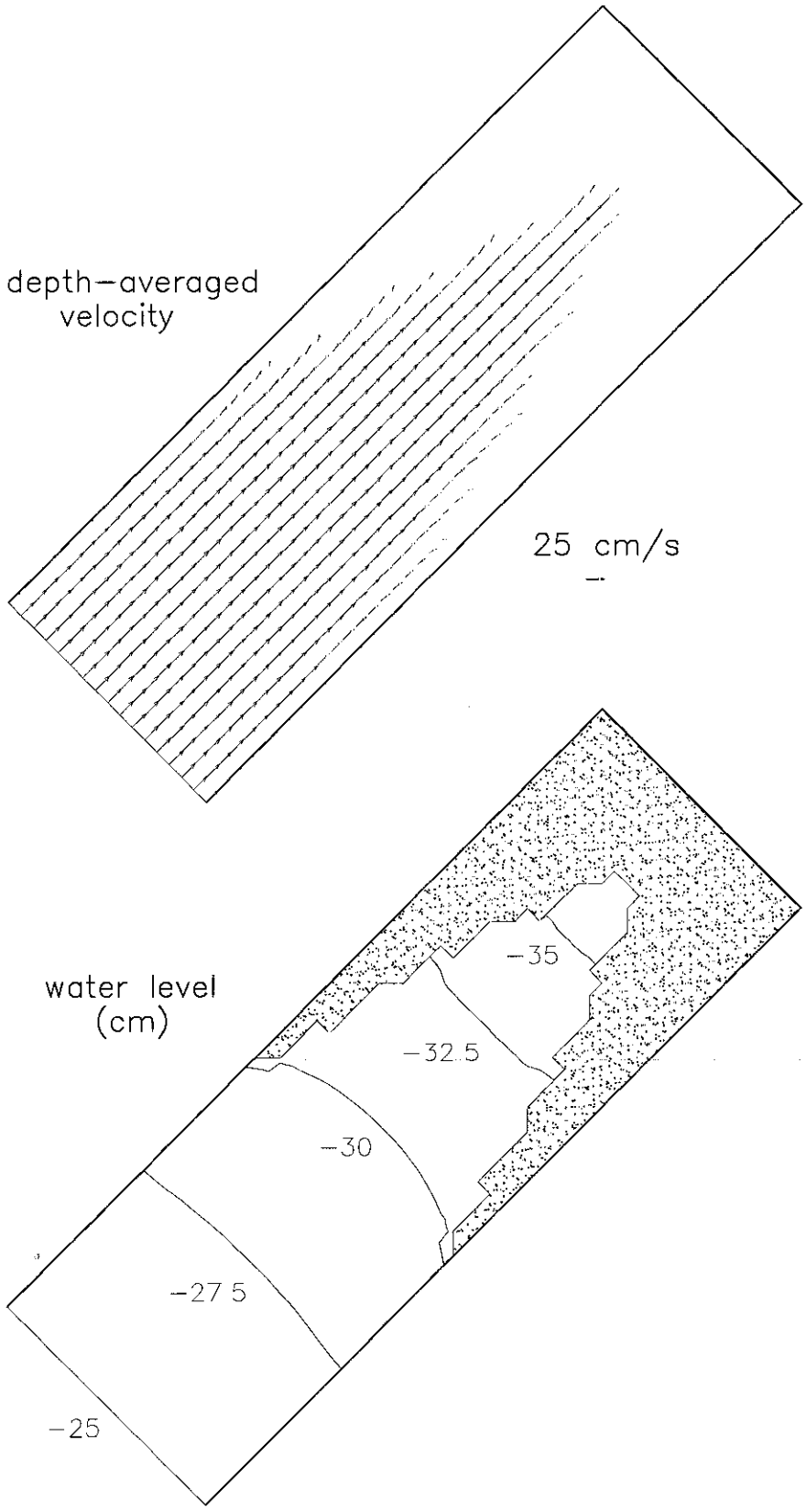

Figure 6i. Test Case #2, time=4.0 hrs

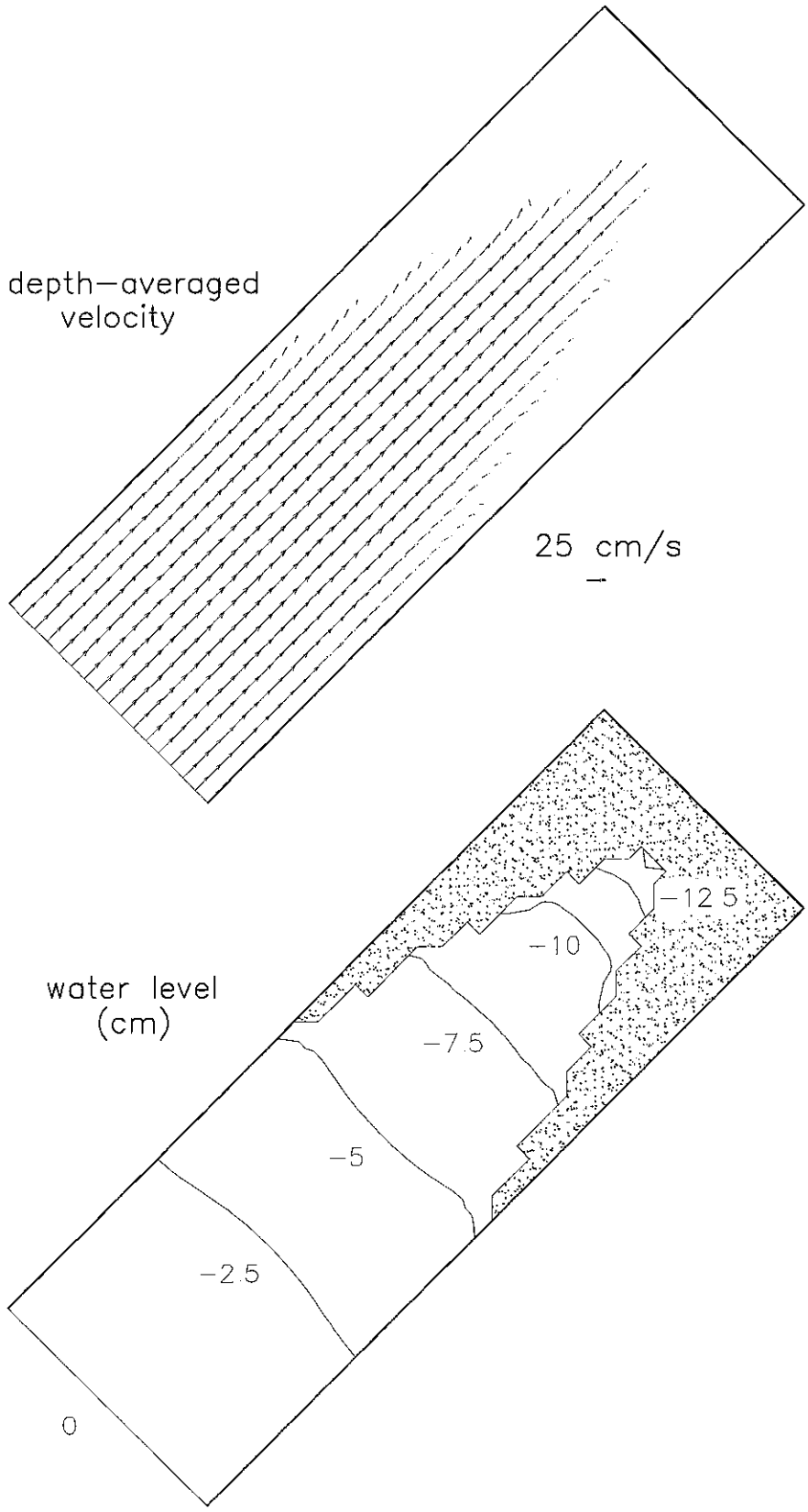

Figure 6j. Test Case #2, time=4.5 hrs

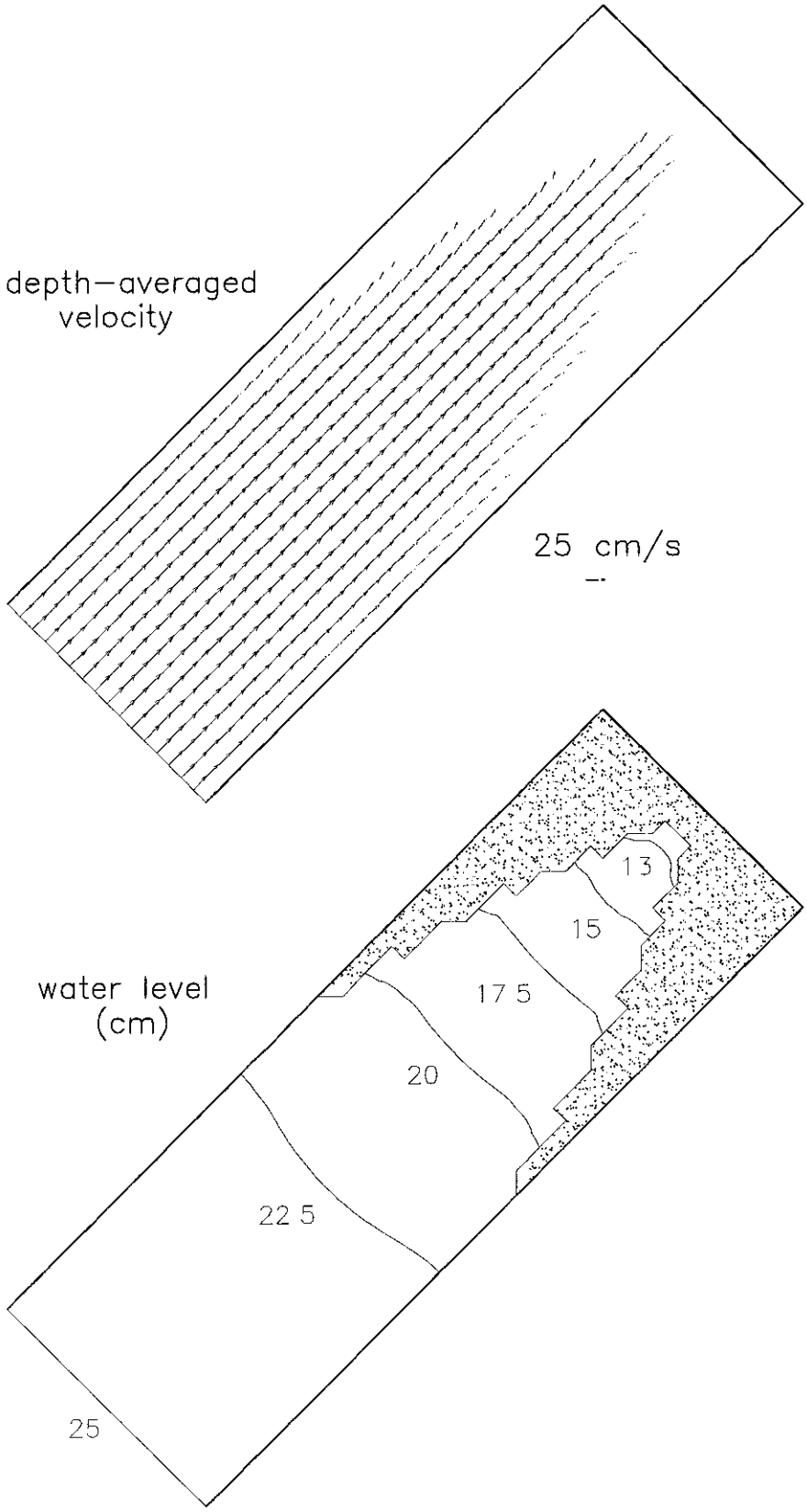

Figure 6k. Test Case #2, time=5.0 hrs

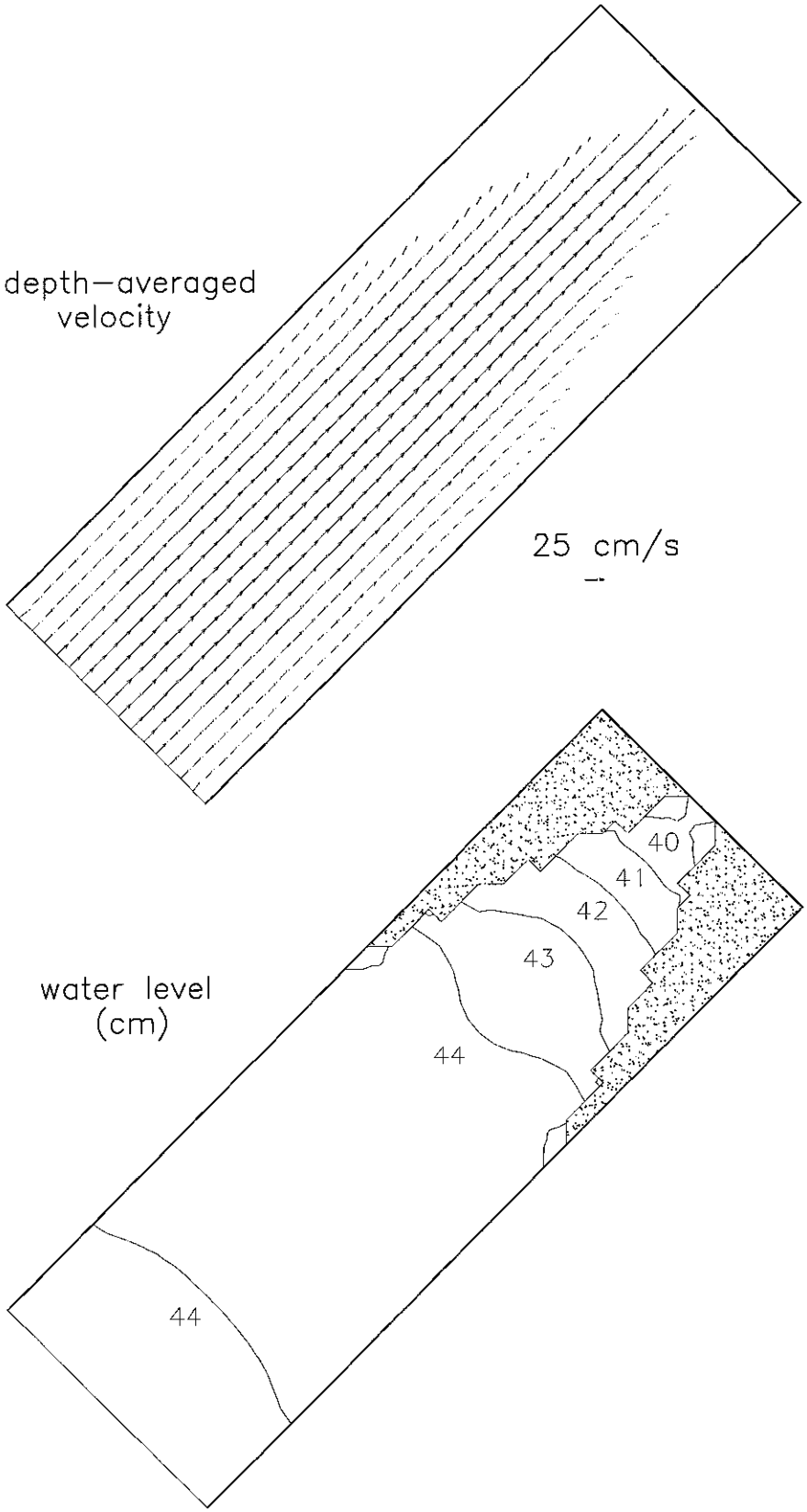

Figure 61. Test Case #2, time=5.5 hrs

Figure 7a. Test Case #2, Node 383

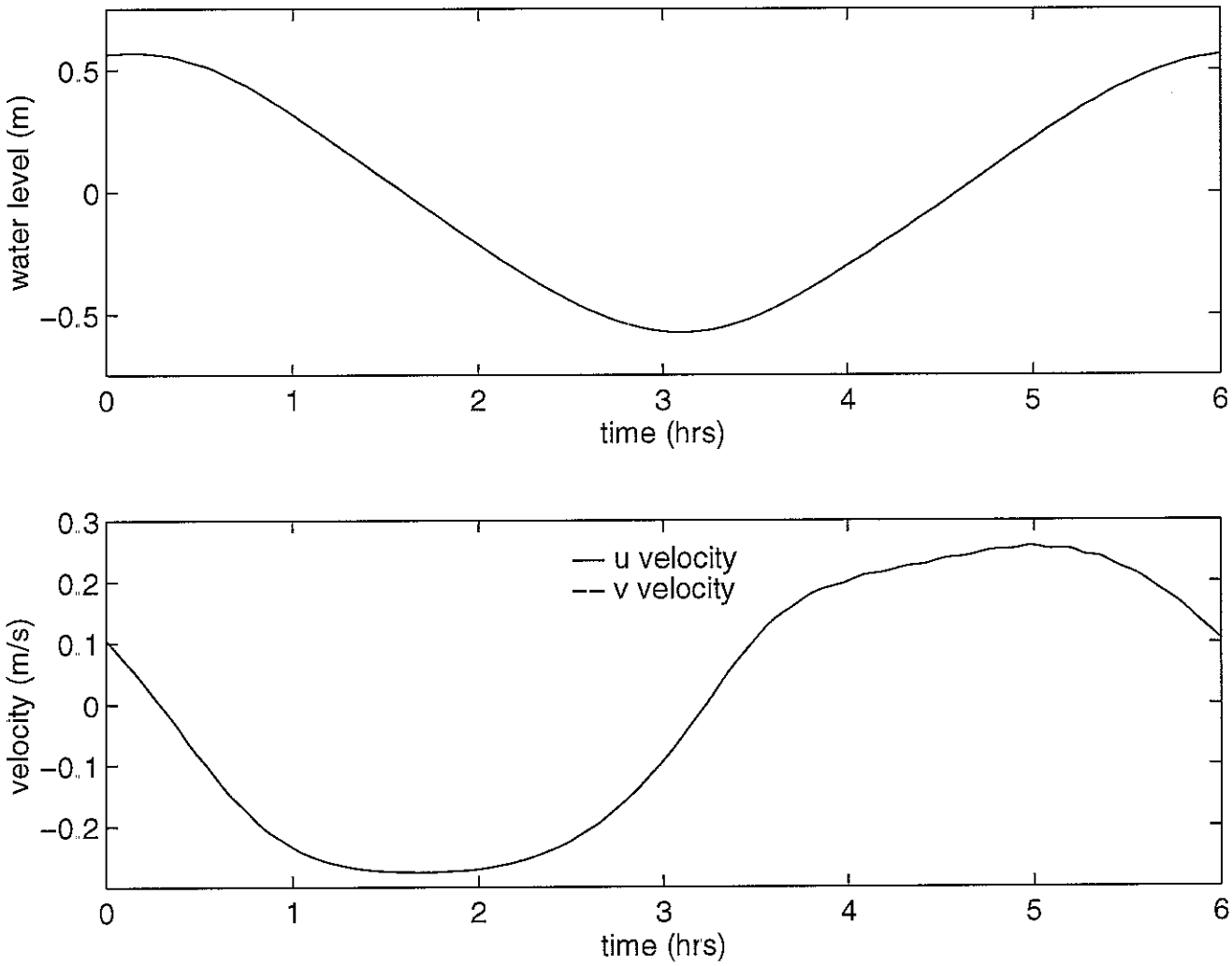

Figure 7b. Test Case #2, Node 553

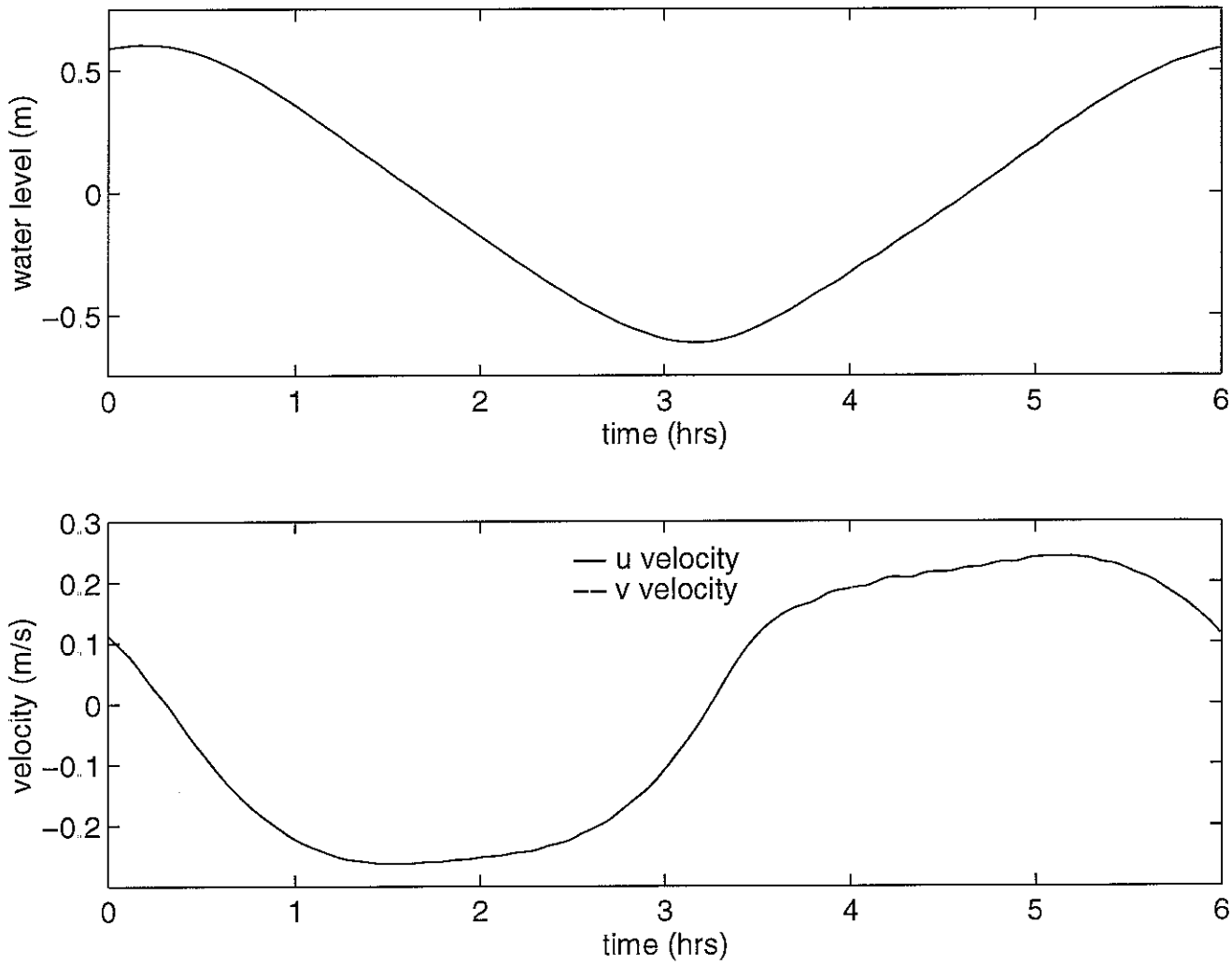

Figure 7c. Test Case #2, Node 706

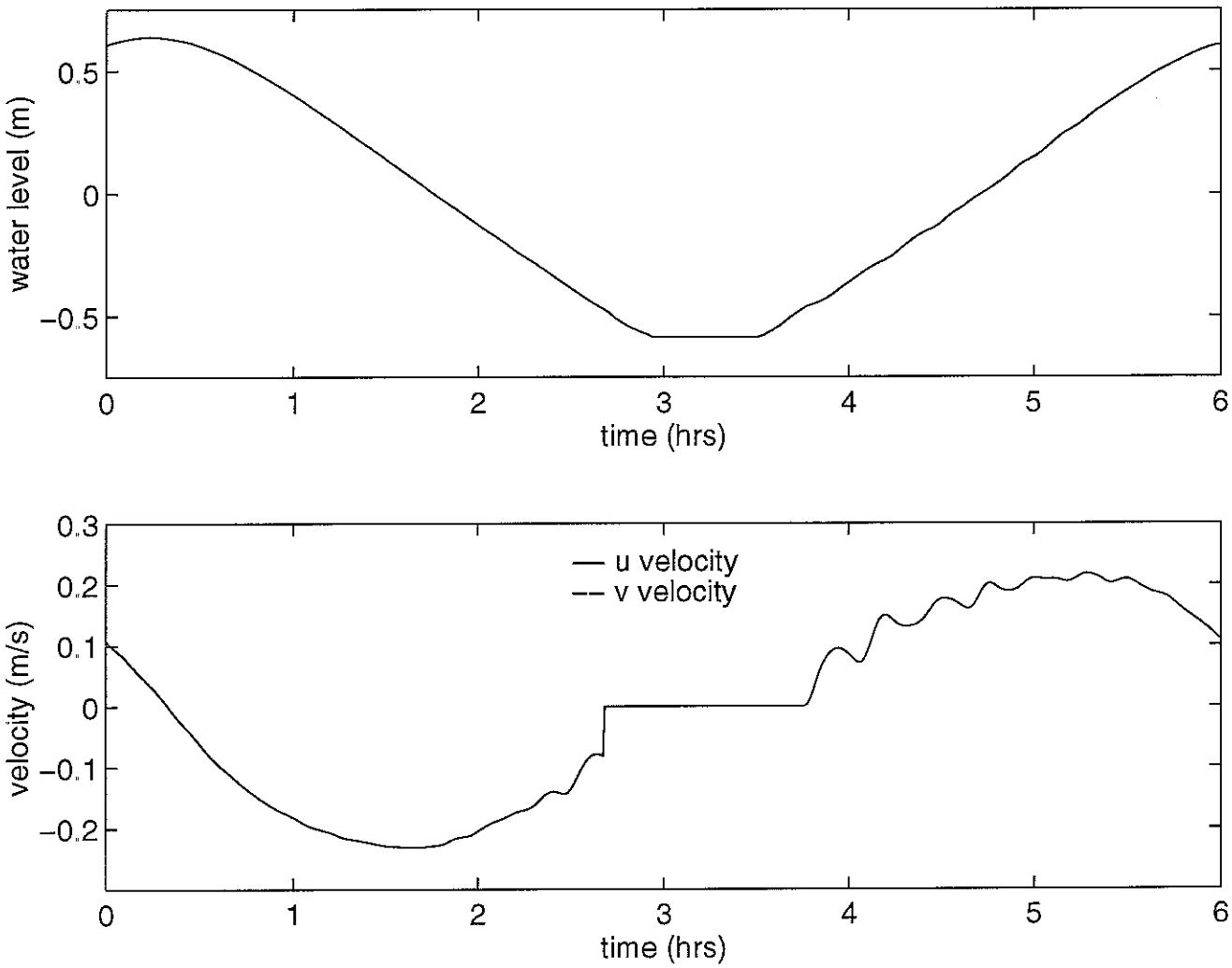

Figure 7d. Test Case #2, Node 705

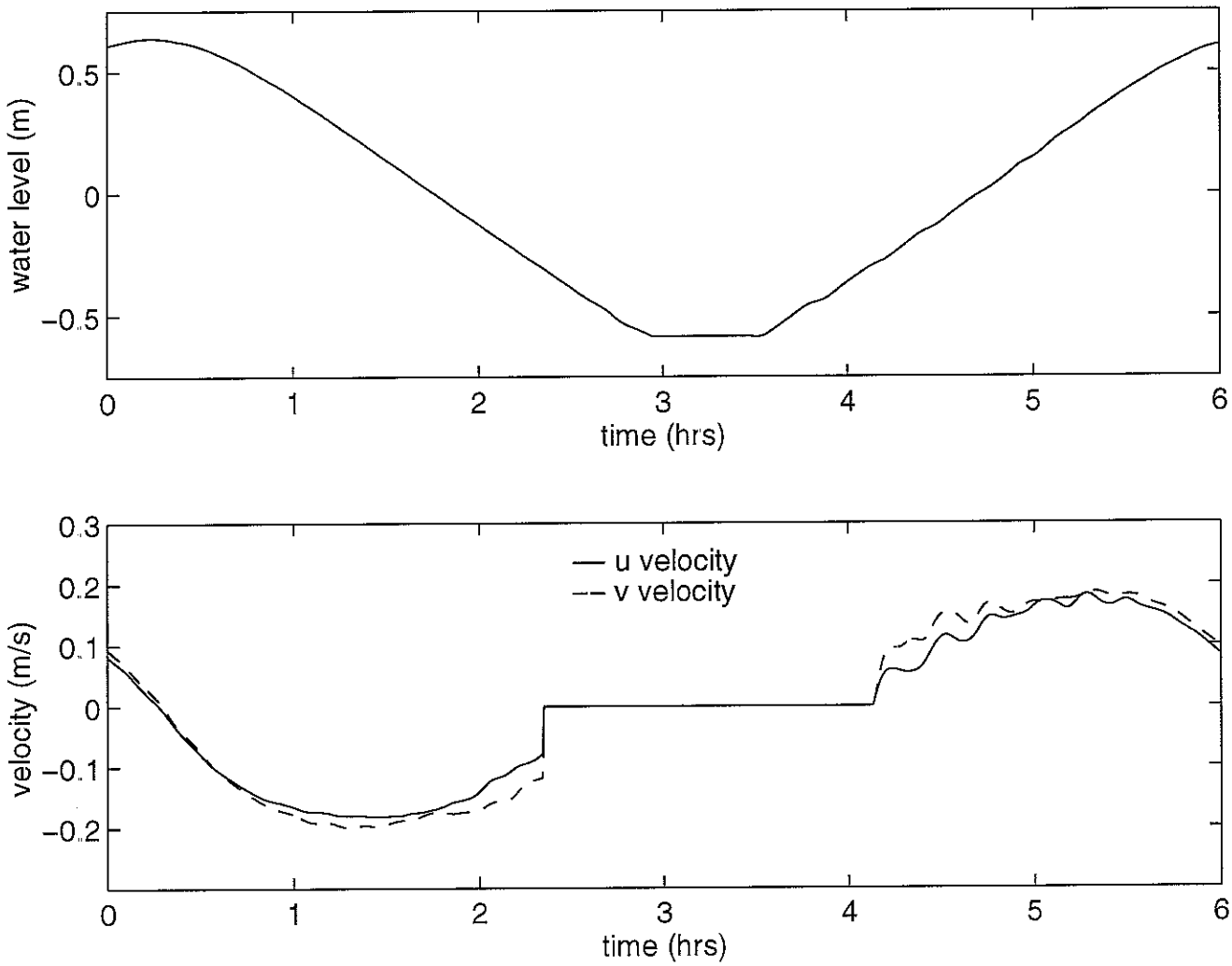

Figure 7e. Test Case #2, Node 704

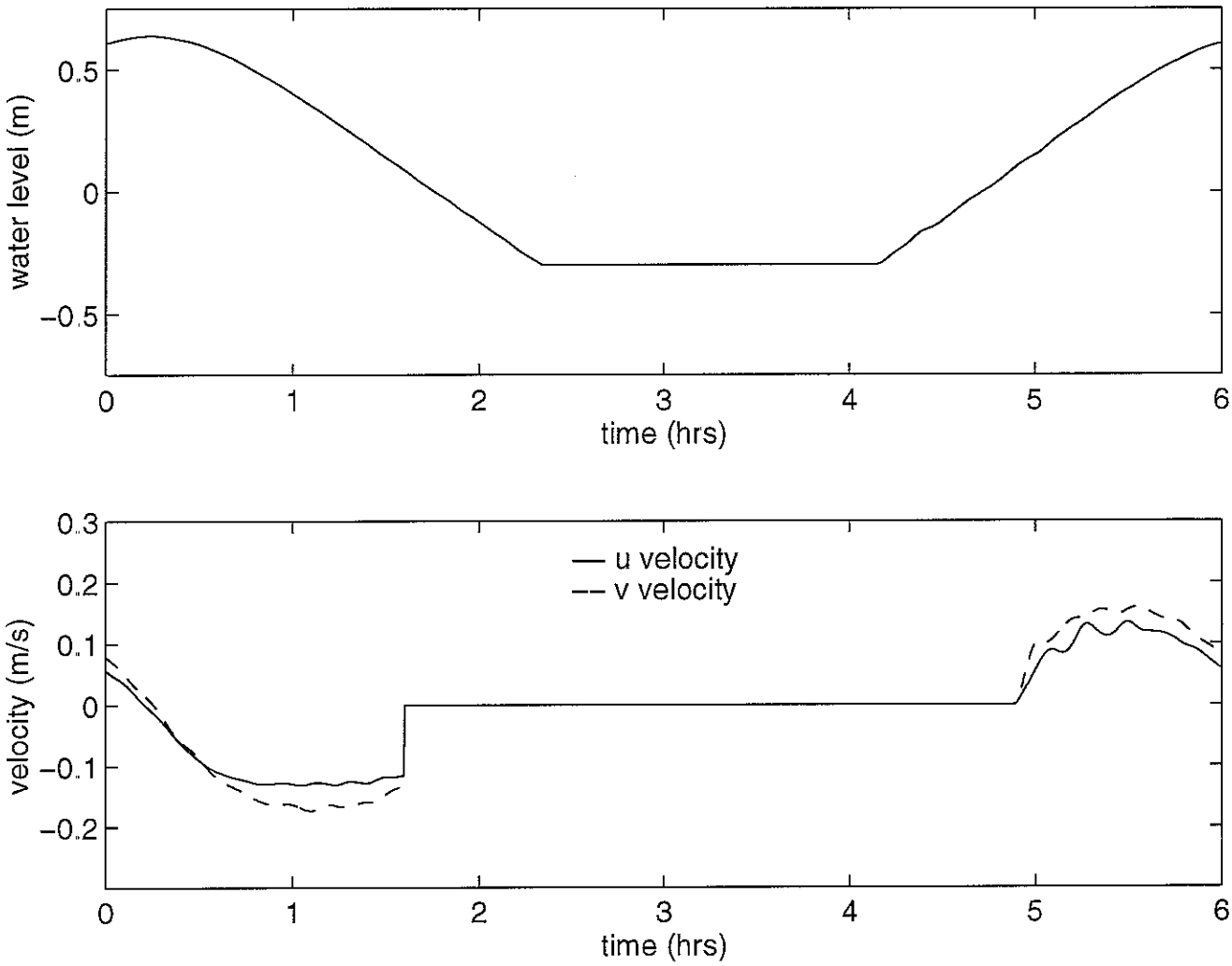

Figure 7f. Test Case #2, Node 703

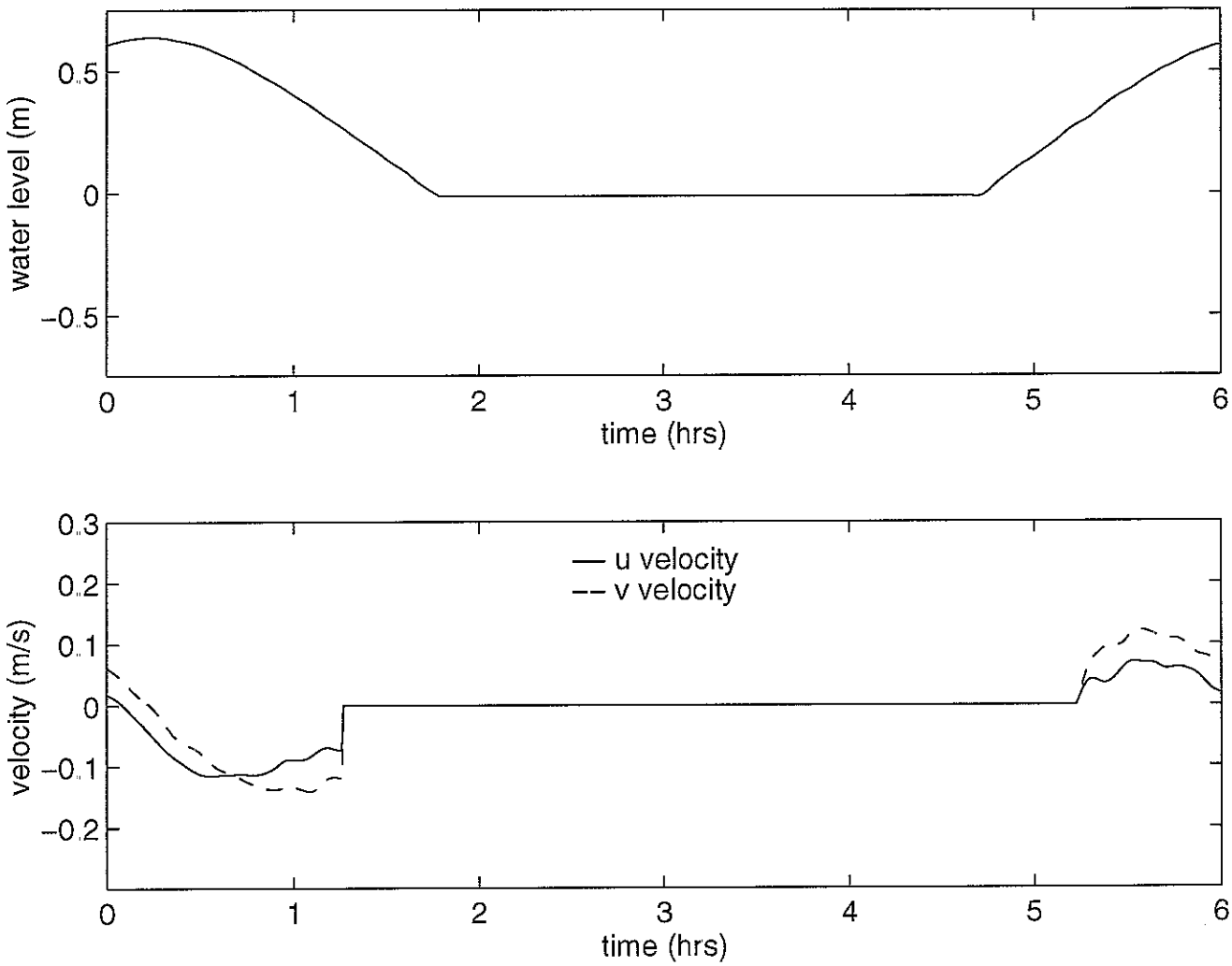

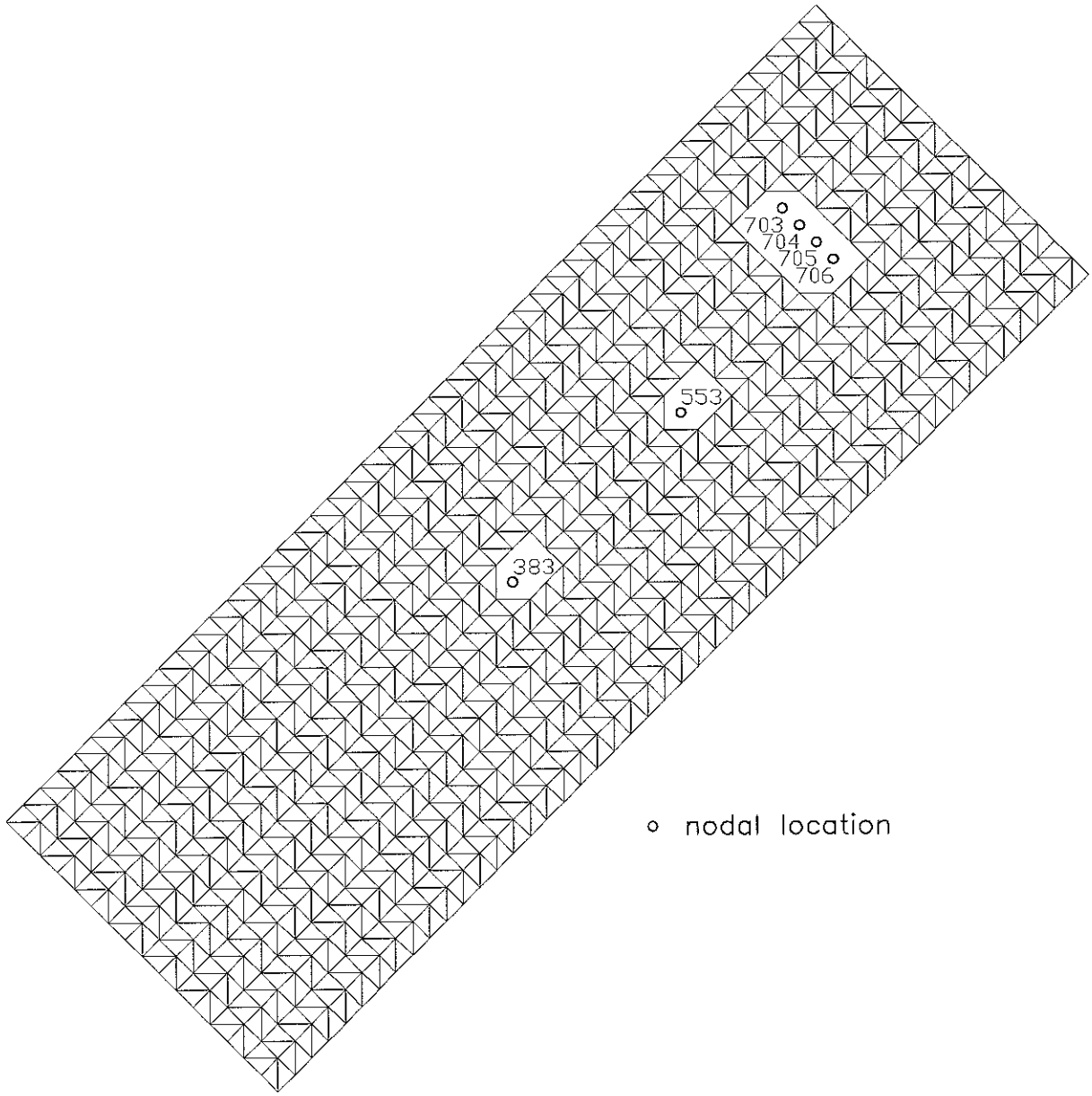

Figure 8. Location of time series nodes

Figure 9a. Test Case #3, Time = 0*T/10

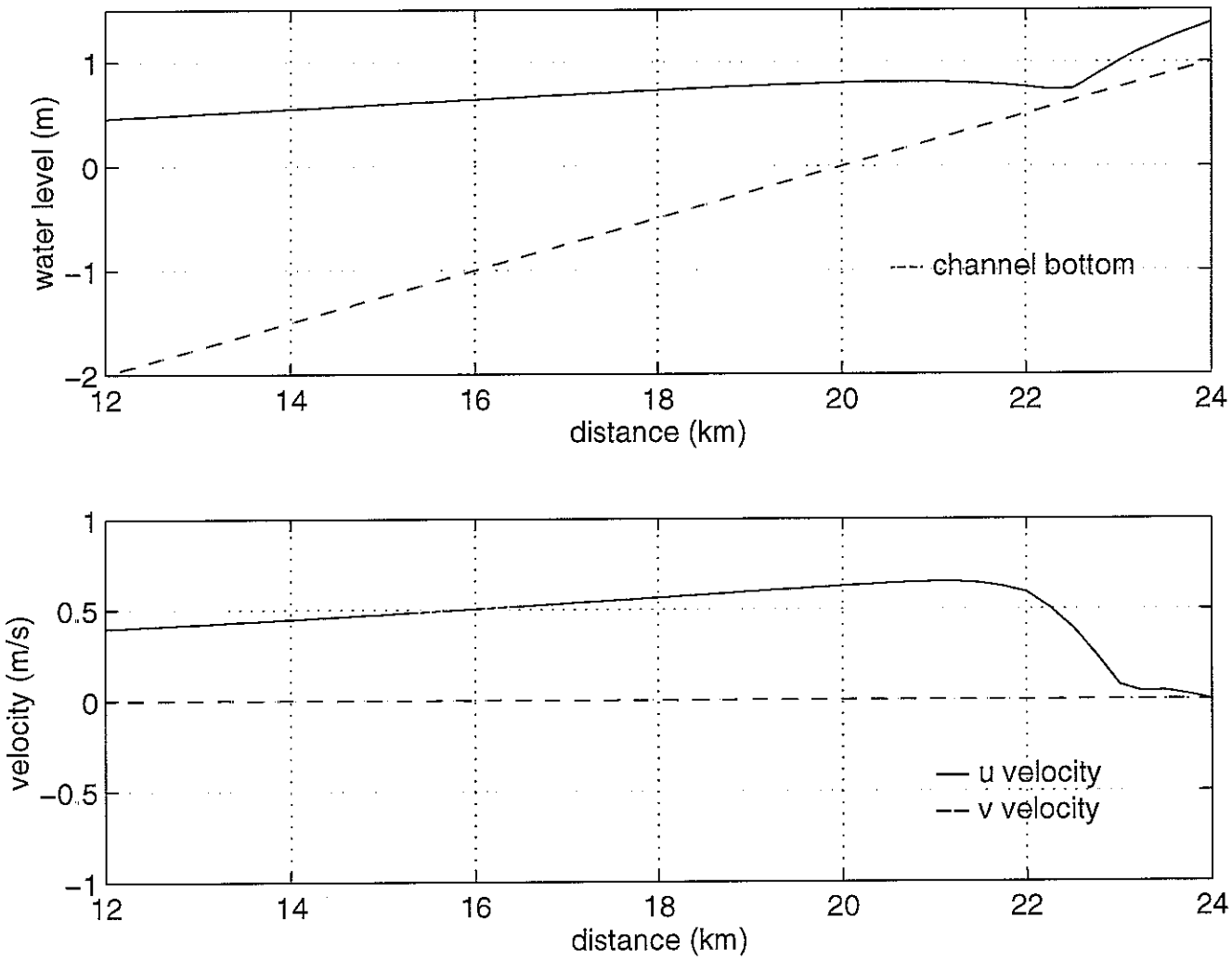

Figure 9b. Test Case #3, Time = 1*T/10

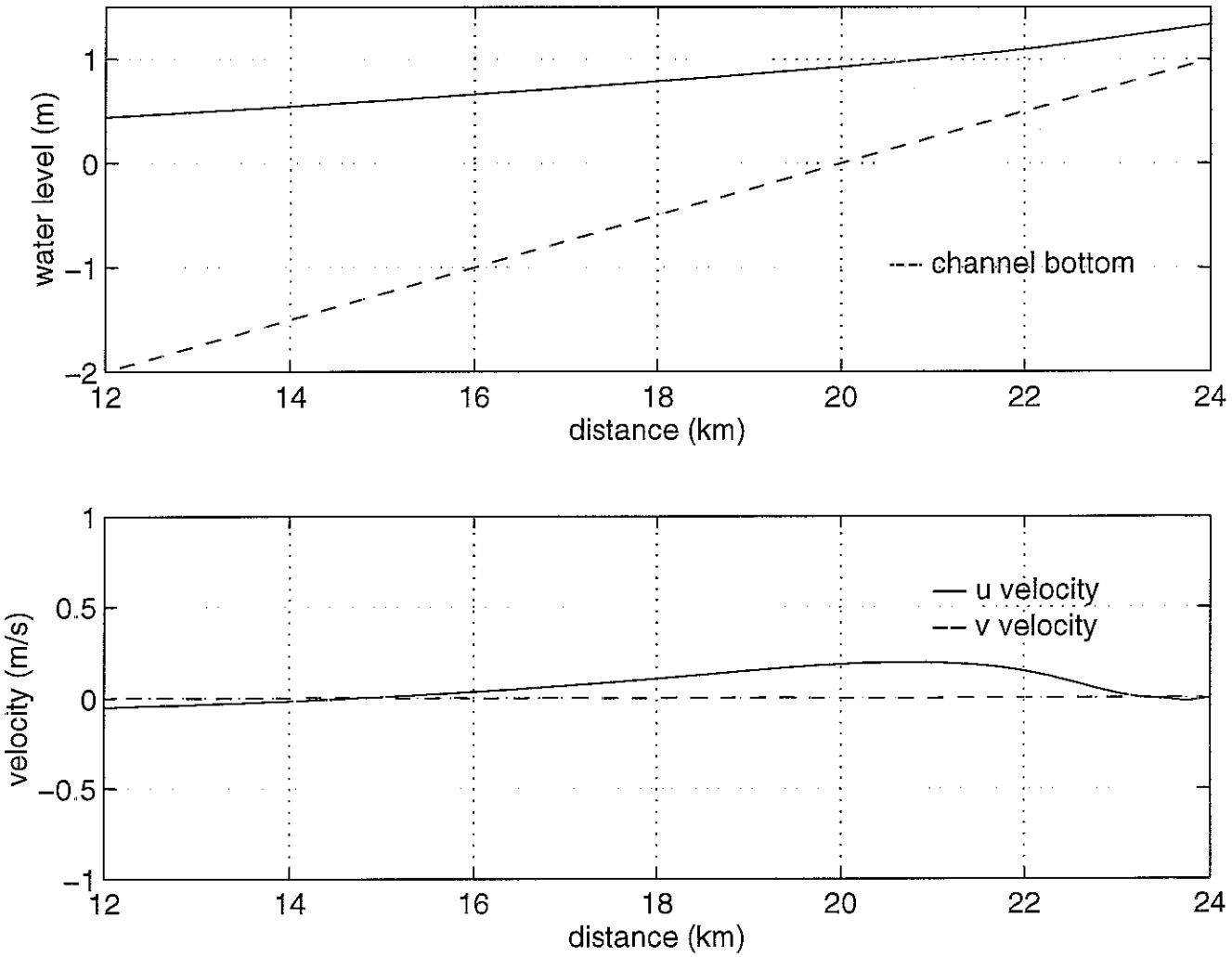

Figure 9c. Test Case #3, Time = 2*T/10

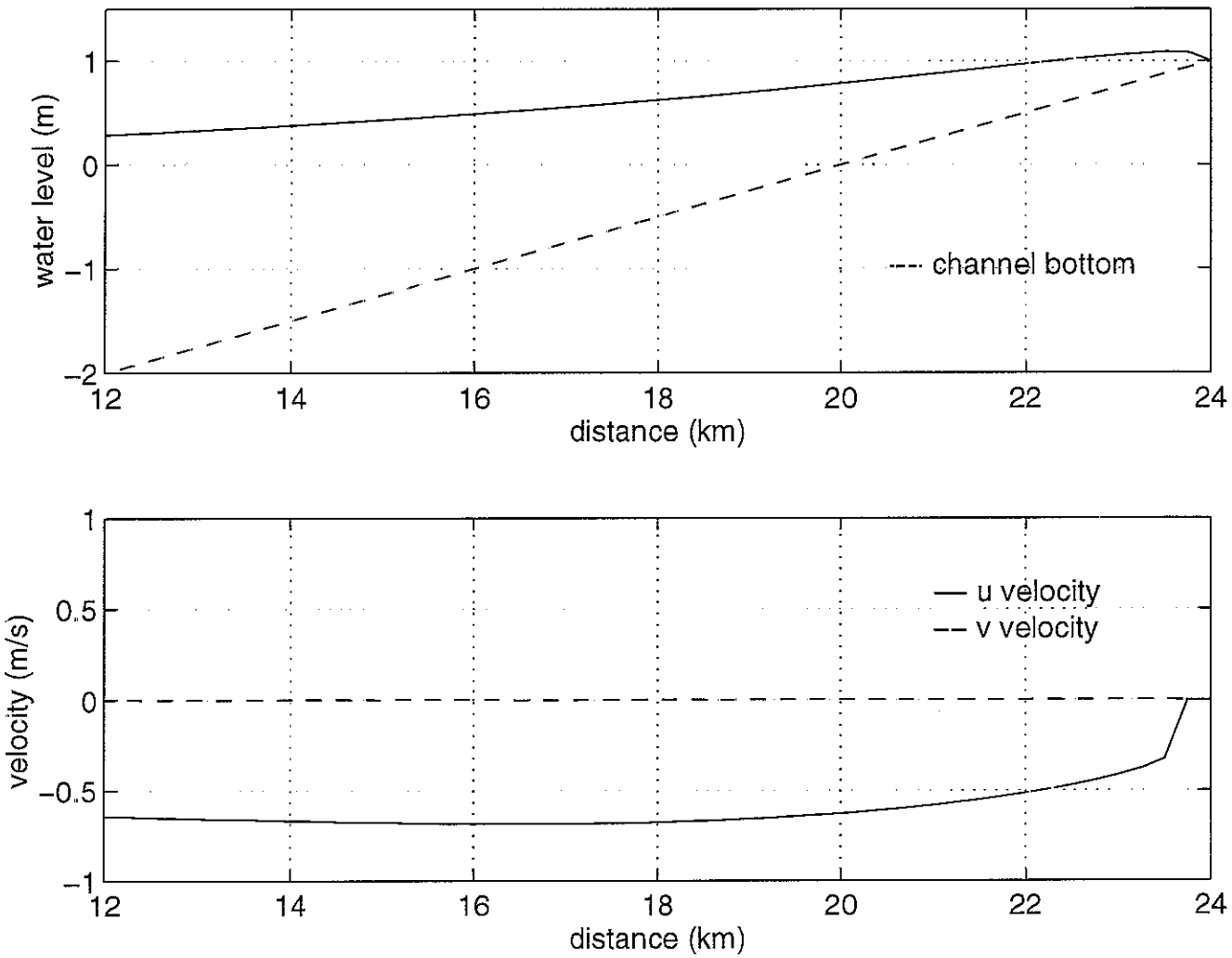

Figure 9d. Test Case #3, Time = 3*T/10

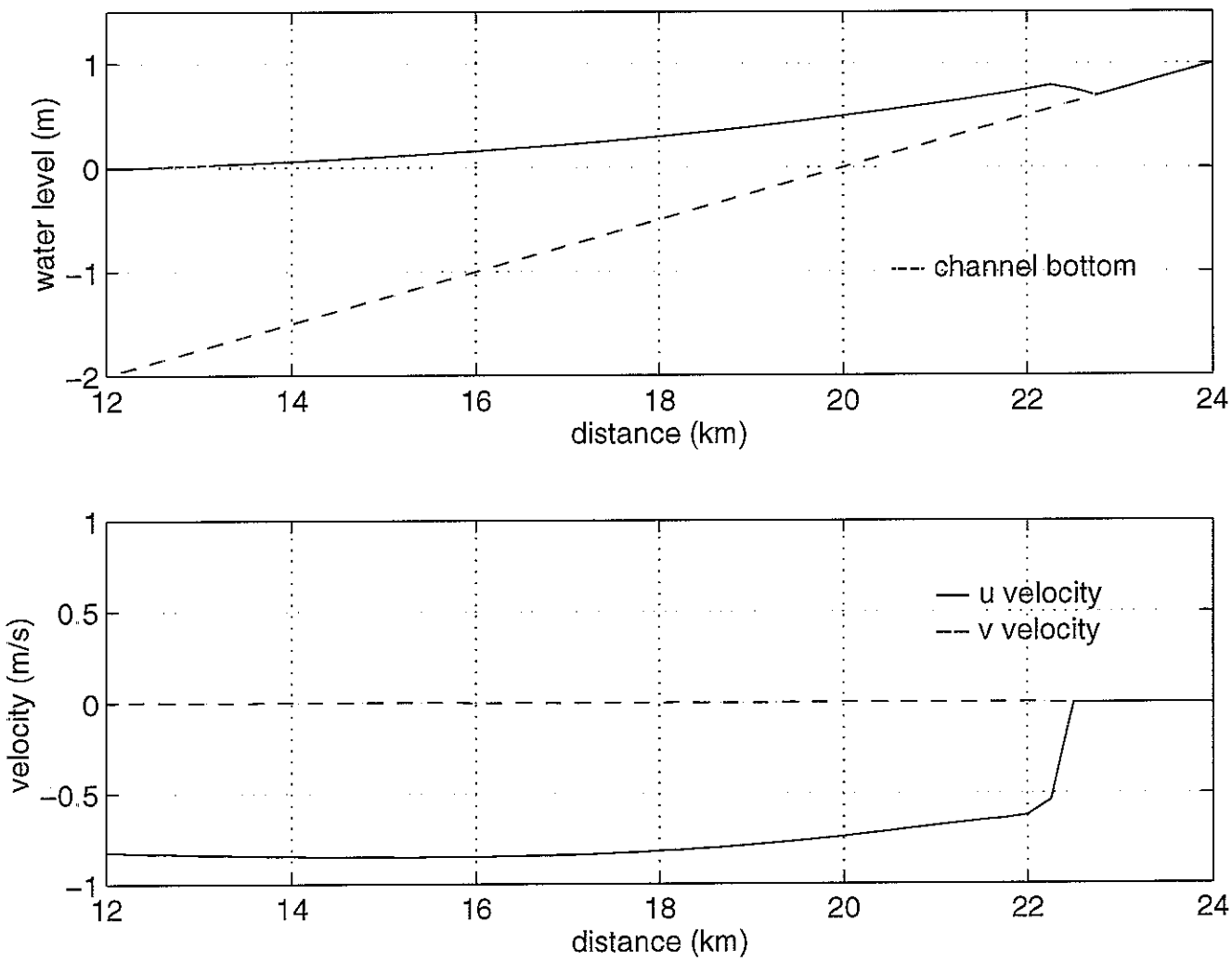

Figure 9e. Test Case #3, Time = 4*T/10

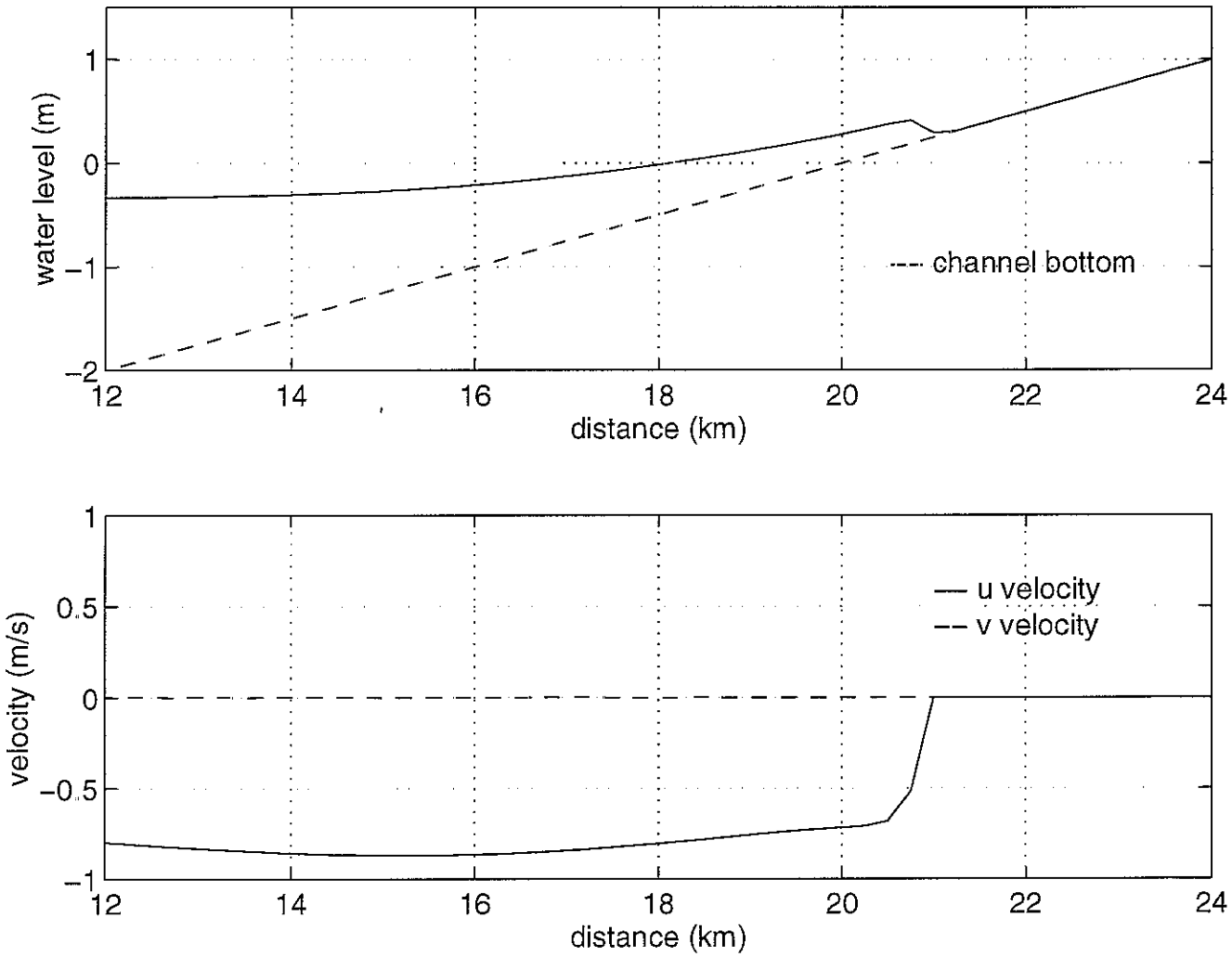

Figure 9f. Test Case #3, Time = 5*T/10

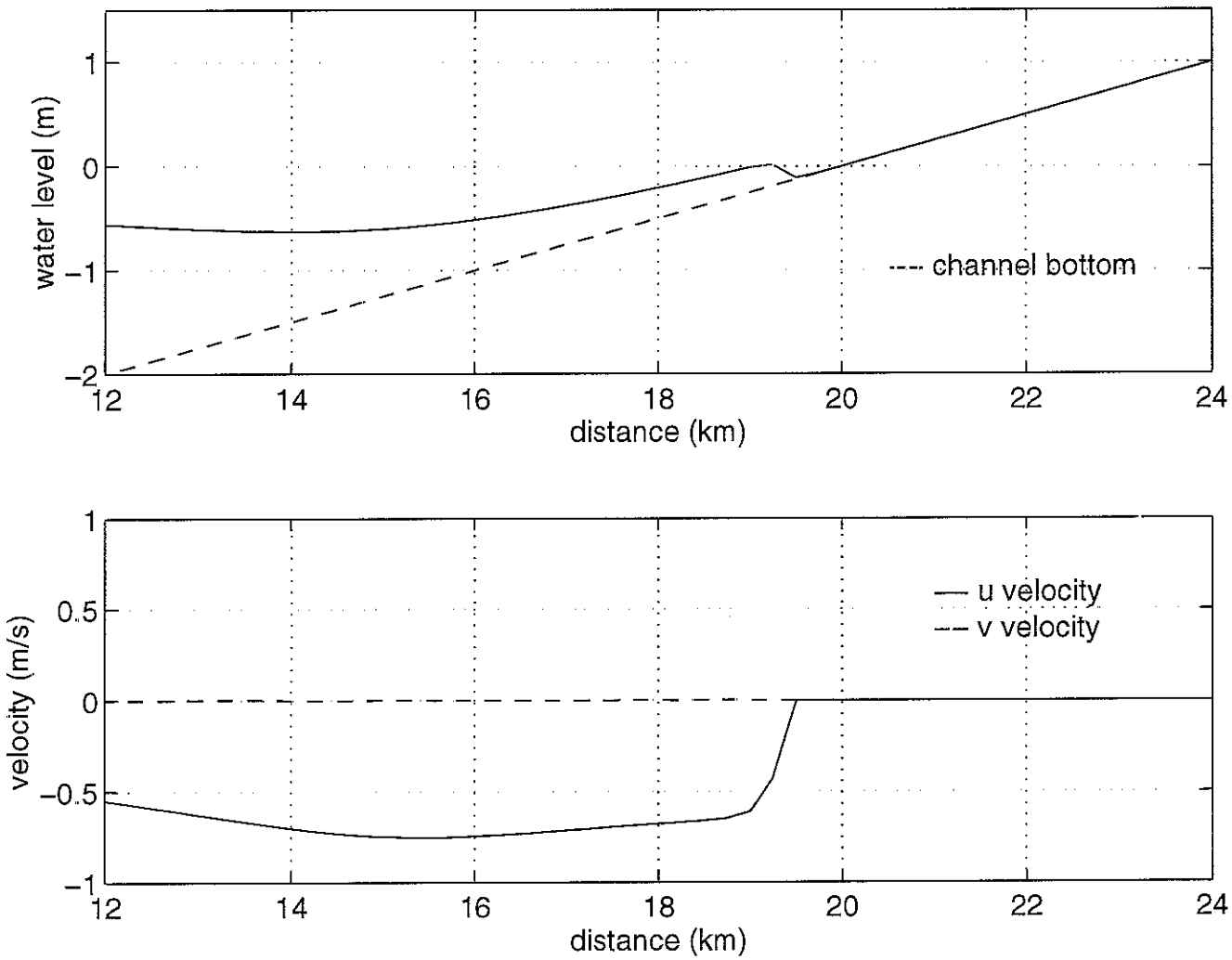

Figure 9g. Test Case #3, Time = 6*T/10

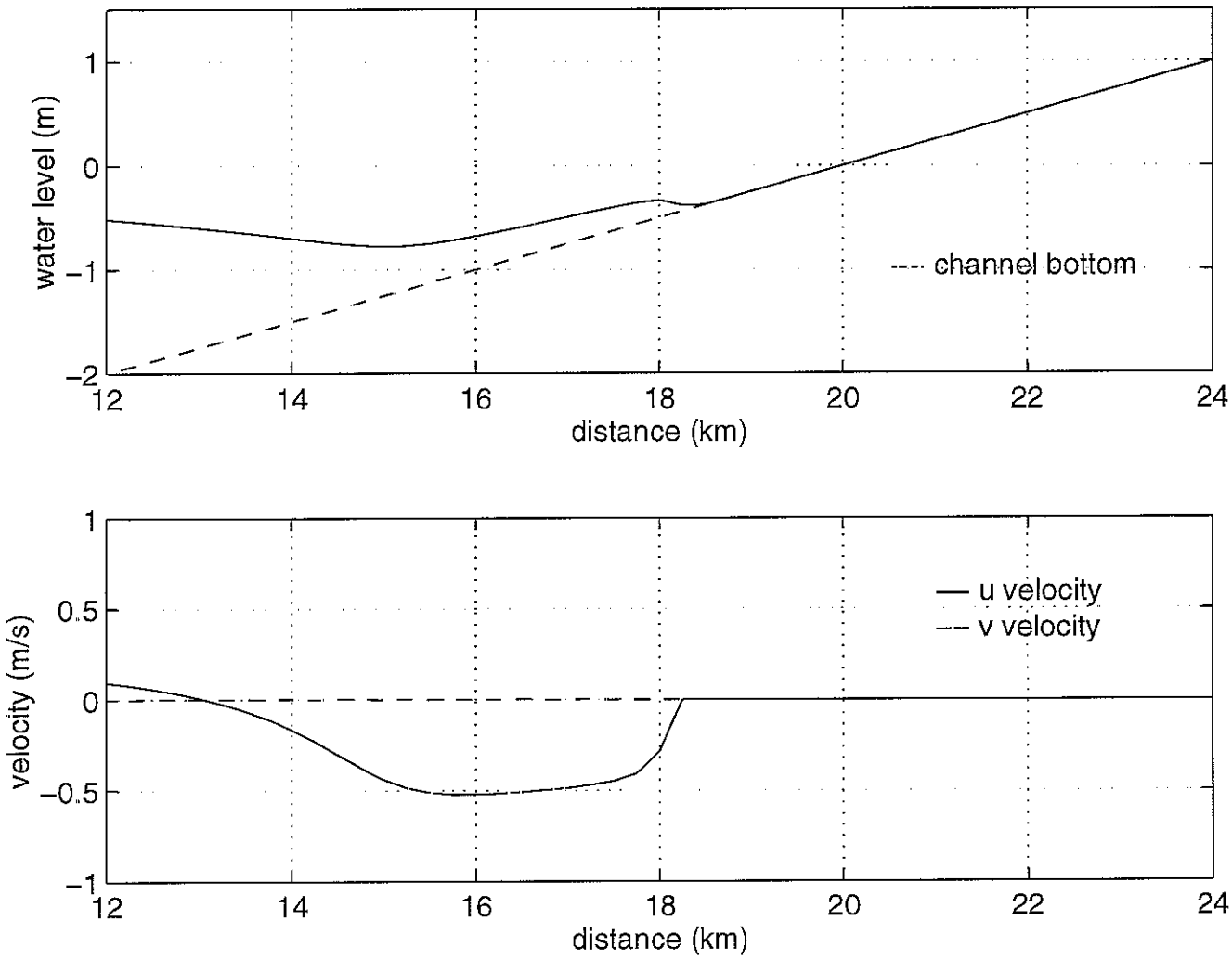

Figure 9h. Test Case #3, Time = 7*T/10

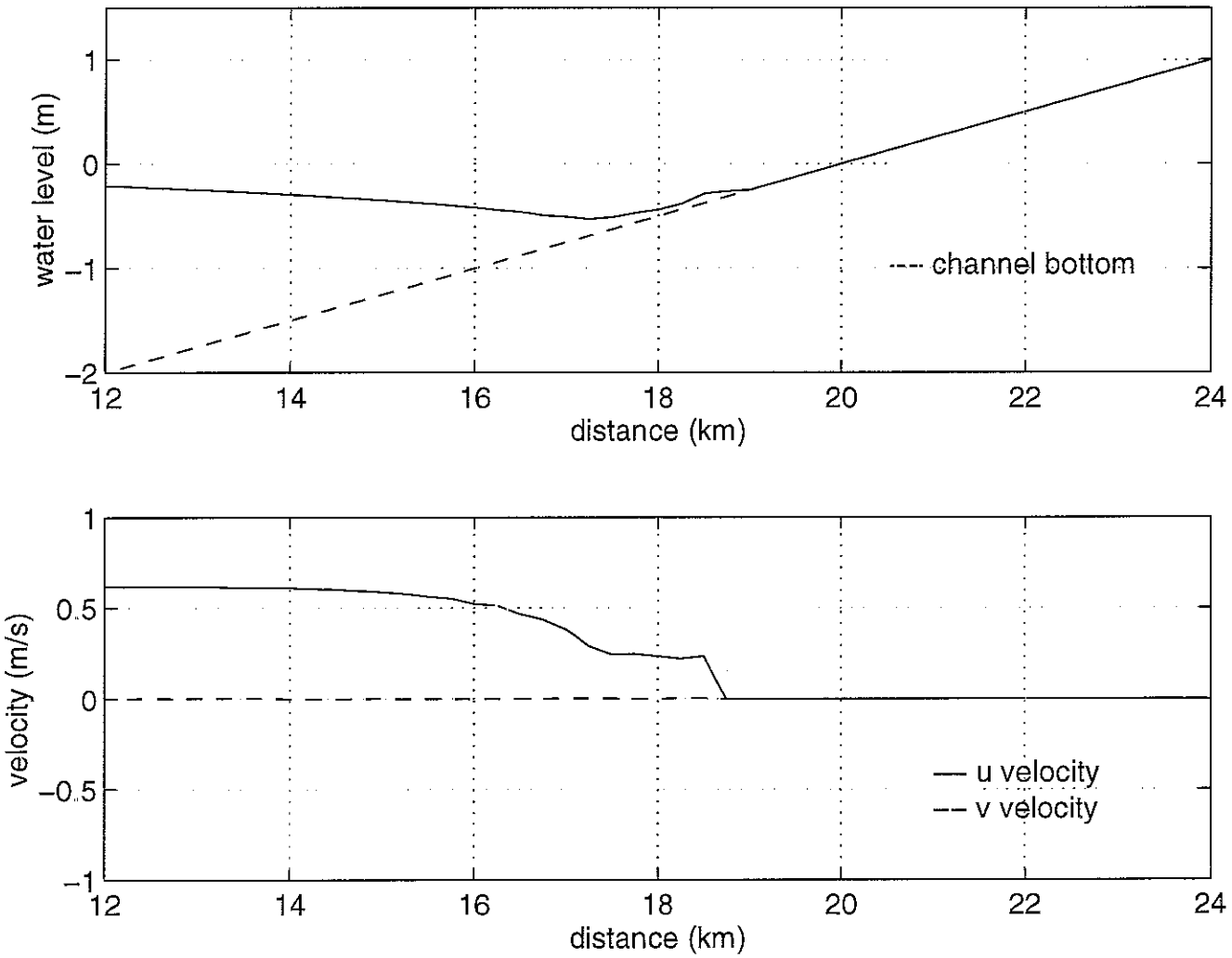

Figure 9i. Test Case #3, Time = 8*T/10

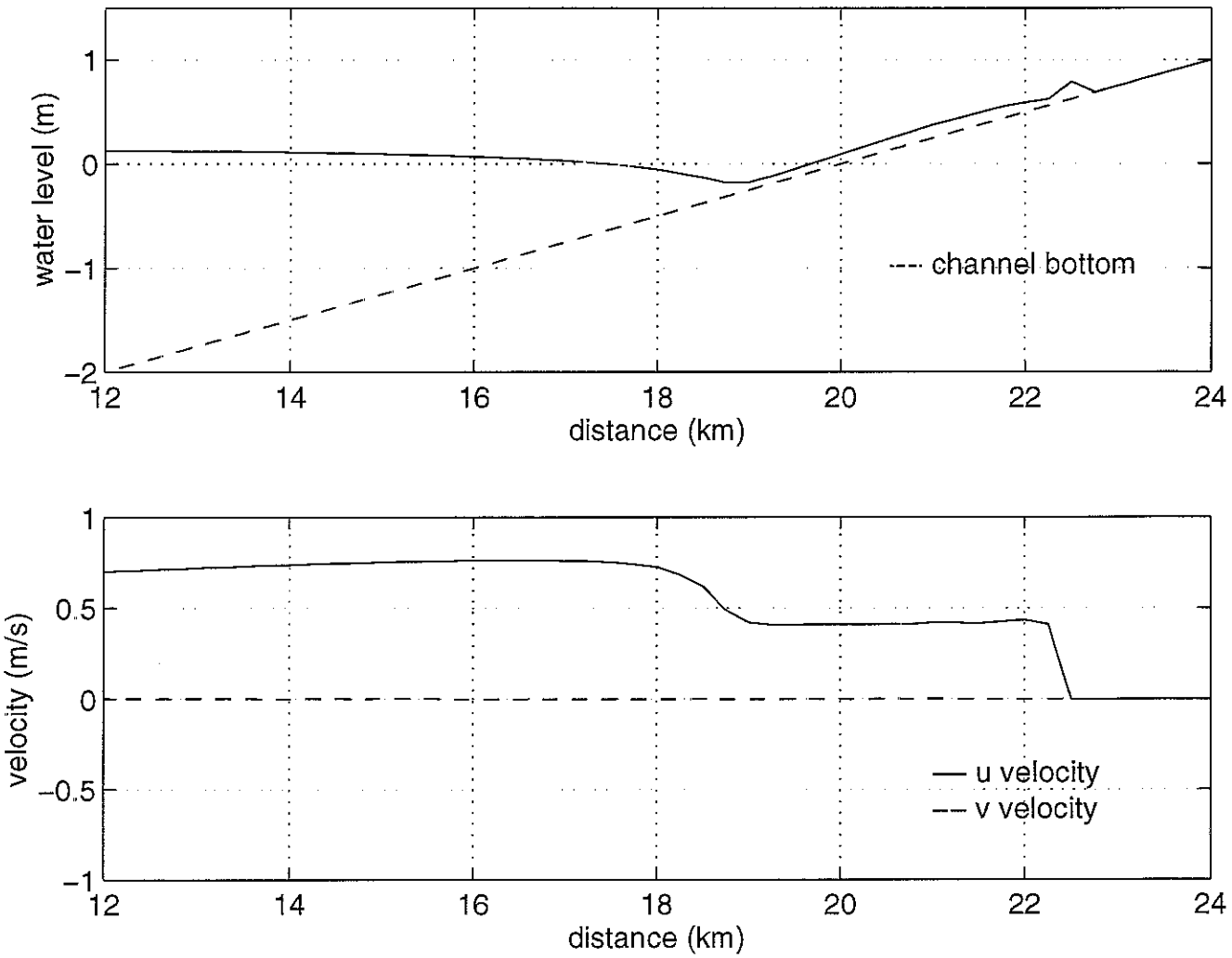

Figure 9j. Test Case #3, Time = 9*T/10

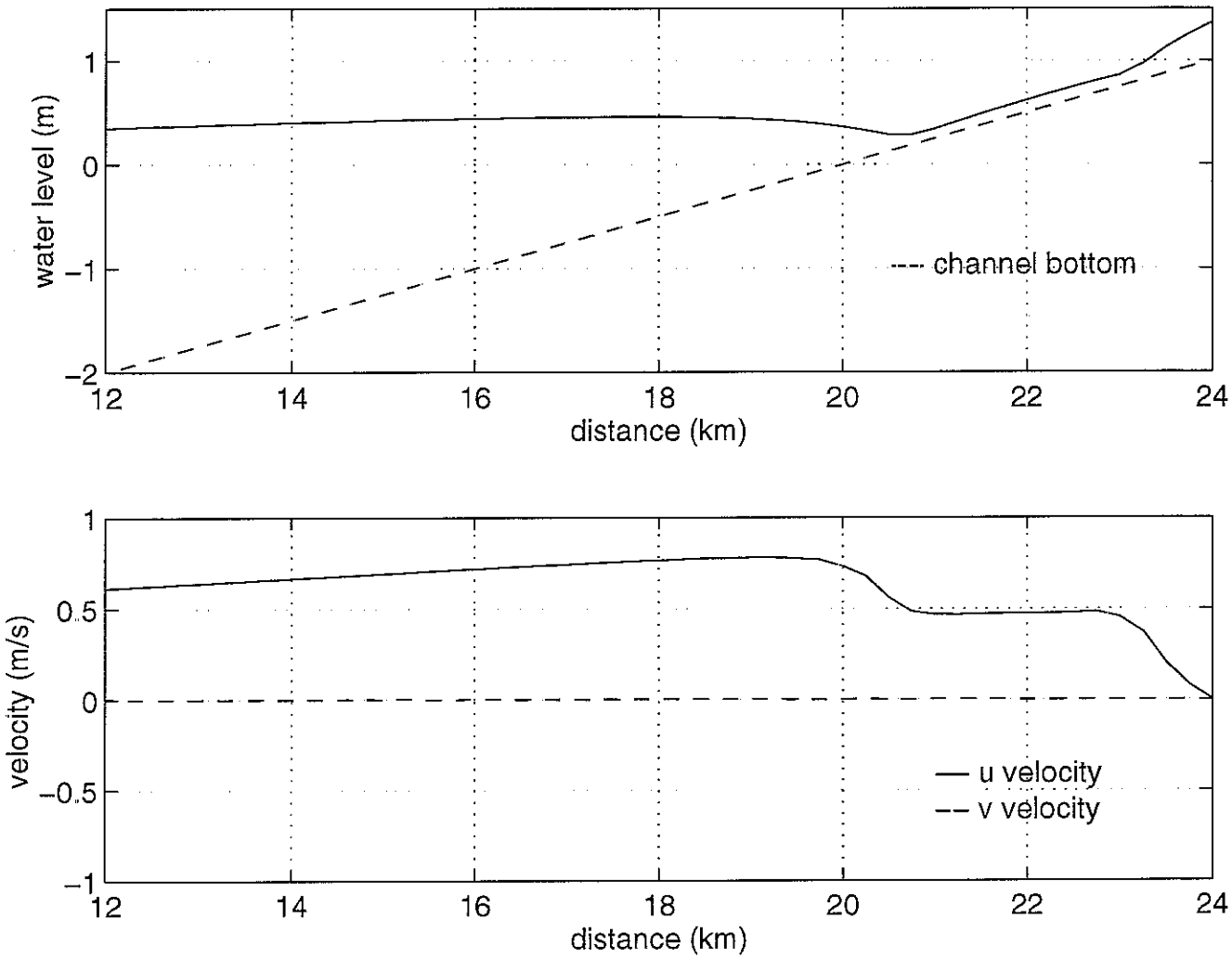

Figure 10a. Test Case #3, Distance = 12.75 km

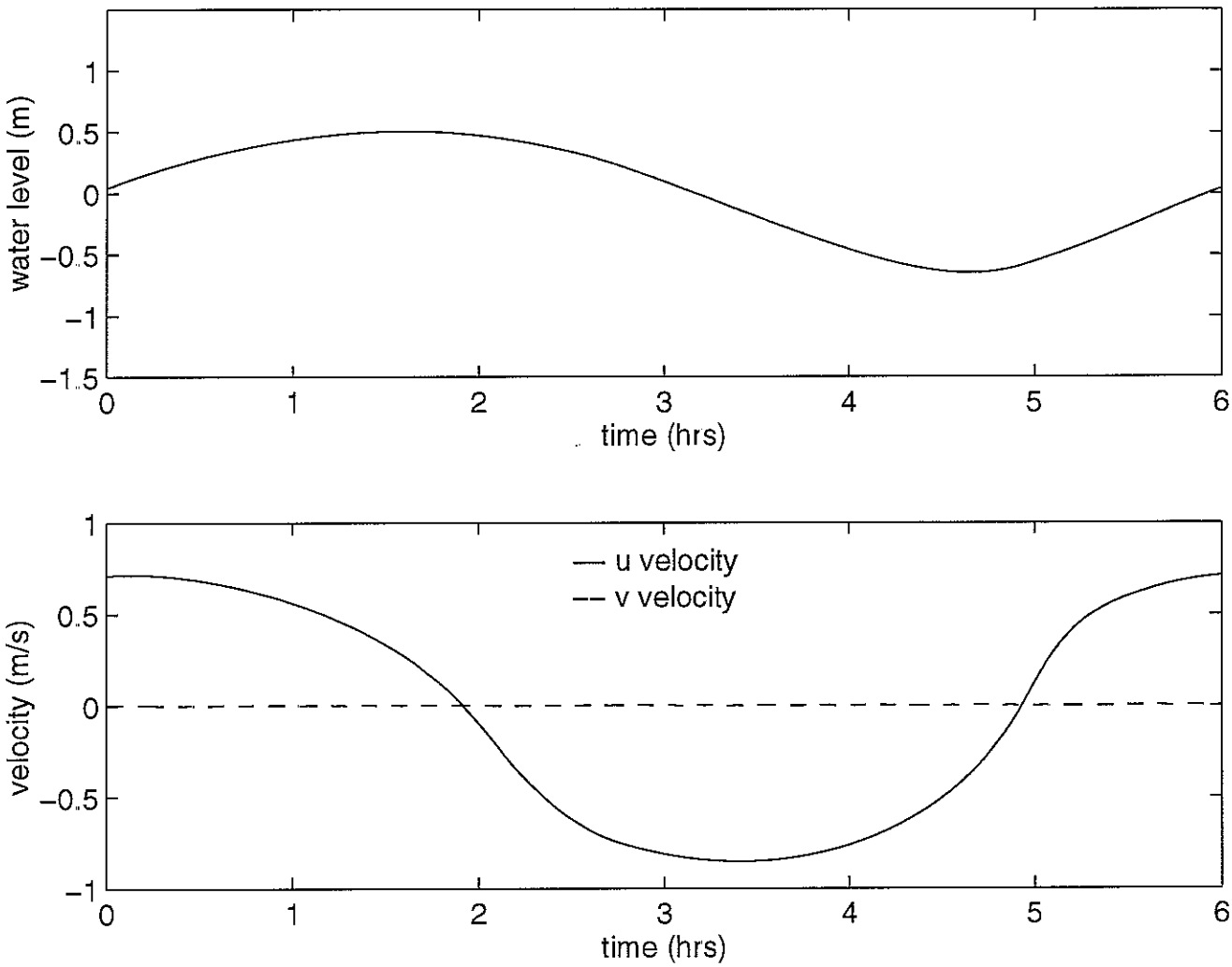

Figure 10b. Test Case #3, Distance = 17.75 km

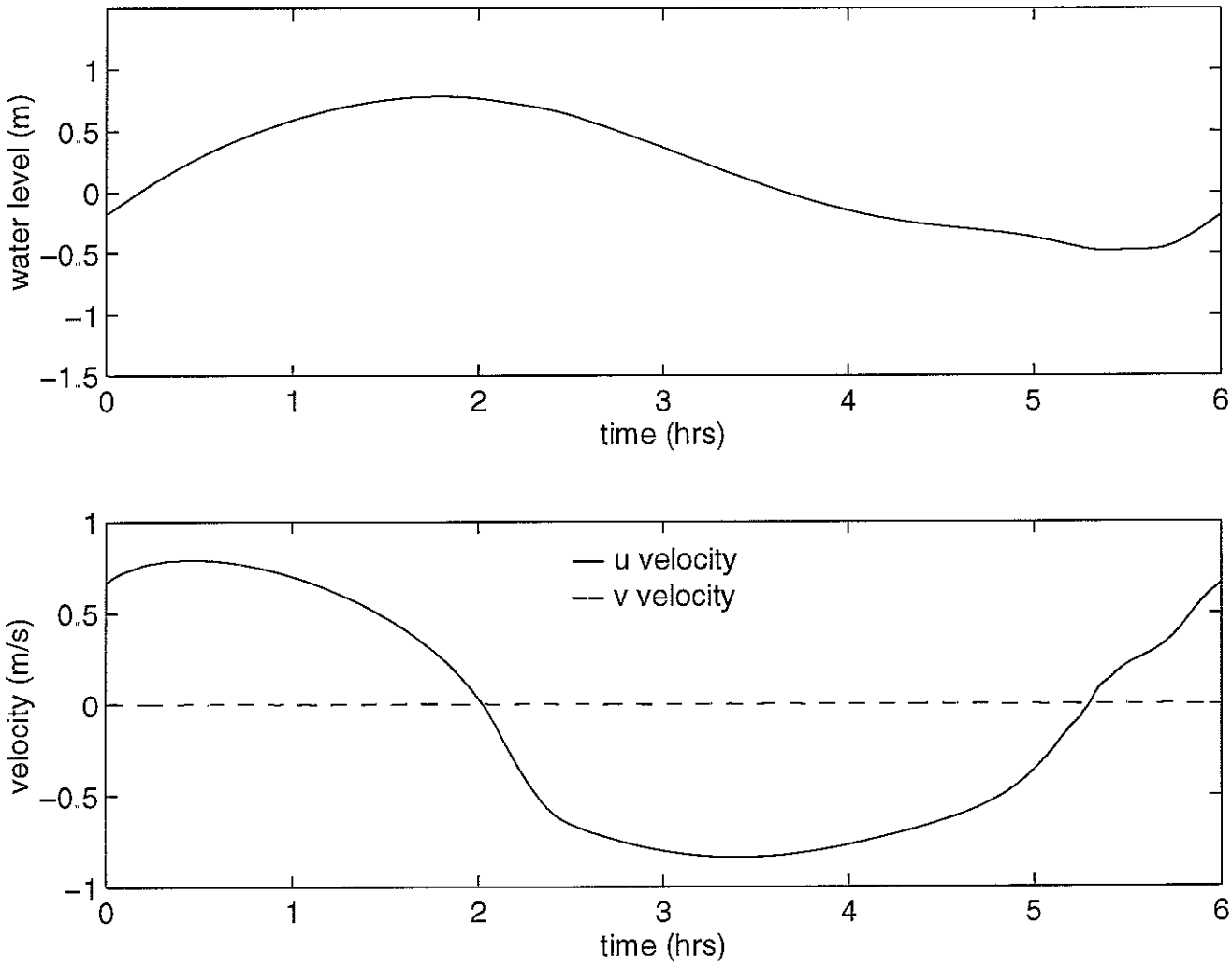

Figure 10c. Test Case #3, Distance = 18.50 km

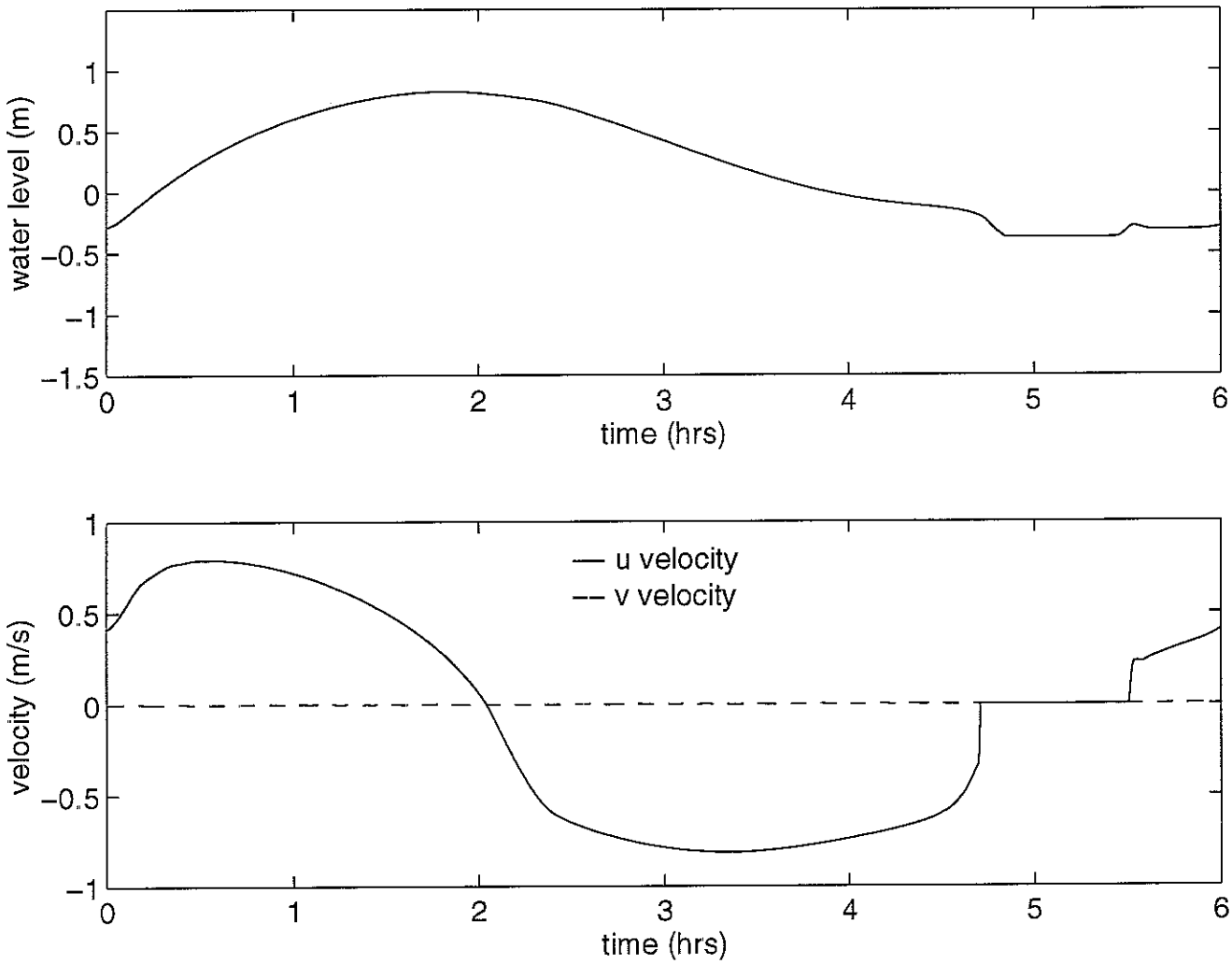

Figure 10d. Test Case #3, Distance = 20.50 km

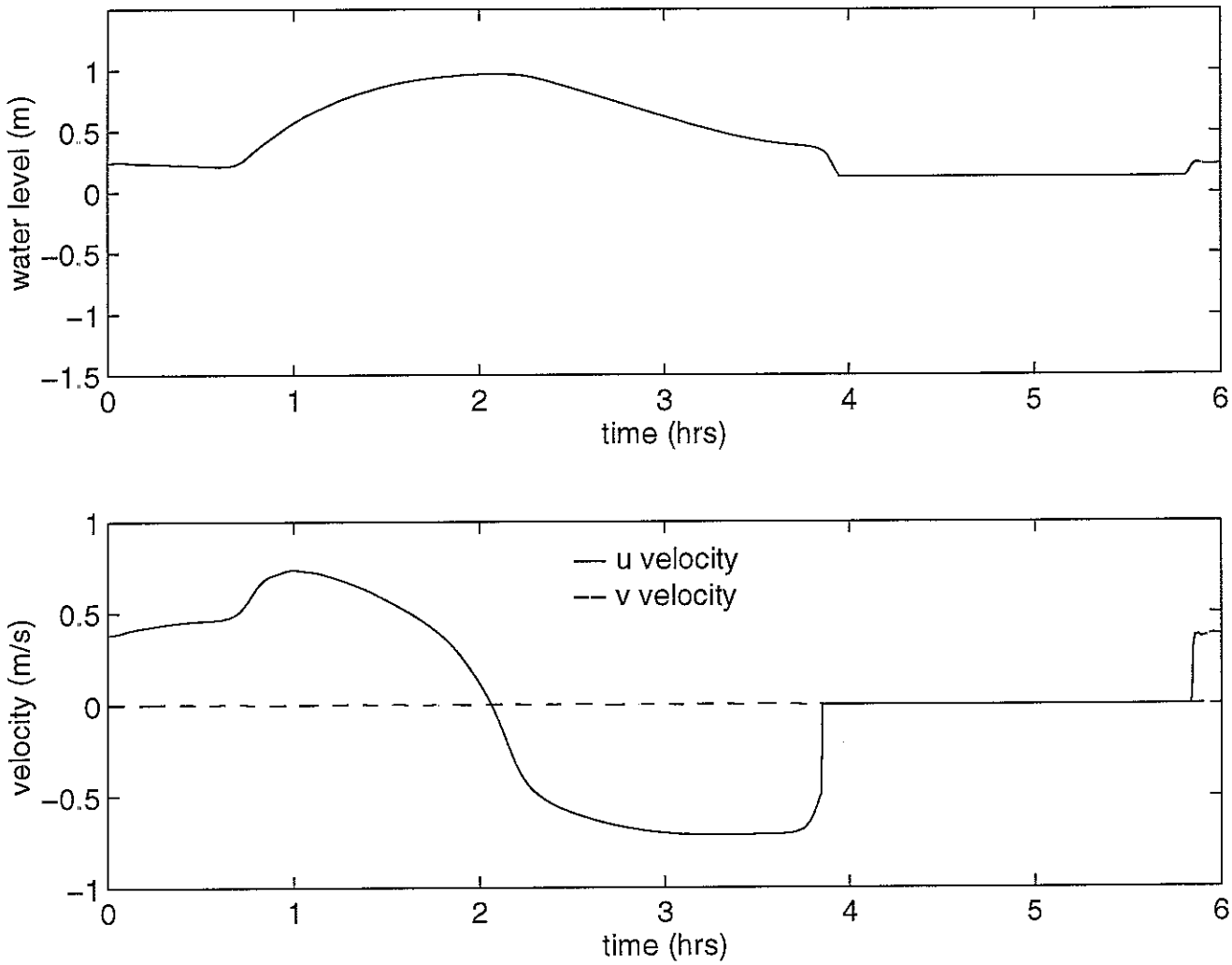

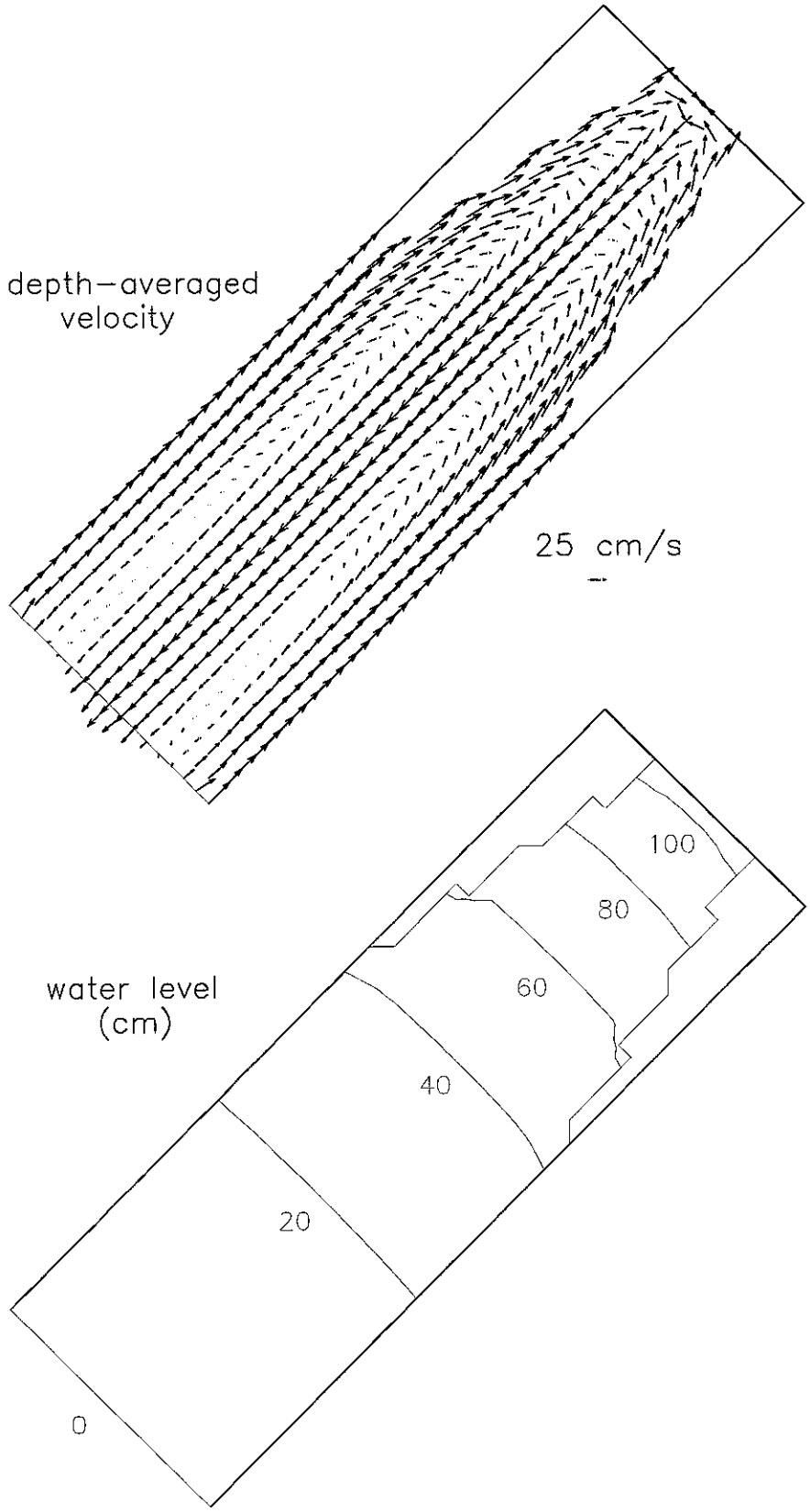

Figure 11a. Test Case #4, time=0.0 hrs

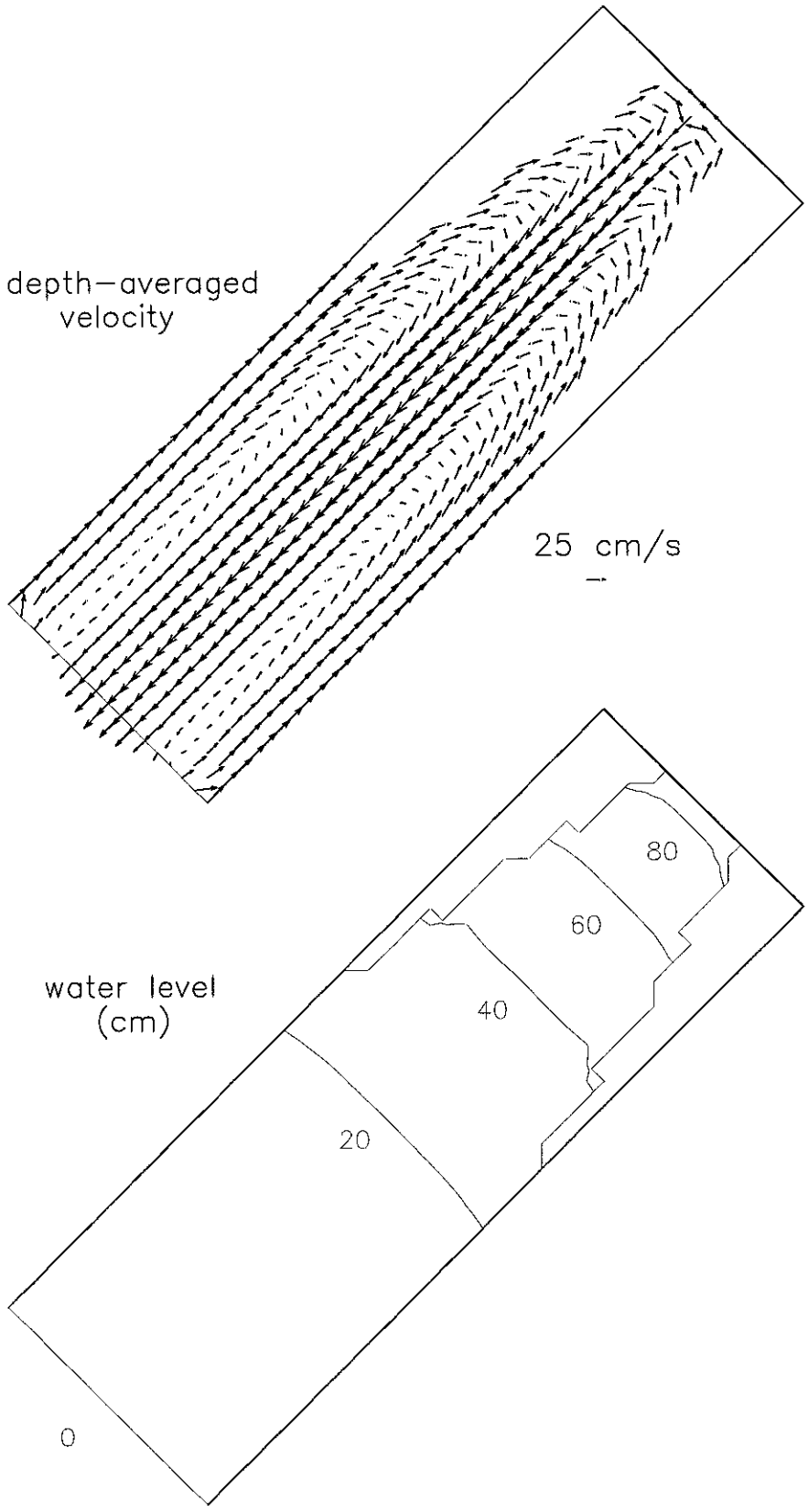

Figure 11b. Test Case #4, time=0.5 hrs

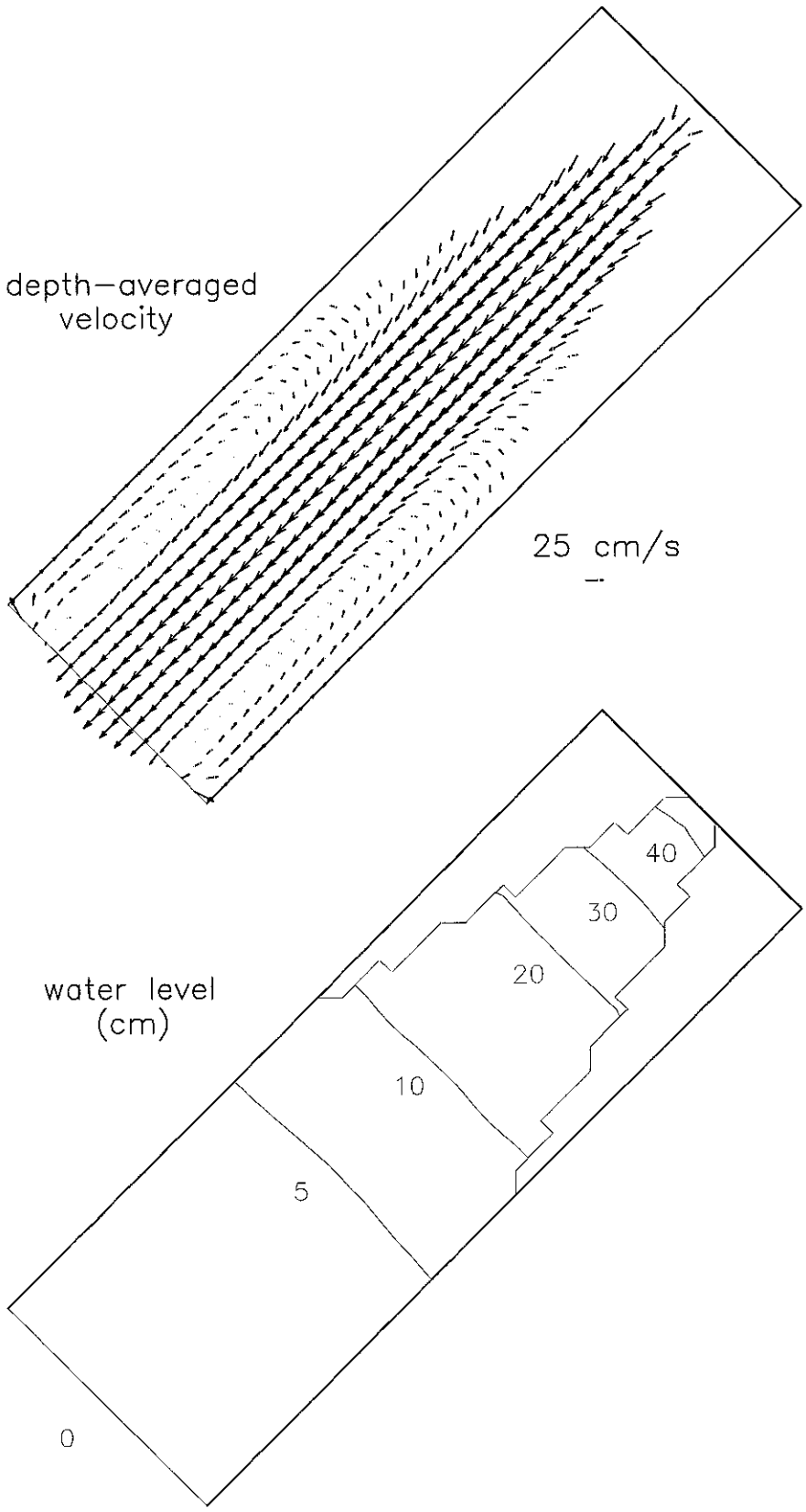

Figure 11c. Test Case #4, time=1.0 hrs

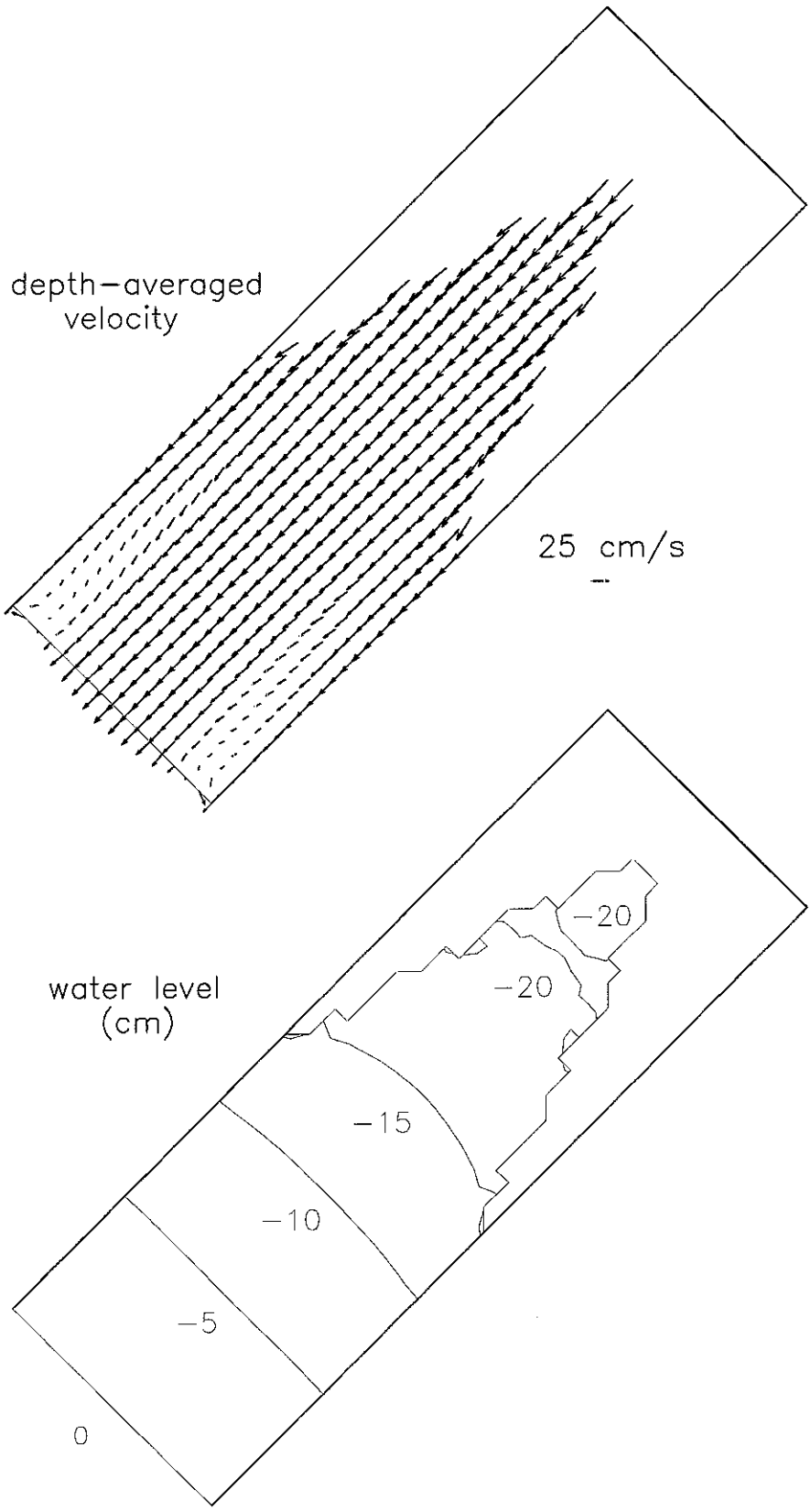

Figure 11d. Test Case #4, time=1.5 hrs

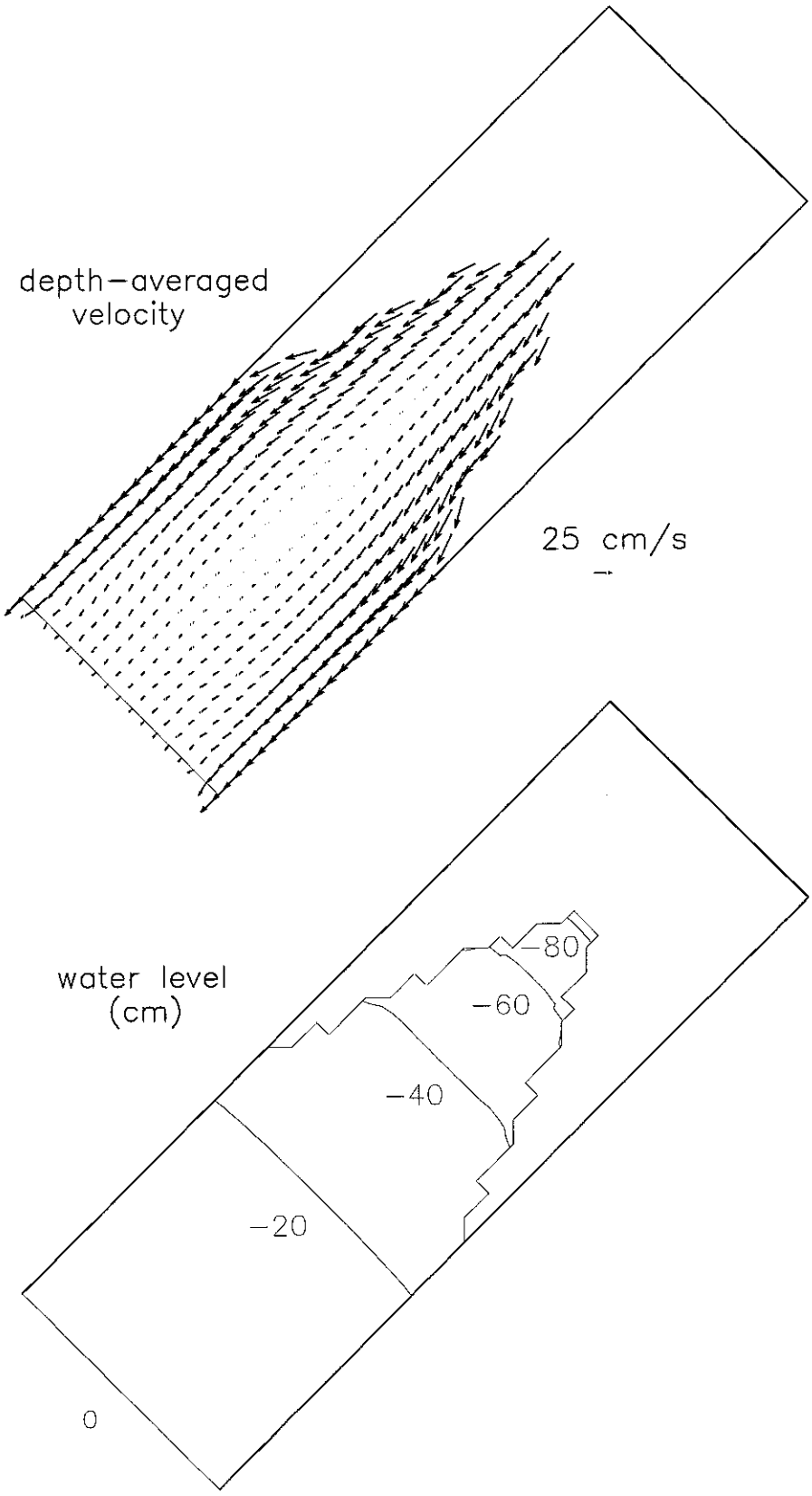

Figure 11e. Test Case #4, time=2.0 hrs

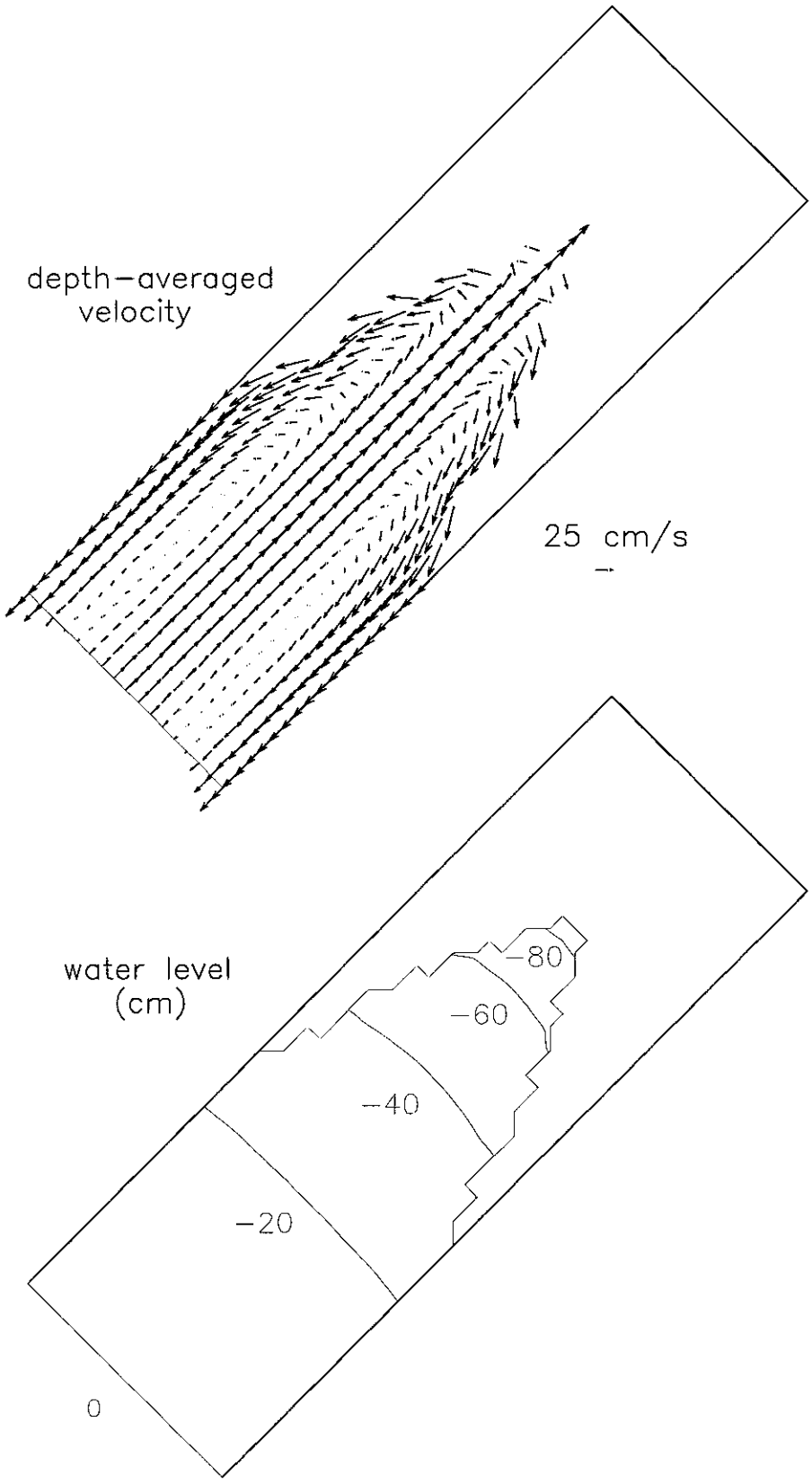

Figure 11f. Test Case #4, time=2.5 hrs

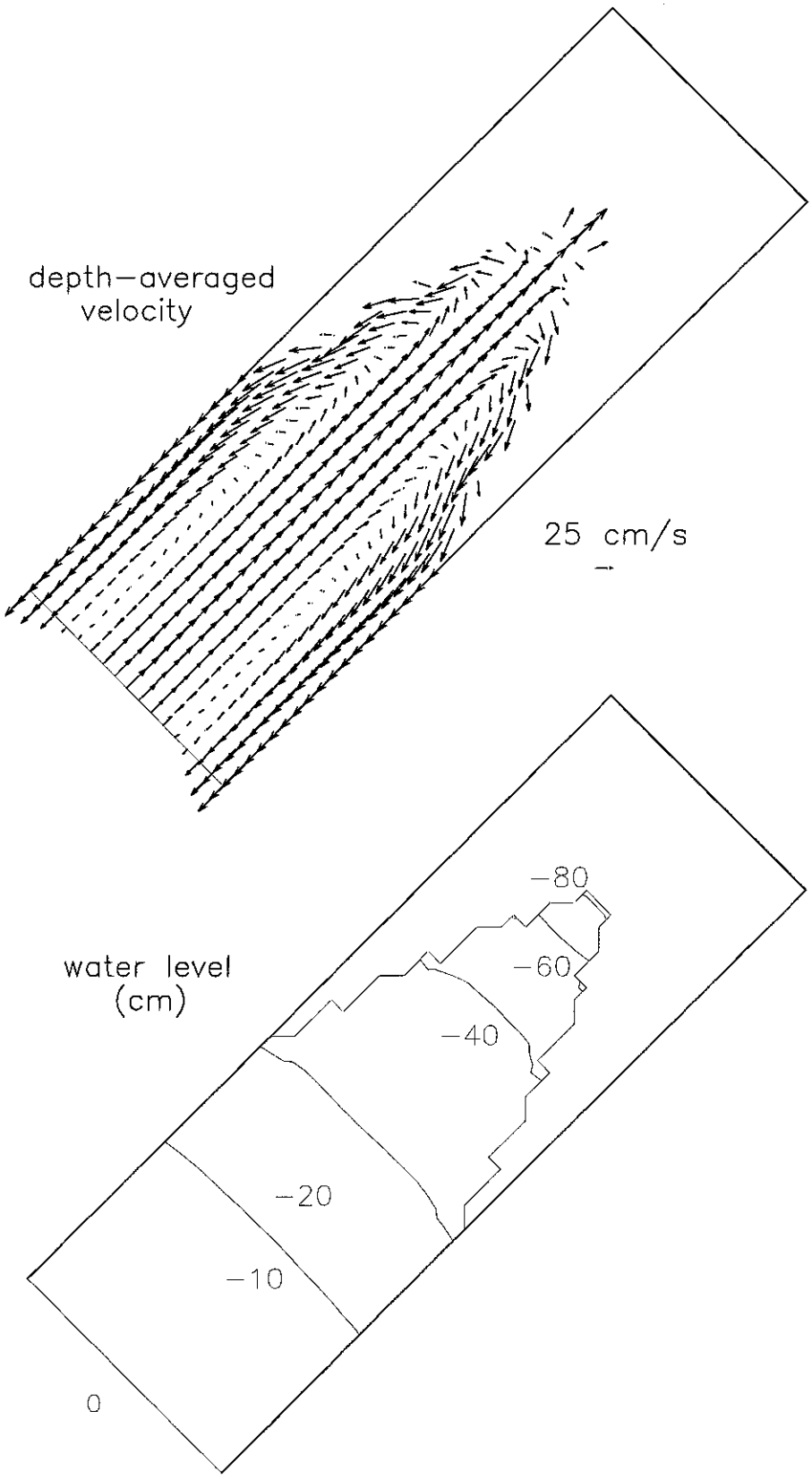

Figure 11g. Test Case #4, time=3.0 hrs

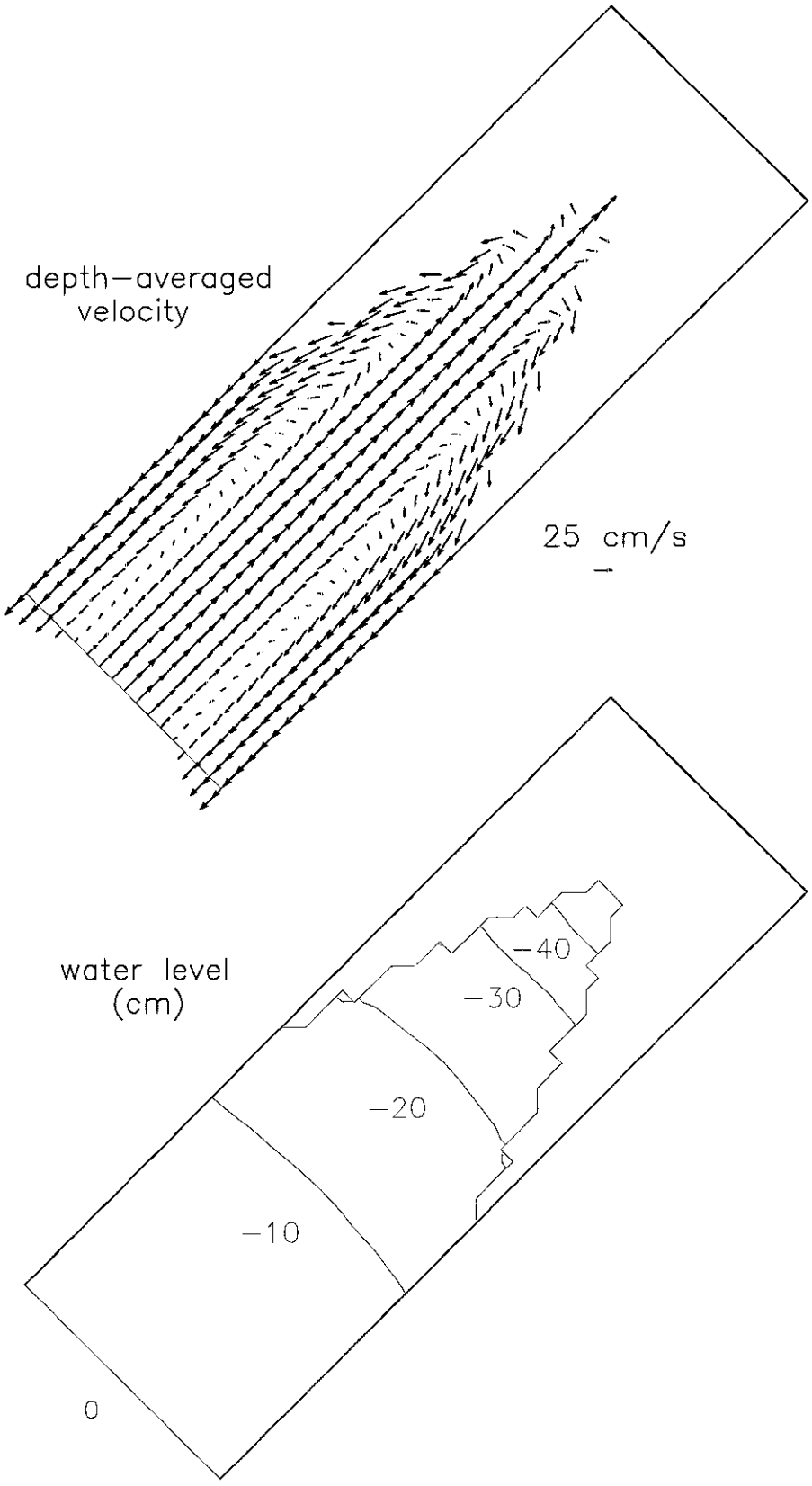

Figure 11h Test Case #4, time=3.5 hrs

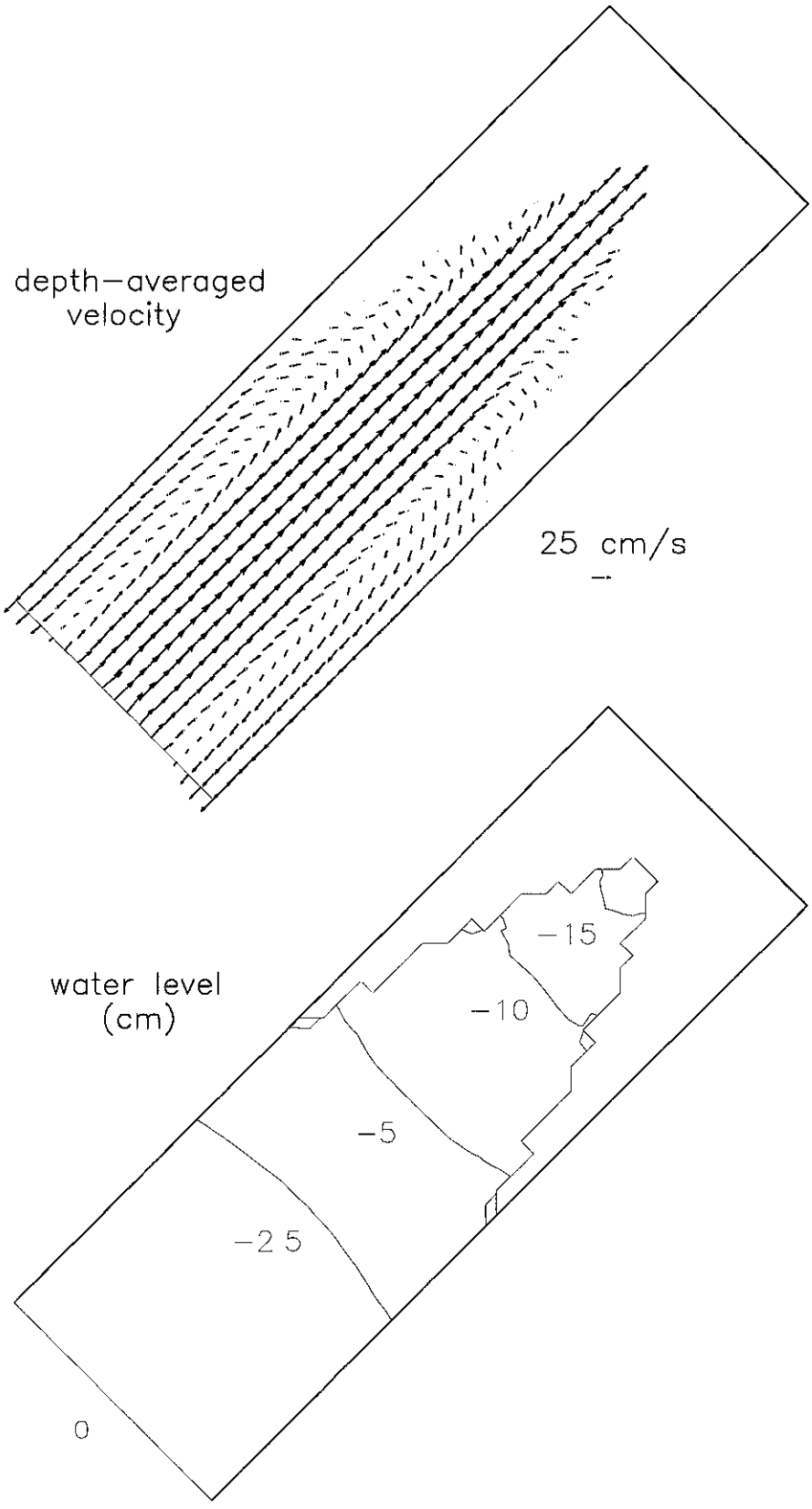

Figure 11i. Test Case #4, time=4.0 hrs

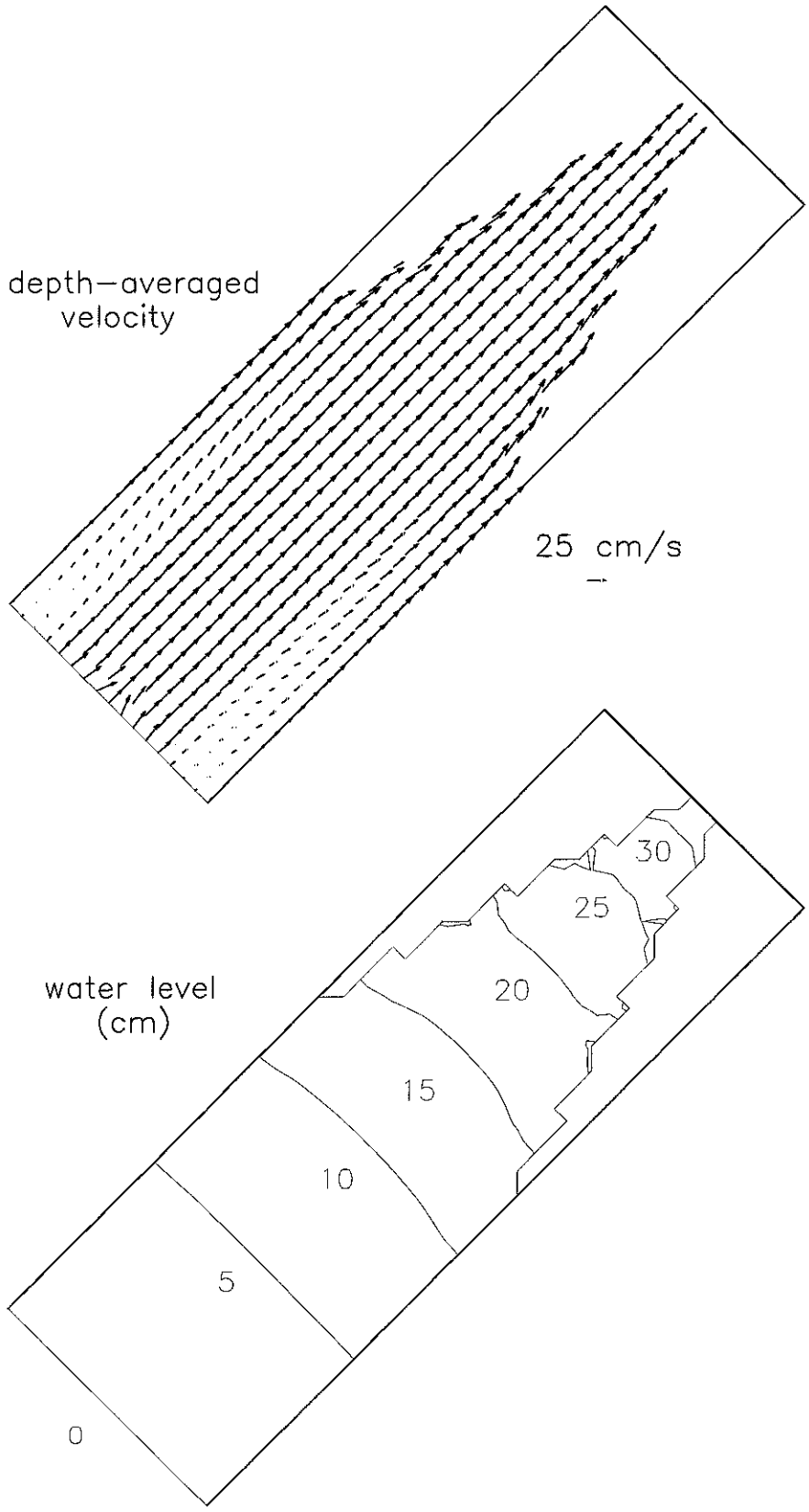

Figure 11j. Test Case #4, time=4.5 hrs

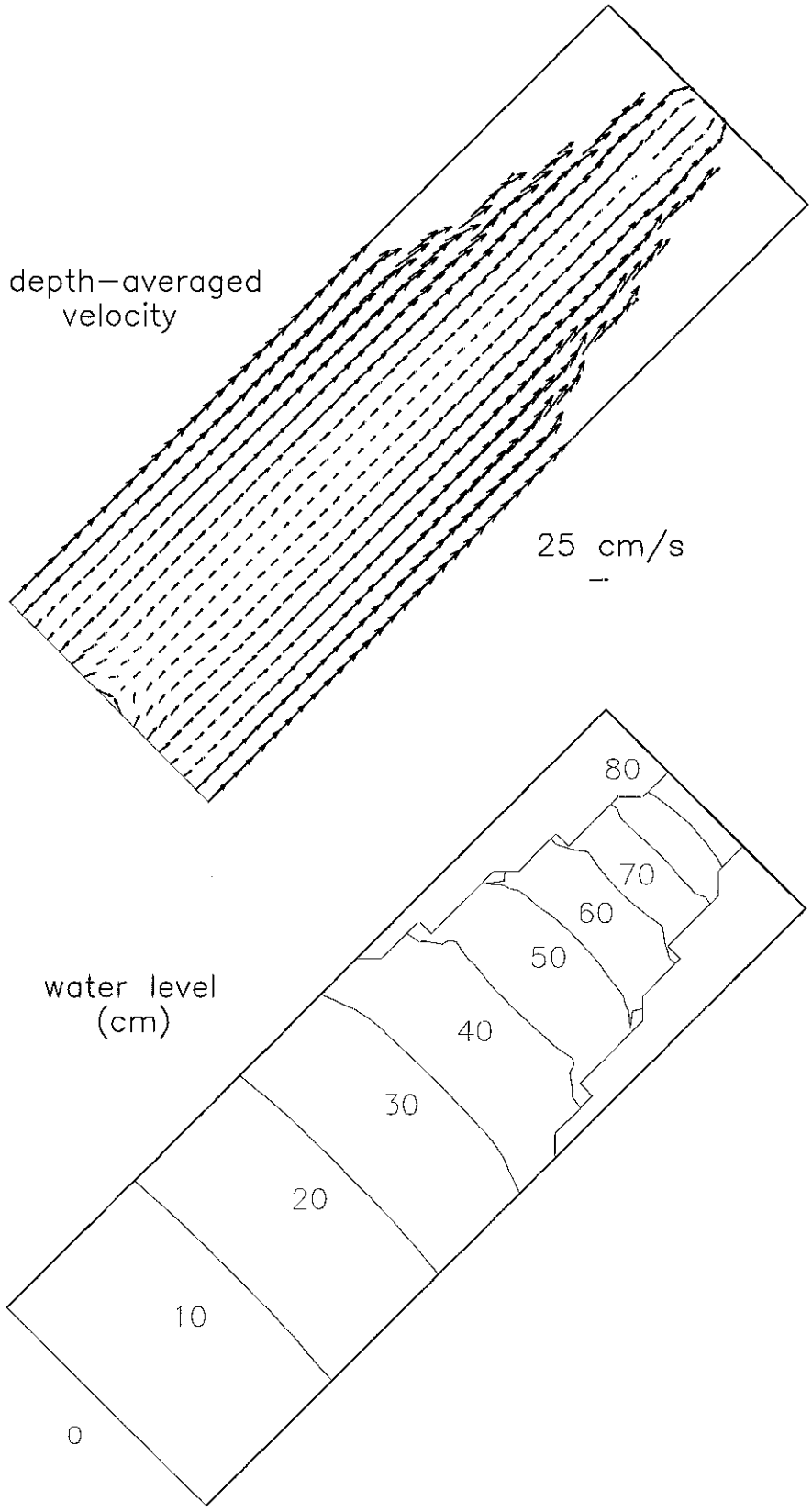

Figure 11k. Test Case #4, time=5.0 hrs

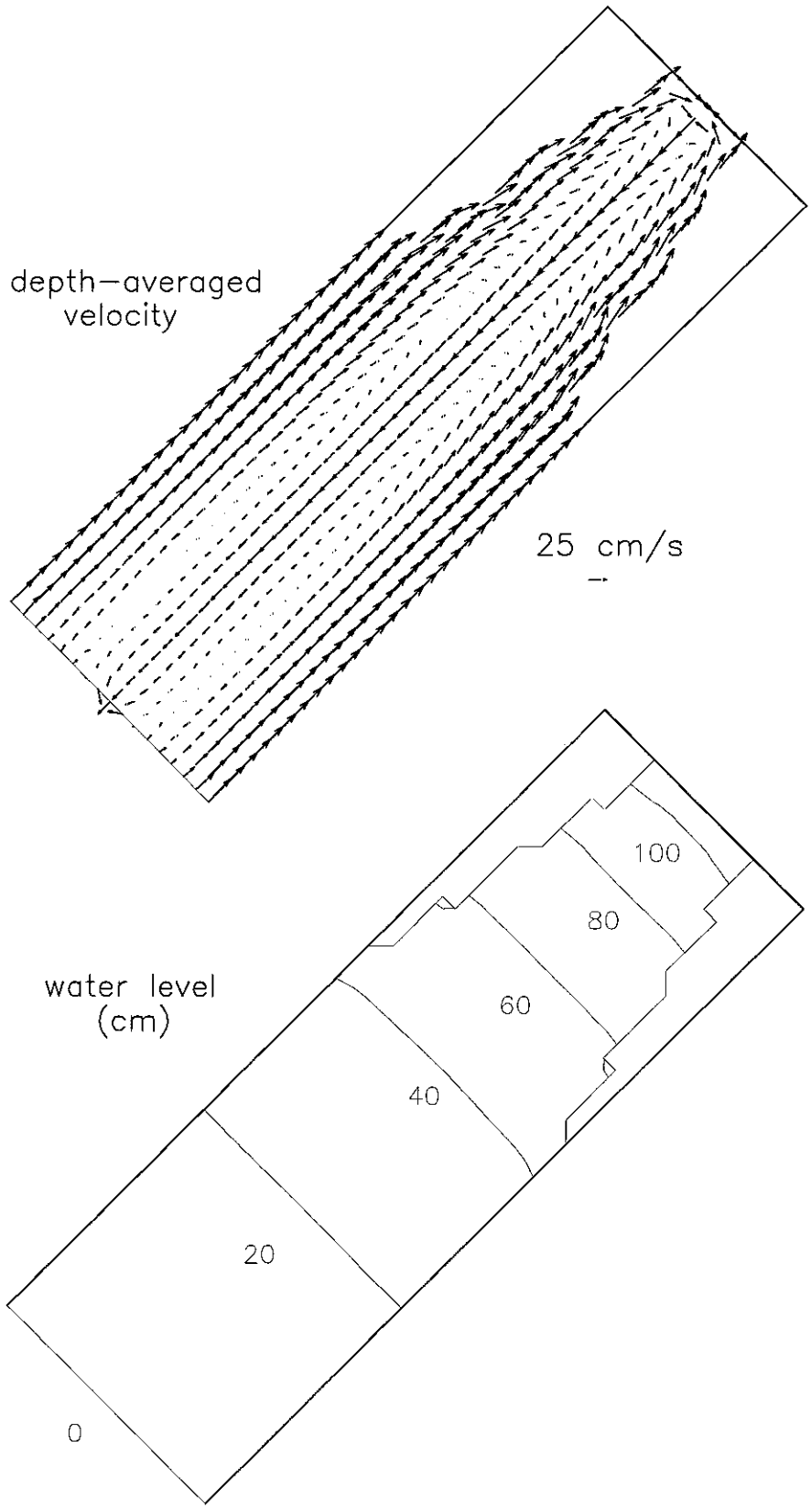

Figure 11l. Test Case #4, time=5.5 hrs

Figure 12a. Test Case #4, Node 383

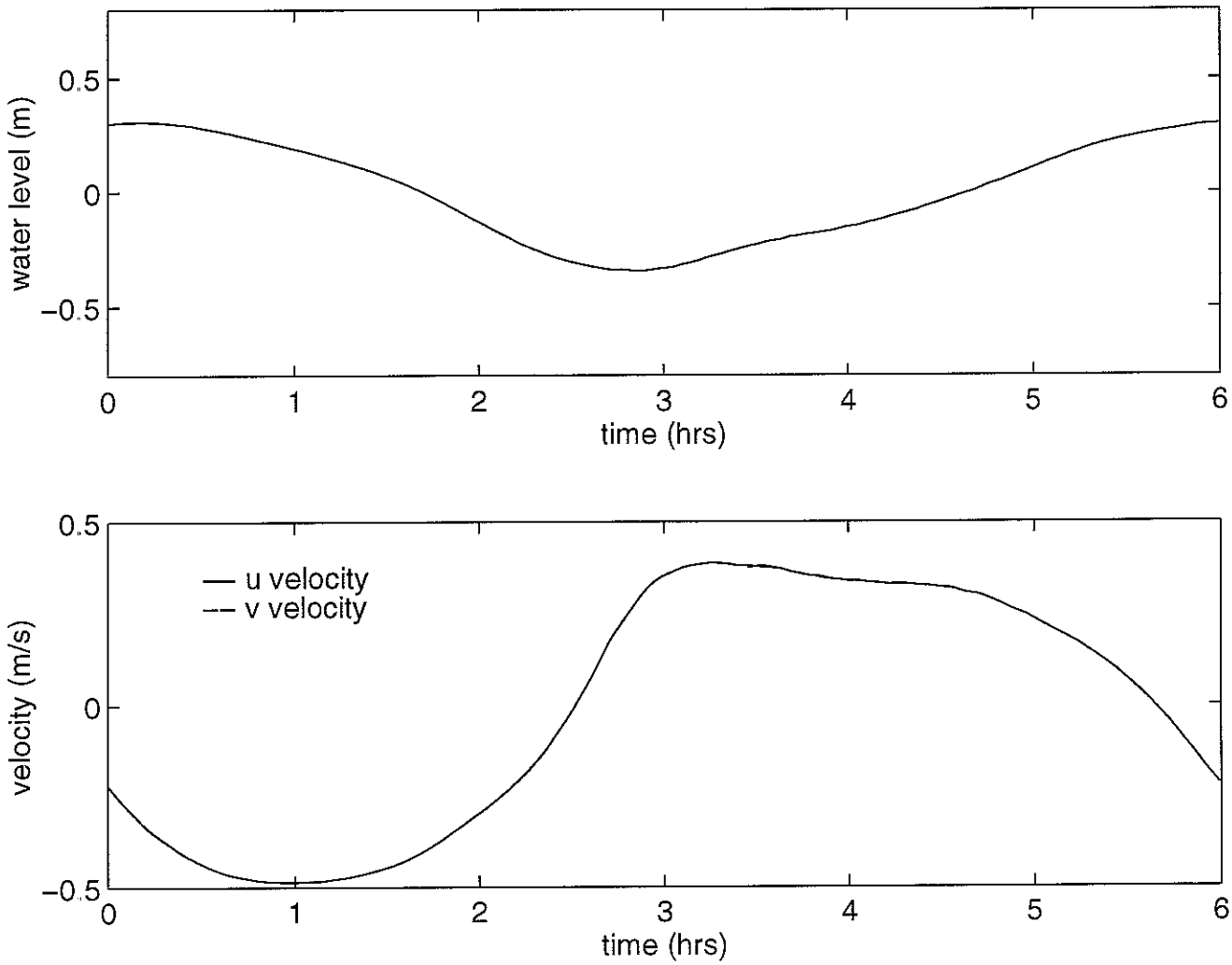

Figure 12b. Test Case #4, Node 553

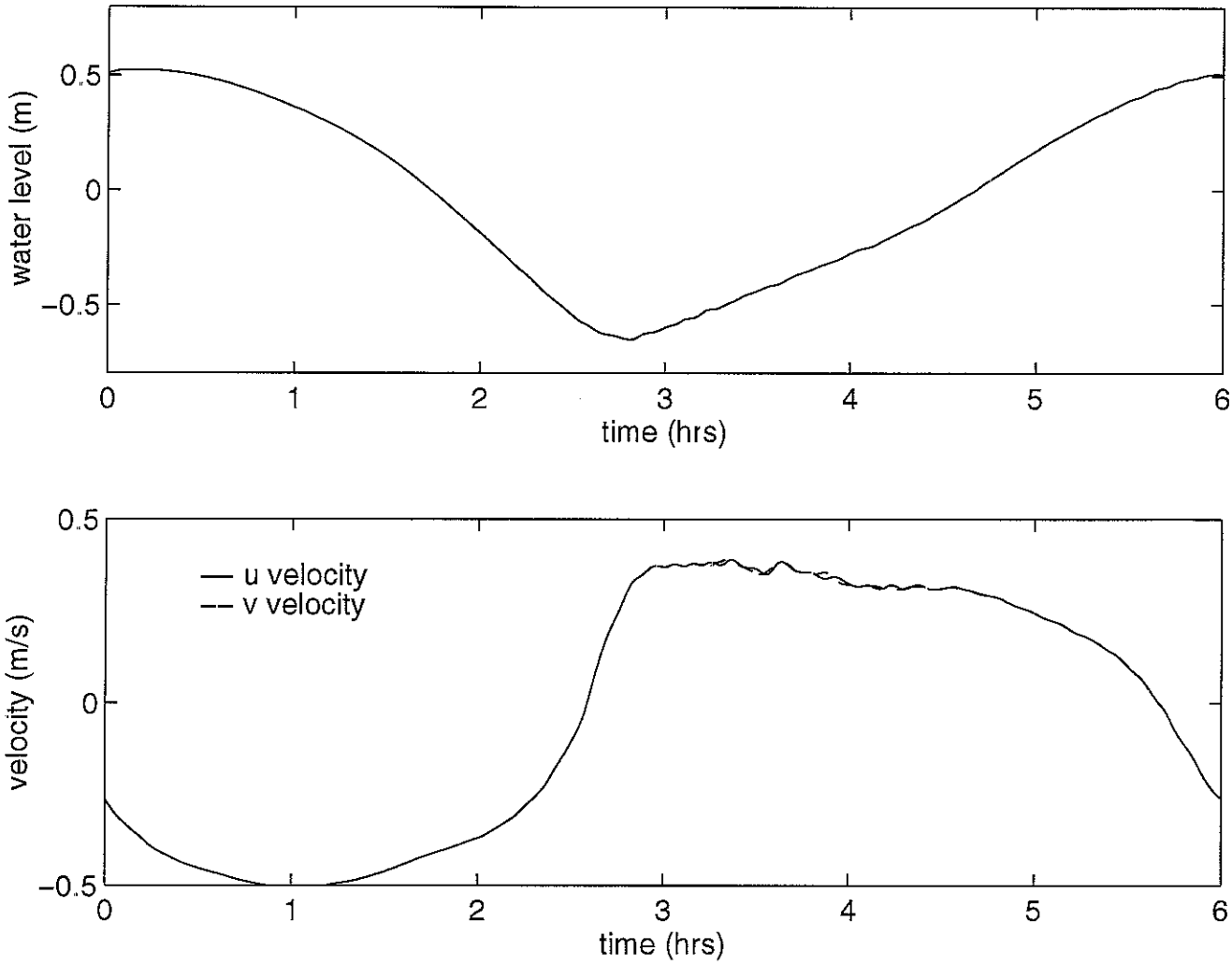

Figure 12c. Test Case #4, Node 706

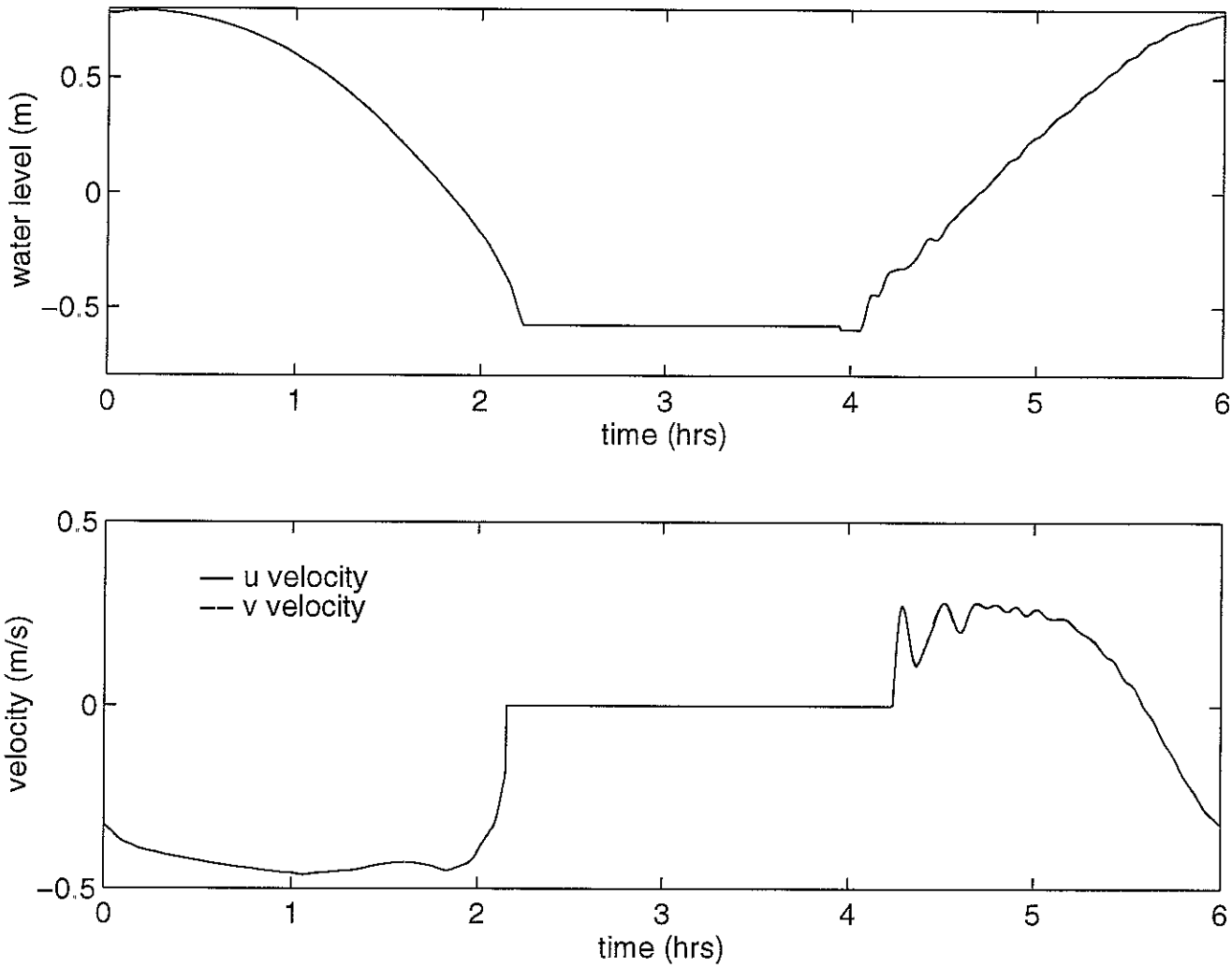

Figure 12d. Test Case #4, Node 705

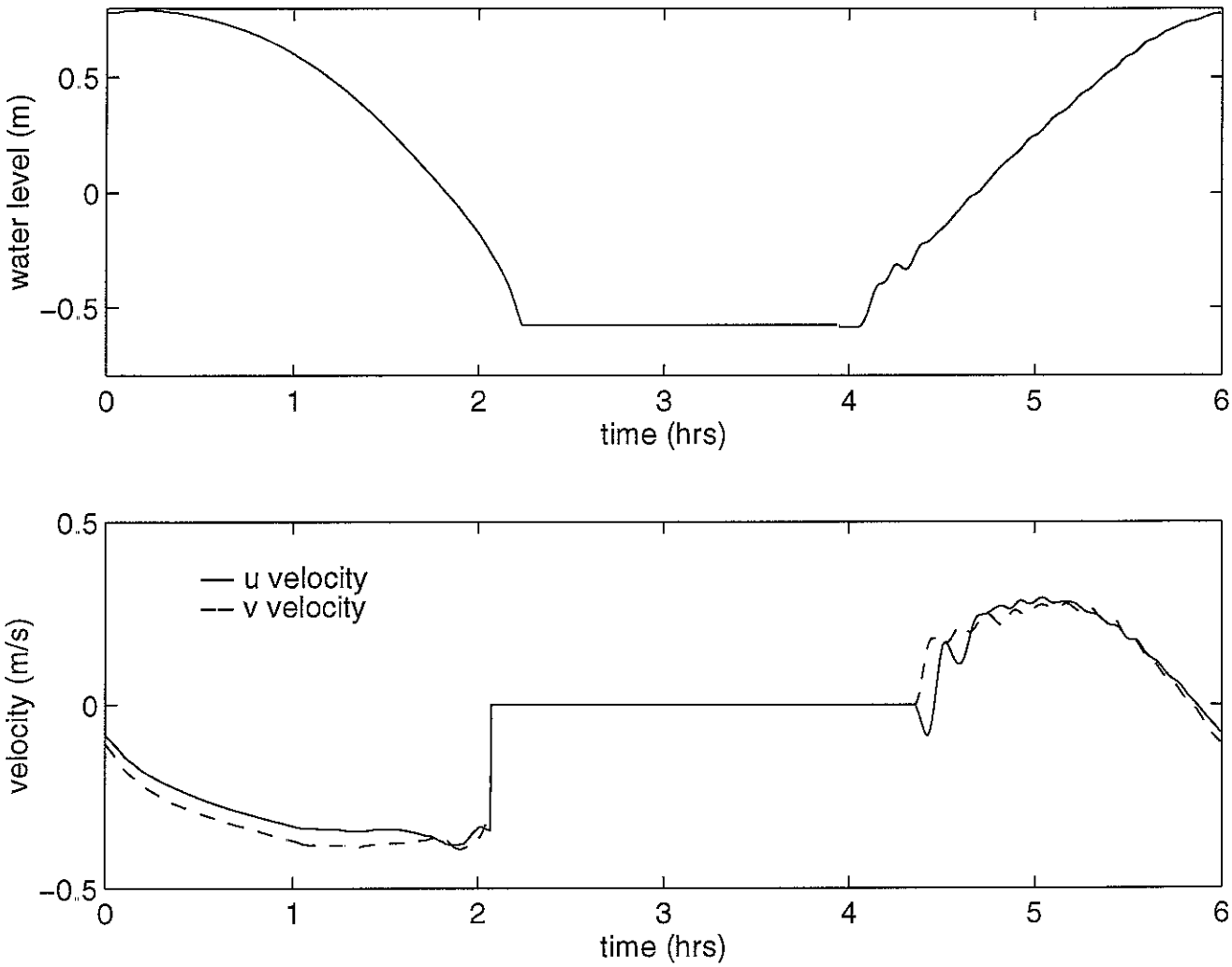

Figure 12e. Test Case #4, Node 704

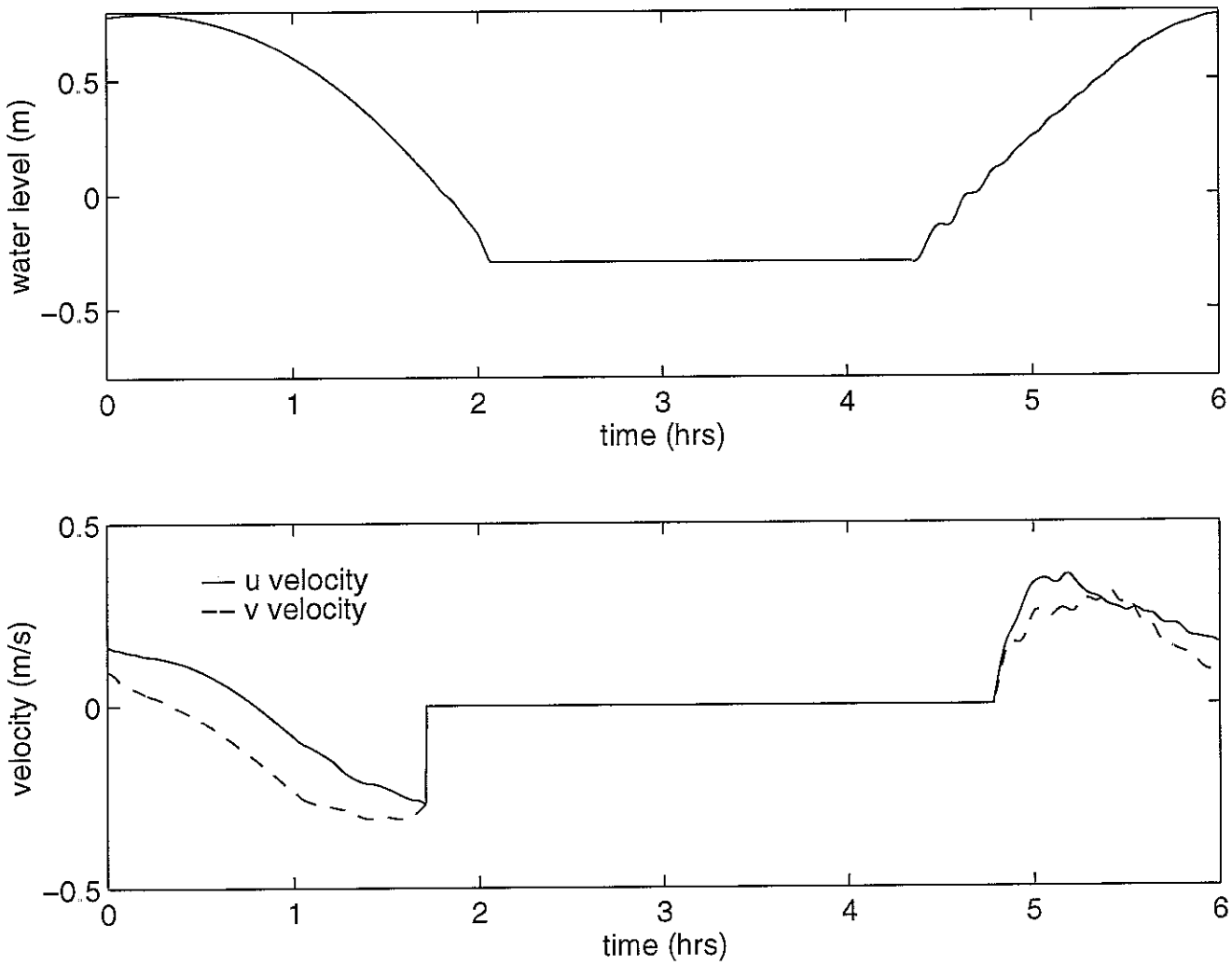

Figure 12f. Test Case #4, Node 703